

QUANTUM MECHANICAL STUDY OF PROPYLENE EPOXIDATION
ON VARIOUS METAL OXIDE SURFACES

A THESIS SUBMITTED TO
THE GRADUATE SCHOOL OF NATURAL AND APPLIED SCIENCES
OF
MIDDLE EAST TECHNICAL UNIVERSITY

BY

İLKER TEZSEVİN

IN PARTIAL FULFILLMENT OF THE REQUIREMENTS
FOR
THE DEGREE OF DOCTOR OF PHILOSOPHY
IN
CHEMICAL ENGINEERING

JANUARY 2018

Approval of the thesis:

**QUANTUM MECHANICAL STUDY OF PROPYLENE EPOXIDATION
ON VARIOUS METAL OXIDE SURFACES**

submitted by **İLKER TEZSEVİN** in partial fulfillment of the requirements for the degree of **Doctor of Philosophy in Chemical Engineering Department, Middle East Technical University** by,

Prof. Dr. Gülbin Dural
Dean, Graduate School of **Natural and Applied Sciences** _____

Prof. Dr. Halil Kalıpçılar
Head of Department, **Chemical Engineering Dept.** _____

Prof. Dr. Işık Önal
Supervisor, **Chemical Engineering Dept.** _____

Examining Committee Members:

Prof. Dr. Mehmet Çakmak
Physics Dept., Gazi University _____

Prof. Dr. Işık Önal
Chemical Engineering Dept., METU _____

Asst. Prof. Dr. Harun Koku
Chemical Engineering Dept., METU _____

Assoc. Prof. Dr. Çerağ Dilek Hacıhabiboğlu
Chemical Engineering Dept., METU _____

Asst. Prof. Dr. Engin Durgun
UNAM, Bilkent University _____

Date: 11.01.2018

I hereby declare that all information in this document has been obtained and presented in accordance with academic rules and ethical conduct. I also declare that, as required by these rules and conduct, I have fully cited and referenced all material and results that are not original to this work.

Name, Last name: İLKER TEZSEVİN

Signature:

ABSTRACT

QUANTUM MECHANICAL STUDY OF PROPYLENE EPOXIDATION ON VARIOUS METAL OXIDE SURFACES

Tezsevin, İlker

Ph.D., Department of Chemical Engineering

Supervisor: Prof. Dr. Işık Önal

January 2018, 97 pages

Silver is a very successful catalyst for the ethylene oxide synthesis, however, its performance for propylene oxide (PO) production is very limited. This thesis work aims to investigate the reasons of the low PO selectivity on the silver catalyst and to study the possible enhancements to make PO formation feasible. In order to investigate the reason of the low PO performance, the partial oxidation mechanism of propylene on silver catalyst is examined by using density functional theory (DFT) calculations. Ag₂O (001) surface is used as the active oxide phase of the catalyst through the study. The mechanistic study on an ideal surface revealed that even though the direct propylene oxide formation on the silver oxide catalyst is the most probable pathway, the high desorption barrier of propylene oxide leads to allyl radical formation causing further oxidation reactions. After finding the reason behind the problem, possible enhancements were studied to make PO desorption easier and to block undesired allyl formation pathways. For this aim, effects of gold and chlorine doping on the Ag₂O (001) surface were investigated both individually and together in seven different scenarios. It is observed that gold doping alters the binding properties of the oxygen atom responsible for the PO and PO isomer formation and decreases the desorption

barrier of the PO from the surface. On the other hand, only gold doping cannot inhibit allyl formation pathways, which are still easier than the PO desorption. Chlorine promotion shows two different effects. First, Cl addition slightly decreases the PO desorption barrier. Second, Cl blocks the oxygen site responsible for allyl formation. It is found that, in order to block the allyl formation pathway completely, two neighboring O atoms of the central oxygen should be replaced with Cl atoms. Therefore, silver oxide unit cell modified with 2 Cl gives better results and favors PO production without allyl formation problem. Studies for combined effects of gold and chlorine doping show that one gold-silver and two oxygen-chlorine replacements gives the best performance among the Au & Cl doped scenarios by both reducing the PO desorption barrier and blocking the allyl formation paths. As a result, this study shows that silver can be an effective catalyst for the propylene oxide production with appropriate modifications. This study also encourages experimental researchers for further effort on the modified silver (oxide) catalyst for the direct propylene epoxidation.

Keywords: DFT, Propylene Oxide, Ag₂O Catalyst, Mechanism, Doping Effect

ÖZ

ÇEŞİTLİ METAL OKSİT YÜZEYLERDE PROPİLEN EPOKSİDASYONUNUN KUANTUM MEKANİK ÇALIŞMASI

Tezsevin, İlker

Doktora, Kimya Mühendisliği Bölümü

Tez Yöneticisi: Prof. Dr. Işık Önal

Ocak 2018, 97 sayfa

Gümüş, etilen oksit sentezi için oldukça başarılı bir katalizördür, ancak propilen oksit (PO) üretimindeki performansı sınırlıdır. Bu tez gümüş katalizörü üzerinde düşük PO seçiciliğinin sebeplerini incelemeyi ve PO oluşumunu elverişli bir hale getirmek için gerekli iyileştirmeleri çalışmayı amaçlamaktadır. Düşük PO performansının sebebini incelemek amacıyla, kısmi propilen oksidasyon mekanizması gümüş katalizör üzerinde yoğunluk fonksiyoneli teorisi (DFT) hesaplamaları kullanılarak çalışılmıştır. Ag₂O (001) yüzeyi katalizörün aktif oksit fazı olarak tez boyunca kullanılmıştır. İdeal yüzey üzerindeki mekanizma çalışması göstermiştir ki, gümüş oksit katalizör üzerinde doğrudan propilen oksit oluşumu en olası yol olmasına karşın, propilen oksidin yüksek desorpsiyon bariyeri ileri oksidasyon tepkimelerine sebep olan allil radikal oluşumuna yol açmaktadır. Problemin sebebi bulunduğundan sonra PO desorpsiyonunu kolaylaştırmak ve istenmeyen allil oluşumu yollarını engellemek için olası iyileştirmeler çalışılmıştır. Bu amaçla, Ag₂O (001) yüzeyinde altın ve klorun etkisi yalnız başlarına ve birlikte olmak üzere yedi farklı senaryoda incelenmiştir. Altın katkısının PO ve PO izomer oluşumundan sorumlu oksijen atomunun bağ yapma özelliklerini değiştirdiği ve PO'nun yüzeyden desorpsiyon bariyerini azalttığı gözlemlenmiştir. Diğer taraftan, yalnızca altın katkısı, halen PO desorpsiyonundan

daha kolay olan allil oluşumu yollarını engelleyememiştir. Klor desteği iki farklı etki göstermektedir. Birincisi, Cl eklemesi PO desorpsiyon bariyerini kısmen azaltmaktadır. İkincisi, Cl allil oluşumundan sorumlu oksijen sitelerini engellemektedir. Allil oluşumu yollarını tamamen engellemek için merkezdeki oksijen atomunun komşusu olan iki O atomunun da Cl atomları ile yer değiştirilmesi gerektiği bulunmuştur. Bu sebeple 2 Cl eklentisi ile değiştirilmiş gümüş oksit birim hücresi daha iyi sonuç vermekte ve allil oluşumu problemi olmadan PO üretimini kolaylaştırmaktadır. Altın ve klor katkılarının karma etkileri çalışmaları bir altın-gümüş ve iki oksijen-klor değişiminin hem PO desorpsiyon bariyerini azaltarak hem de allil oluşumu yollarını engelleyerek Au & Cl katkılı senaryolar arasında en iyi performansı verdiğini göstermiştir. Sonuç olarak, bu çalışma gümüşün gerekli değiştirmelerle propilen oksit üretiminde etkili bir katalizör olabileceğini göstermiştir. Bu çalışma ayrıca deneysel araştırmacıları değiştirilmiş gümüş (oksit) katalizörü konusunda cesaretlendirmektedir.

Anahtar Kelimeler: DFT, Propilen Oksit, Ag₂O Katalizör, Mekanizma, Doping Etkisi

ACKNOWLEDGEMENTS

First of all, I would like to thank my supervisor Prof. Işık Önal for his invaluable guidance, encouragement and helpful suggestions during my research. I would like to thank Prof. Dr. Mehmet Çakmak and Asst. Prof. Dr. Harun Koku for their critical questions and inspiring comments during progress comity meetings. I would also like to thank to Prof. Dr. Rutger van Santen and Prof. Dr. Emiel Hensen for their comments and for inviting me to the Netherlands to enrich my knowledge on computational catalysis.

I would like to acknowledge The Scientific and Technological Research Council of Turkey (TÜBİTAK) for the financial support under the graduate scholarship programs BİDEB 2211 and 2214-A. I deeply acknowledge TUBITAK ULAKBIM, High Performance and Grid Computing Centre (TRUBA resources) for the computational power. All the calculations in this work are performed at TRUBA resources.

I would also like to thank to Dr. M. Ferdi Fellah, Dr. M. Oluş Özbek and Dr. Derya Düzenli for sharing their knowledge on catalysis. I thank all the members of METU Computational Catalysis Research laboratory and the members of TU/e Inorganic Materials Chemistry Group for their friendship.

I would like to thank my mother Fatma Nur Tezsevin for her patience and support without any expectation. I would like to dedicate this thesis to my father Mehmet Tezsevin, who I lost during my doctoral studies. Without his support and encouragement, I could not achieve many things.

Finally, I would like to express my special thanks to my precious wife Yasemin Tezsevin for her love, support, patience and for all the time we spend together.

TABLE OF CONTENTS

ABSTRACT	v
ÖZ	vii
ACKNOWLEDGEMENTS	ix
TABLE OF CONTENTS.....	xi
LIST OF TABLES.....	xiii
LIST OF FIGURES	xv
CHAPTERS	
1. INTRODUCTION	1
1.1. Industrial PO Production Processes.....	2
1.1.1. Chlorohydrin Process	2
1.1.2. Hydroperoxide Processes	3
1.1.3. Hydrogen Peroxide Based Propylene Oxide Process (HPPO).....	4
1.1.4. Cumene Hydroperoxide Process	5
1.2. Catalysis.....	5
1.2.1. Catalysis Cycle and Sabatier's Principle	7
1.2.2. Types of Catalysts	7
1.3. Computational Chemistry and Density Functional Theory.....	9
1.3.1. Density Functional Theory	9
1.3.2. Formulation of Density Functional Theory	10
1.3.3. Approximations of Density Functional Theory	14
2. HISTORY OF PROPYLENE EPOXIDATION RESEARCH	17
2.1. Photocatalyst Studies	17
2.2. Alternative Oxygen Source Studies.....	18
2.3. Direct Epoxidation Studies.....	21
3. MOTIVATION, COMPUTATIONAL METHOD AND SURFACE MODELS	29
3.1. Motivation and Goals.....	29
3.2. Computational Method and Surface Models	30

4. RESULTS AND DISCUSSIONS	35
4.1. Construction of the Partial Oxidation Mechanism of Propylene.....	35
4.2. Completion of Catalysis Cycle for Propylene Epoxidation	36
4.3. Energetics on the Unpromoted Silver Oxide Slabs	37
4.3.1. Energetics on the Silver Oxide ($\text{Ag}_{32}\text{O}_{16}$) Slab	37
4.3.2. Energetics on the Silver Oxide Slab with Oxygen Vacancy ($\text{Ag}_{32}\text{O}_{15}$).....	41
4.4. Energetics on the Silver Oxide Slabs with Gold Doping	47
4.4.1. Energetics on the $\text{Ag}_{31}\text{Au}_1\text{O}_{16}$ (001) Slab	47
4.4.2. Energetics on the $\text{Ag}_{30}\text{Au}_2\text{O}_{16}$ (001) Slab	52
4.5. Energetics on the Silver Oxide Slabs with Chlorine Doping	56
4.5.1. Energetics on the $\text{Ag}_{32}\text{O}_{15}\text{Cl}_1$ (001) Slab	56
4.5.2. Energetics on the $\text{Ag}_{32}\text{O}_{14}\text{Cl}_2$ (001) Slab	62
4.6. Energetics on the Silver Oxide Slabs with both Gold and Chlorine Doping	66
4.6.1. Energetics on the $\text{Ag}_{31}\text{Au}_1\text{O}_{15}\text{Cl}_1$ (001) Slab	66
4.6.2. Energetics on the $\text{Ag}_{31}\text{Au}_1\text{O}_{14}\text{Cl}_2$ (001) Slab	72
4.6.3. Energetics on the $\text{Ag}_{30}\text{Au}_2\text{O}_{14}\text{Cl}_2$ (001) Slab	76
5. CONCLUSIONS.....	81
REFERENCES	85
CURRICULUM VITAE	95

LIST OF TABLES

TABLES

Table 1: Distribution of world propylene oxide capacity by technology [6]	2
Table 2: Activation barriers and reaction energies on $\text{Ag}_{32}\text{O}_{16}$ (001) slab.....	41
Table 3: Activation barriers and reaction energies on $\text{Ag}_{32}\text{O}_{15}$ (001) slab.....	46
Table 4: Activation barriers and reaction energies on $\text{Ag}_{31}\text{Au}_1\text{O}_{16}$ (001) slab.....	51
Table 5: Activation barriers and reaction energies on $\text{Ag}_{30}\text{Au}_2\text{O}_{16}$ (001) slab.....	55
Table 6: Activation barriers and reaction energies on $\text{Ag}_{32}\text{O}_{15}\text{Cl}_1$ (001) slab.....	61
Table 7: Activation barriers and reaction energies on $\text{Ag}_{32}\text{O}_{14}\text{Cl}_2$ (001) slab.....	65
Table 8: Activation barriers and reaction energies on $\text{Ag}_{31}\text{Au}_1\text{O}_{15}\text{Cl}_1$ (001) slab.....	71
Table 9: Activation barriers and reaction energies on $\text{Ag}_{31}\text{Au}_1\text{O}_{14}\text{Cl}_2$ (001) slab.....	75
Table 10: Activation barriers and reaction energies on $\text{Ag}_{30}\text{Au}_2\text{O}_{14}\text{Cl}_2$ (001) slab.....	78

LIST OF FIGURES

FIGURES

Figure 1: Steps of chlorohydrin process [17]	3
Figure 2: Steps of PO/SM Process [9]	3
Figure 3: Steps of PO/TBA Process [2]	4
Figure 4: Reaction for HPPO Process [2]	4
Figure 5: Steps of Cumene Hydroperoxide Process [18]	5
Figure 6: Trend of DFT publications over years [47].....	10
Figure 7: Geometries of optimized $\text{Ag}_{32}\text{O}_{16}$ (001) and $\text{Ag}_{32}\text{O}_{15}$ (001) Slabs (Grey atoms = silver, Red atoms = oxygen)	31
Figure 8: Schematic diagram of the steps followed through the study	32
Figure 9: Geometries of $\text{Ag}_{31}\text{Au}_1\text{O}_{16}$, $\text{Ag}_{30}\text{Au}_2\text{O}_{16}$, $\text{Ag}_{32}\text{O}_{15}\text{Cl}_1$ and $\text{Ag}_{32}\text{O}_{14}\text{Cl}_2$ (001) slabs after optimization (Grey atoms = silver, Red atoms = oxygen, Yellow atoms = gold, Green atoms = chlorine)	34
Figure 10: Geometries of $\text{Ag}_{31}\text{Au}_1\text{O}_{15}\text{Cl}_1$, $\text{Ag}_{31}\text{Au}_1\text{O}_{14}\text{Cl}_2$ and $\text{Ag}_{30}\text{Au}_2\text{O}_{14}\text{Cl}_2$ (001) slabs after optimization (Grey atoms = silver, Red atoms = oxygen, Yellow atoms = gold, Green atoms = chlorine)	34
Figure 11: Partial oxidation mechanism of propylene on Ag_2O (001) Surface	36
Figure 12: Energetics of direct propylene-surface interactions on $\text{Ag}_{32}\text{O}_{16}$ (001) slab.....	38
Figure 13: Energetics of the reactions through OMP1 on $\text{Ag}_{32}\text{O}_{16}$ (001) slab.....	39
Figure 14: Energetics of the reactions through OMP2 on $\text{Ag}_{32}\text{O}_{16}$ (001) slab.....	40
Figure 15: The most probable pathway on $\text{Ag}_{32}\text{O}_{16}$ (001) slab.....	41
Figure 16: Energetics of direct propylene-surface interactions on $\text{Ag}_{32}\text{O}_{15}$ (001) slab.....	42
Figure 17: Energetics of the reactions through OMP1 on $\text{Ag}_{32}\text{O}_{15}$ (001) slab.....	43
Figure 18: Energetics of the reactions through OMP2 on $\text{Ag}_{32}\text{O}_{15}$ (001) slab.....	43
Figure 19: Energetics of the reactions through adsorbed propylene on $\text{Ag}_{32}\text{O}_{15}$ (001) slab ..	45
Figure 20: The most probable pathway on $\text{Ag}_{32}\text{O}_{15}$ (001) slab.....	46
Figure 21: Energetics of direct propylene-surface interactions on $\text{Ag}_{31}\text{Au}_1\text{O}_{16}$ (001) slab....	47
Figure 22: Energetics of the reactions through Au-OMP1 on $\text{Ag}_{31}\text{Au}_1\text{O}_{16}$ (001) slab.....	49
Figure 23: Energetics of the reactions through Au-OMP2 on $\text{Ag}_{31}\text{Au}_1\text{O}_{16}$ (001) slab.....	49

Figure 24: Energetics of the reactions through Ag-OMP1 on $\text{Ag}_{31}\text{Au}_1\text{O}_{16}$ (001) slab.....	50
Figure 25: Energetics of the reactions through Ag-OMP2 on $\text{Ag}_{31}\text{Au}_1\text{O}_{16}$ (001) slab.....	51
Figure 26: The most probable pathway on $\text{Ag}_{31}\text{Au}_1\text{O}_{16}$ (001) slab.....	52
Figure 27: Energetics of direct propylene-surface interactions on $\text{Ag}_{30}\text{Au}_2\text{O}_{16}$ (001) slab ...	53
Figure 28: Energetics of the reactions through OMP1 on $\text{Ag}_{30}\text{Au}_2\text{O}_{16}$ (001) slab.....	54
Figure 29: Energetics of the reactions through OMP2 on $\text{Ag}_{30}\text{Au}_2\text{O}_{16}$ (001) slab.....	54
Figure 30: The most probable pathway on $\text{Ag}_{30}\text{Au}_2\text{O}_{16}$ (001) slab.....	56
Figure 31: Reaction directions on $\text{Ag}_{32}\text{O}_{15}\text{Cl}_1$ (001) slab	56
Figure 32: Energetics of direct propylene-surface interactions on $\text{Ag}_{32}\text{O}_{15}\text{Cl}_1$ (001) slab	57
Figure 33: Energetics of the reactions through OMP1 on $\text{Ag}_{32}\text{O}_{15}\text{Cl}_1$ (001) slab on Direction A	58
Figure 34: Energetics of the reactions through OMP2 on $\text{Ag}_{32}\text{O}_{15}\text{Cl}_1$ (001) slab on Direction A	59
Figure 35: Energetics of the reactions through OMP1 on $\text{Ag}_{32}\text{O}_{15}\text{Cl}_1$ (001) slab on Direction B.....	60
Figure 36: Energetics of the reactions through OMP2 on $\text{Ag}_{32}\text{O}_{15}\text{Cl}_1$ (001) slab on Direction B.....	60
Figure 37: The most probable pathway on $\text{Ag}_{32}\text{O}_{15}\text{Cl}_1$ (001) slab.....	62
Figure 38: Energetics of direct propylene-surface interactions on $\text{Ag}_{32}\text{O}_{14}\text{Cl}_2$ (001) slab	63
Figure 39: Energetics of the reactions through OMP1 on $\text{Ag}_{32}\text{O}_{14}\text{Cl}_2$ (001) slab	64
Figure 40: Energetics of the reactions through OMP2 on $\text{Ag}_{32}\text{O}_{14}\text{Cl}_2$ (001) slab	64
Figure 41: The most probable pathway on $\text{Ag}_{32}\text{O}_{14}\text{Cl}_2$ (001) slab.....	66
Figure 42: Reaction directions on $\text{Ag}_{31}\text{Au}_1\text{O}_{15}\text{Cl}_1$ (001) slab.....	67
Figure 43: Energetics of direct propylene-surface interactions on $\text{Ag}_{31}\text{Au}_1\text{O}_{15}\text{Cl}_1$ (001) slab	67
Figure 44: Energetics of the reactions through OMP1 on $\text{Ag}_{31}\text{Au}_1\text{O}_{15}\text{Cl}_1$ (001) slab on Direction A.....	68
Figure 45: Energetics of the reactions through OMP2 on $\text{Ag}_{31}\text{Au}_1\text{O}_{15}\text{Cl}_1$ (001) slab on Direction A.....	69
Figure 46: Energetics of the reactions through OMP1 on $\text{Ag}_{31}\text{Au}_1\text{O}_{15}\text{Cl}_1$ (001) slab on Direction B.....	70
Figure 47: Energetics of the reactions through OMP2 on $\text{Ag}_{31}\text{Au}_1\text{O}_{15}\text{Cl}_1$ (001) slab on Direction B.....	70
Figure 48: The most probable pathway on $\text{Ag}_{31}\text{Au}_1\text{O}_{15}\text{Cl}_1$ (001) slab.....	72

Figure 49: Energetics of direct propylene-surface interactions on $\text{Ag}_{31}\text{Au}_1\text{O}_{14}\text{Cl}_2$ (001) slab	73
Figure 50: Energetics of the reactions through OMP1 on $\text{Ag}_{31}\text{Au}_1\text{O}_{14}\text{Cl}_2$ (001) slab.....	74
Figure 51: Energetics of the reactions through OMP2 on $\text{Ag}_{31}\text{Au}_1\text{O}_{14}\text{Cl}_2$ (001) slab.....	74
Figure 52: The most probable pathway on $\text{Ag}_{31}\text{Au}_1\text{O}_{14}\text{Cl}_2$ (001) slab	75
Figure 53: Energetics of direct propylene-surface interactions on $\text{Ag}_{30}\text{Au}_2\text{O}_{14}\text{Cl}_2$ (001) slab	76
Figure 54: Energetics of the reactions through OMP1 on $\text{Ag}_{30}\text{Au}_2\text{O}_{14}\text{Cl}_2$ (001) slab.....	77
Figure 55: Energetics of the reactions through OMP2 on $\text{Ag}_{30}\text{Au}_2\text{O}_{14}\text{Cl}_2$ (001) slab.....	78
Figure 56: The most probable pathway on $\text{Ag}_{30}\text{Au}_2\text{O}_{14}\text{Cl}_2$ (001) slab	79

CHAPTER 1

INTRODUCTION

Propylene oxide (PO, $\text{CH}_3\text{-CH}(\text{O})\text{-CH}_2$) is an important product in chemical industry and mainly used as a building block to produce high variety of products. PO is a colorless and highly volatile liquid and very reactive. Due to its high reactivity, PO is an important intermediate and used in textile, furniture, food, cosmetic, pharmaceutical, automotive, aviation and maritime industries to produce thousands of everyday products. According to 2015 data, global production capacity of PO reaches 22 billion pounds. [1–6]

Propylene oxide is one of the top 50 chemicals produced in the world and approximately 10% of the propylene produced is used for the production of propylene oxide [7,8]. However, traditional chlorohydrin and hydroperoxide processes to produce PO are either energy intensive, environmental unfriendly or not economic [9–12]. In recent years, some new technologies, namely hydrogen peroxide based PO (HPPO) and cumene PO, are introduced but these methods still have additional feed requirements or some by-products to process. Due to limitations of these conventional processes, direct gas phase epoxidation of propylene to propylene oxide by molecular oxygen, which is also the subject of this thesis, has received considerable attention as a cheaper and cleaner chemical process [13–16]. In the following sections of this chapter conventional PO production processes mentioned above are explained.

Moreover, information about catalysis phenomena and density functional theory is also given in this chapter to prepare readers to the recent finding in the literature and this study.

1.1. Industrial PO Production Processes

Currently, PO can be produced economically in only world-scale plants with capacities above 100,000 tons/year [1]. Table 1 shows the shares of the conventional production methods used to produce propylene oxide according to data of 2010. According to Table 1 the oldest PO production method, namely chlorohydrin process, still has the biggest share in the PO market. Details of the industrial production methods of PO are explained below.

Table 1: Distribution of world propylene oxide capacity by technology [6]

Production Technology	Percentage
Hydrogen Peroxide Based Propylene Oxide Process	4%
Cumene Hydroperoxide Process	5%
Hydroperoxide Processes PO/TBA	15%
Hydroperoxide Processes PO/SM	33%
Chlorohydrin Process	43%

1.1.1. Chlorohydrin Process

The chlorohydrin method, the most traditional method, is a multi-step process to produce PO with alkali salt byproduct. This method is a moderate temperature reaction in an aqueous solution and requires 1.4 tons of chlorine, one ton of calcium hydroxide and several tens of tons water for one ton of PO. Approximately two tons of calcium chloride is also produced as a byproduct with each ton of PO. The chemistry of this process is given in Figure 1. In order to provide chlorine, facility should be integrated with a large caustic soda/chlorine plant. Due to the high energy requirement, electricity

supply and prices influence the production costs. Also the amount of waste water with alkali salt content causes environmental problems [17,18].

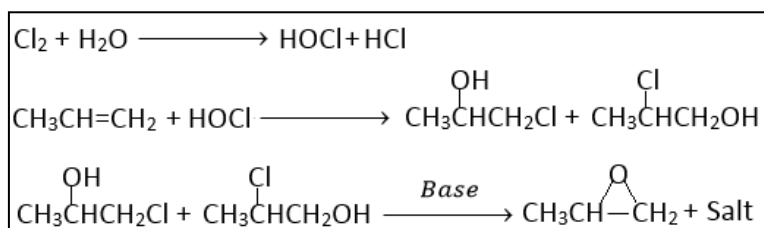


Figure 1: Steps of chlorohydrin process [17]

1.1.2. Hydroperoxide Processes

a. Hydroperoxide Process with Styrene Co-Product (PO/SM)

The process uses the ethylbenzene hydroperoxide intermediate produced by the liquid phase oxidation of ethyl benzene with air. This hydroperoxide is reacted with propylene in the presence of a catalyst solution to form α -methylbenzyl alcohol and propylene oxide. Obtained alcohol is dehydrated to styrene in a catalytic reaction. Chemistry of this process is given in Figure 2. At the end of this process approximately 2.5 tons of styrene is produced for every ton of PO. Storage of co-product, additional requirements for dehydration step and market conditions of co-product directly affect economy of the process [2,17,18].

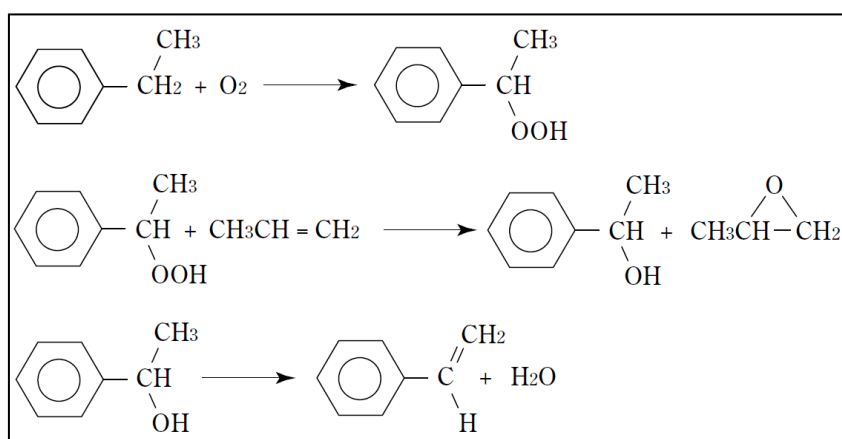


Figure 2: Steps of PO/SM Process [9]

b. Hydroperoxide Process with Tert-Butanol Co-Product (PO/TBA)

This process uses the tert-butyl hydroperoxide intermediate produced by the liquid phase oxidation of isobutane with air. Produced tert-butyl hydroperoxide reacts with propylene in the presence of a catalyst solution to form propylene oxide and tert-butyl alcohol as co-product. Chemistry of this process is given in Figure 3. At the end of this process approximately 2.1 tons of tert-butyl alcohol is produced for every ton of PO. This process also suffers from the same problems with styrene co-product process [2,17,18].

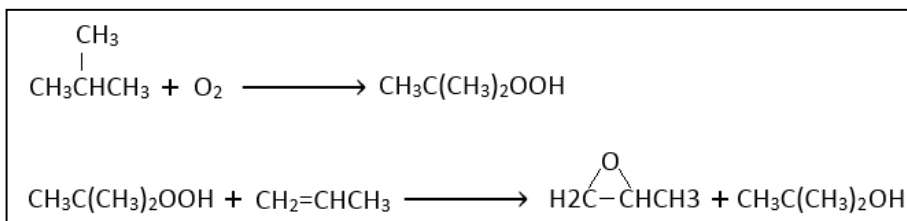


Figure 3: Steps of PO/TBA Process [2]

1.1.3. Hydrogen Peroxide Based Propylene Oxide Process (HPPO)

HPPO process uses hydrogen peroxide to produce propylene oxide from propylene in liquid phase in the presence of catalyst. Hydrogen peroxide can be either fed directly or produced by introducing H₂ and O₂ feed to the system. In this method presence of water in the system can result in product loss due to the reactions of propylene oxide and water [1,17]. Chemistry of this process is given in Figure 4. Production cost of hydrogen peroxide and hazard potential of presence of concentrated hydrogen peroxide solutions are the main disadvantages of this method.

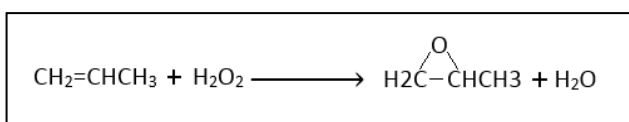


Figure 4: Reaction for HPPO Process [2]

1.1.4. Cumene Hydroperoxide Process

In cumene hydroperoxide process, cumene hydroperoxide is obtained by the auto-oxidation of cumene by oxygen without catalyst presence. Then, cumene hydroperoxide and propylene react in the presence of catalyst to produce propylene oxide and dimethyl benzyl alcohol. After separation processes, dimethyl benzyl alcohol reacts with hydrogen to reproduce cumene. This final hydrogenation step is followed by additional separation processes before recycling of cumene. Requirement of additional separation and reactions steps for cumene recycle affect the economy of this production method [17,18]. Chemistry of this process is given in Figure 5.

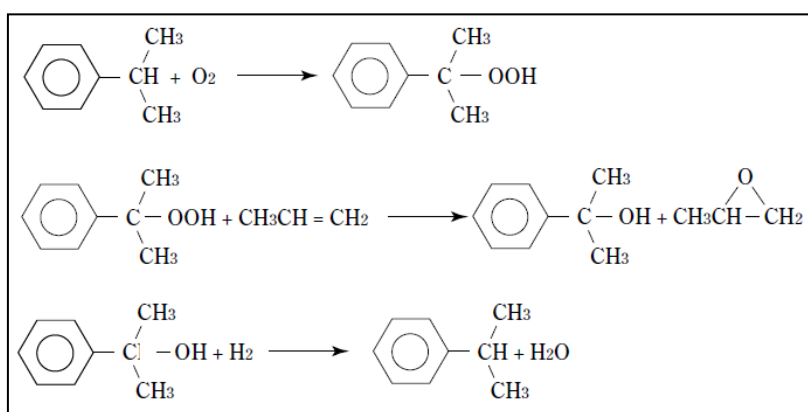


Figure 5: Steps of Cumene Hydroperoxide Process [18]

1.2. Catalysis

Catalysis can be named as one of the most important technologies of our time. Like in the epoxidation of propylene to propylene oxide, catalysis is used for more than 80% of the industrial processes involving chemical conversions [19–22]. Use of catalyst is essential for the petroleum and chemical industry to enhance the selectivity and the reaction rate towards the target products. Industrial catalysts enable the customers to have high quality products like fuels, foods, tools, fertilizers, drugs and clothes with reasonable prices [23]. Catalysts are not only used for the synthesis processes. Catalysts are used in the fuel cells and batteries as electrodes. In order to protect our environment, catalysts are used in the waste treatment and conversion of the pollutants into harmless products. Most importantly, catalysts (enzymes) are important agents in

human bodies for the biological processes to maintain vital functions. Therefore, catalytic activities are important processes affecting our daily life [22–25]. According to the market report for the global catalyst market published in 2015, average investment in catalysts was 2% of total investment in chemical processes in 2014. According to same report, the global demand on the catalyst materials was higher than 33.5 billion dollars [26].

Even though catalyst materials have been used by humankind to make bread, cheese and alcoholic beverages for over thousands of years, “catalysis” term is first mentioned in 1835 by Berzelius [19,27]. Berzelius combined the findings of previous researchers and stated that the presence of some substances is affecting the course of chemical reactions without being consumed. He called this unknown internal force exerted by these substances as “Catalytic Force” and called the process caused by this force as “Catalysis”. According to the definition of Berzelius, catalytic force is related with the electrochemical affinity of the material and a material with catalytic force has the ability to awaken the affinities of the reactants by just its presence in the reaction medium [28,29].

At the end of 19th century, Ostwald expanded the Berzelius’s definition of the catalyst. According to Ostwald’s definition, catalysts increase the rate of a reaction without being consumed and without affecting the equilibrium thermodynamics between the reactants and the products. Therefore, a catalyst cannot turn a thermodynamically unfeasible reaction into a feasible reaction [19,21,28]. Consequently, the target reaction could take place without catalyst even if it takes thousand years to reach its equilibrium. Formation of water from hydrogen and oxygen molecules can be given as a perfect example for this condition. Formation of water from hydrogen and oxygen is a thermodynamically feasible, exothermic reaction. However, without the presence of any catalytic material, hydrogen and oxygen atoms seem to have no affinity towards each other at room temperature. On the other hand, the introduction of platinum to the reaction medium lead to rapid water formation reaction [22,27]. Catalysis only affects the kinetics of the reaction and changes the activation energy term in the Arrhenius

equation. Catalysis decreases the energy barrier between the reactants and the products by providing a less energetic pathway [21,23,27,30].

1.2.1. Catalysis Cycle and Sabatier's Principle

As the definition of catalysis states, the catalyst should be unaltered at the end of the process. Boudart defines catalysis as repeated and sustained cyclic series of elementary reactions. During catalysis, reactants adsorb on the catalyst surface and form intermediate reaction complexes. Then, these active complexes react to generate the products on the catalyst surface. Finally, end products desorb from the catalyst surface by regenerating the catalyst surface to its original form. This process is called as “cycle of catalysis” or “catalysis cycle”. The strength of the interactions between the catalyst and reactants and the interaction between the catalyst and the products are important for the performance of the catalyst. Catalyst-reactant interaction should be strong enough to form unstable surface intermediates. Weak interaction between the catalyst and the reactants cannot form activated surface intermediates. On the other hand, too strong catalyst reactant interaction causes stable surface complexes that cannot be involved in the reaction. Therefore, surface intermediates should have an intermediate bond strength with the catalyst surface. Similarly, products obtained after the surface reaction should not bond to the surface strongly. Hence a good catalyst should have optimum interaction energy. This concept is known as “Sabatier's Catalysis Law” or “Sabatier's Principle” [19–22,25].

1.2.2. Types of Catalysts

Catalyst materials can be classified in various ways. Dividing the catalyst types into heterogeneous, homogeneous and biological catalyst is the most common and easiest way of the classification [24,25,31,32].

a. Heterogeneous Catalysis

Heterogeneous catalyst is present in a different phase than the phase of reactants and products. Generally heterogeneous catalyst are solid particles used to accelerate gas or liquid phase reactions. Therefore, heterogeneous catalysis is sometimes mentioned as

surface catalysis. Being in a separate phase from the reaction mixture, heterogeneous catalysts have an advantage over the homogeneous catalysts which has costly separation procedures. Therefore, using heterogeneous catalysts in the continuous processes is easier than using homogeneous catalysts. Over 80% of the catalytic process in the chemical industry and 90% of the reactions in the petroleum industry uses heterogeneous catalysis. Bulk or supported metals, supported inorganic metal complexes, supported organometallic complexes, metal oxides and sulfides can be listed as the most general kinds of the heterogeneous catalysts [20–22,25,32,33].

b. Homogeneous Catalysis

Homogeneous catalyst is present in the same phase with the reaction mixture either in liquid or gas phase. Because of the presence of catalyst and the reaction mixture in the same phase, separation of homogeneous catalyst is harder than the separation of the heterogeneous catalyst from the products. Therefore batch-type processes are generally used for the homogeneous catalysis.

Homogeneous catalysts are generally used in the production of pharmaceuticals, fine chemicals and agrochemicals with highly selective reactions requiring less purification steps. Homogeneous catalysts are organometallic complexes which are metals chelated with organic ligands [23,25,32,34].

c. Biological Catalysis

Biological catalysis can be defined as special branch of heterogeneous catalysis dealing with enzymes and microorganisms. As all living organisms, our bodies use enzymes to sustain biological activities. Biocatalysts (enzymes) have limited temperature and pressure ranges. Industrial use of biological catalysts requires significant purification operations. Biocatalysts are used in the production of fine chemicals, pharmaceuticals and foods [24,25,31]

1.3. Computational Chemistry and Density Functional Theory

Theoretical chemistry can be considered as the translation of chemistry to the mathematics and formulates new methods to mathematical description of chemistry. On the other hand, computational (quantum) chemistry takes the well-defined expressions of theoretical chemistry that can be automated for the computer application and use them to solve chemical problems [35,36]. Computational chemistry is an important tool enabling calculation of the spectroscopic properties of the model systems to analyze spectra and to designate chemical intermediates. Furthermore, computational chemistry allows the calculation of the energies of atoms/molecules to compare the relative stability of the different atomic/molecular arrangements and helps scientist to predict reaction pathways [37,38]. Quantum chemical methods can be classified as ab-initio, semi-empirical, density functional, molecular mechanics, molecular dynamics and Monte Carlo simulation methods [39,40]. This chapter only focuses on the density functional methods.

1.3.1. Density Functional Theory

The origins of the density functional theory (DFT) goes back to late 1920s. However, publications of Hohenberg and Kohn in 1964 and Kohn and Sham in 1965 are considered as the beginning of modern DFT. After 1990s, DFT has become one of the most popular methods in computational chemistry applications [41,42]. In 1998 Walter Kohn was awarded by Nobel Prize in Chemistry for “for his development of the density-functional theory” with John A. Pople “for his development of computational methods in quantum chemistry” [39,43,44]. DFT’s high accuracy without compromising computational time, its applicability over many different systems including metals and metal oxides combined with the very fast developing computer technology and has resulted in DFT to become a standard research tool for many areas [39,42,45,46]. According to Figure 6 generated from the data of Web of Science database, number of DFT papers published in 1988 (the year Kohn was awarded with a Nobel Prize) was around 1800 and the total number of DFT papers

until that day have reached to 7700. After 2015, annual DFT publications were reported around 13100 and total DFT publications exceeded 130000 publications [47].

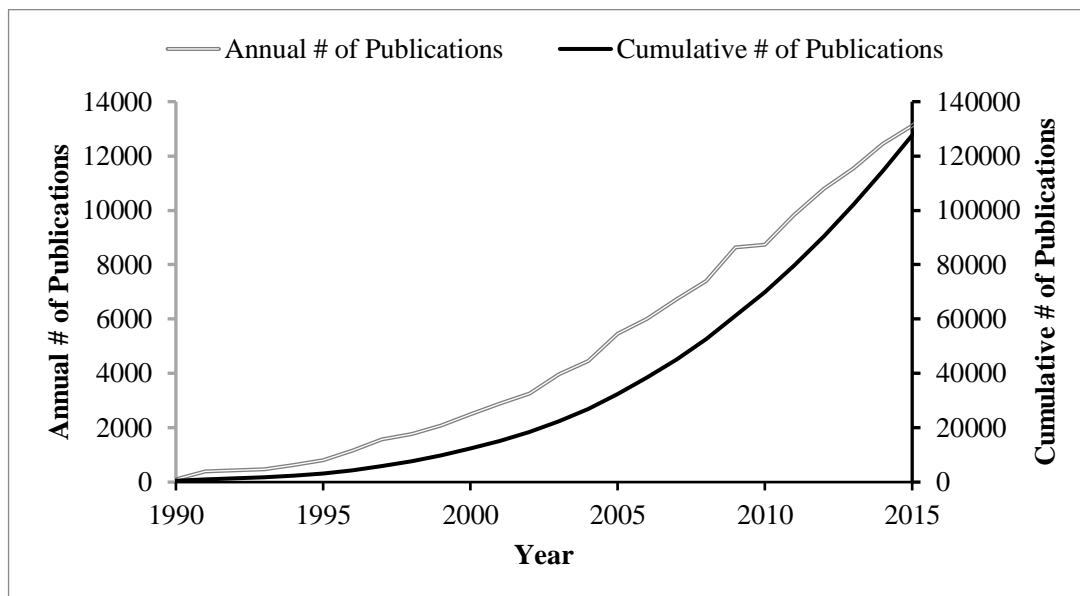


Figure 6: Trend of DFT publications over years [47]

1.3.2. Formulation of Density Functional Theory

Density functional theory uses electron density (a physical observable property of the material) to define the properties of the molecules whereas classical quantum mechanical methods are using wavefunction to solve Schrödinger equation. DFT defines energy of the molecule as a function of electron density which is also a function of x , y and z coordinates of the electrons of the molecule. According to assumption of Thomas and Fermi, electrons are uniformly dispersed in the six-dimensional space and properties of the molecule can be found from the information gained from electrons. Modern DFT depends on the works of Hohenberg-Kohn and Kohn-Sham which were developments on top of the basic definition of the Thomas and Fermi. Hohenberg and Kohn proved in their first theorem that “*The ground-state energy from Schrödinger’s equation is a unique functional of the electron density*” [48]. Then, in their second theorem, they stated that “*The electron density that minimizes the energy of the overall functional is the true electron density*”

corresponding to the full solution of the Schrödinger equation” [48]. According to these definitions, equations to solve Schrödinger equation with electron density were formulated by Kohn and Sham.

Like standard quantum chemical (wavefunction) methods, Schrödinger equation for N electrons and M nuclei given in Eqn.1 is also the starting point of the Kohn-Sham formulation.

$$\hat{H}\Psi = E\Psi \quad \text{Eqn.1}$$

In this equation Ψ represents the wavefunction and \hat{H} represents the Hamiltonian operator and E represents the energy.

Wavefunction is a function position vectors (\vec{r}_N) of the N electrons and can be expressed as shown in Eqn.2.

$$\Psi = \Psi(\vec{r}_1, \vec{r}_2, \vec{r}_3, \dots, \vec{r}_N) \quad \text{Eqn.2}$$

Hamiltonian operator of the Schrödinger equation can be separated into its components as shown in Eqn.3 as external potential, \hat{v}_{ext} (Eqn.4), kinetic energy, \hat{T} (Eqn.5) and electron-electron repulsion, \hat{V}_{ee} (Eqn.6), operators.

$$\hat{H} = \hat{v}_{ext} + \hat{T} + \hat{V}_{ee} \quad \text{Eqn.3}$$

According to Born-Oppenheimer approximation, the nuclei are assumed as stationary and are not included in the kinetic energy calculation. Therefore, kinetic energy operator, \hat{T} , only has electronic terms and nuclei only generate an external potential field [49,50].

$$\hat{v}_{ext} = -\sum_{i=1}^N \sum_{A=1}^M \frac{Z_A}{|\vec{R}_A - \vec{r}_i|} \quad \text{Eqn.4}$$

$$\hat{T} = -\frac{1}{2} \sum_{i=1}^N \nabla_i^2 \quad \text{Eqn.5}$$

$$\hat{V}_{ee} = \sum_j^N \sum_{i<j}^N \frac{1}{r_{ij}} \quad \text{Eqn.6}$$

where \vec{R} represents position vector of the nuclei and \vec{r} represents position vector of the electron.

Density functional theory modifies Schrödinger equation to be solved via electron density given in Eqn.7 instead of N-electron wavefunction.

$$\rho(\vec{r}) = N \langle \Psi | \delta(\vec{r} - \vec{r}_i) | \Psi \rangle \quad \text{Eqn.7}$$

Electron density can be expressed for the singular expectation values at any point in the Cartesian space as:

$$\rho(\vec{r}_1) = N \int d\vec{r}_2 d\vec{r}_3 \dots d\vec{r}_N |\Psi(\vec{r}_1, \vec{r}_2, \vec{r}_3, \dots, \vec{r}_N)|^2 \quad \text{Eqn.8}$$

By using electron density, solution of Schrödinger equation for energy becomes:

$$E = \langle \Psi | \hat{H} | \Psi \rangle = \int v_{ext}(\vec{r}) \rho(\vec{r}) d\vec{r} + \langle \Psi | \hat{T} + \hat{V}_{ee} | \Psi \rangle \quad \text{Eqn.9}$$

Eqn.9 shows that the energy is the functional of electronic density for a given external potential v and can be expressed as:

$$E = E_v[\rho] \quad \text{Eqn.10}$$

\hat{T} and \hat{V}_{ee} operators are independent from the external function. Therefore, Hohenberg and Kohn express the second term of Eqn.9 as a universal operator (Eqn.11) which is identical for every system.

$$F[\rho] = \langle \Psi | \hat{T} + \hat{V}_{ee} | \Psi \rangle \quad \text{Eqn.11}$$

Then energy equation becomes:

$$E = E_v[\rho] = \int v(\vec{r}) \rho(\vec{r}) d\vec{r} + F[\rho] \quad \text{Eqn.12}$$

Additional to this energy equation, Hohenberg and Kohn states that for any trivial electron density, ρ^t , $E_v[\rho]$ value calculated via Eqn.12 defines the upper limit of the exact ground state energy.

$$E \leq E_v[\rho^t] \quad \text{Eqn.13}$$

Hohenberg Kohn theorem and their derivation makes preliminary definition for the solution of energy in terms of external potential, electron density and the universal functional. Nevertheless, they do not explain the formulation of the universal functional nor the solution of the energy equation. At this point, Kohn-Sham procedure helps to find universal functional $F[\rho]$ and to solve Schrödinger equation [50].

Kohn-Sham procedure starts with the assumption of a new Hamiltonian operator. In this operator, external potential, v_λ , always gives the electron density, $\rho(r)$, of the real system according to Hohenberg-Kohn theorem.

$$\hat{H}_\lambda = \hat{T} + v_\lambda + \lambda V_{ee} \quad \text{Eqn.14}$$

By using new Hamiltonian operator, Schrödinger equation becomes:

$$\hat{H}_\lambda \Psi_\lambda = E_\lambda \Psi_\lambda \quad \text{Eqn.15}$$

Value (either 0 or 1) of λ in the new Hamiltonian operator and the Schrödinger equation express the reality (or ideality) of the system. $\lambda = 0$ represents the ideal system of non-interacting electrons and $\lambda = 1$ represents the real system with v_{ext} .

In terms of Kohn-Sham formalism, Eqn.12 becomes:

$$E_\lambda = \langle \Psi_\lambda | \hat{H}_\lambda | \Psi_\lambda \rangle = \int v_\lambda(\vec{r}) \rho(\vec{r}) d\vec{r} + \langle \Psi_\lambda | \hat{T} + \lambda V_{ee} | \Psi_\lambda \rangle \quad \text{Eqn.16}$$

After further processing of Eqn.16 with respect to λ , solution gives the difference of the energies of the real, E , and the noninteracting, E_S , systems. In the next step, Eqn.16 yields a new equation, Eqn.17, which is still not solvable due to the integral over λ .

$$E[\rho] = \int v_{ext}(\vec{r}) \rho(\vec{r}) d\vec{r} + T_s + \int_0^1 \langle \Psi_\lambda | V_{ee} | \Psi_\lambda \rangle d\lambda \quad \text{Eqn.17}$$

In order to simplify Eqn.17 further, Kohn and Sham defines the integral with respect to λ as the sum of classical electron-electron energy, $V_{classical}$, and exchange-correlation energy, E_{xc} .

$$\int_0^1 \langle \Psi_\lambda | V_{ee} | \Psi_\lambda \rangle d\lambda = \frac{1}{2} \int \int d\vec{r}_1 d\vec{r}_2 \frac{\rho(\vec{r}_1)\rho(\vec{r}_2)}{|\vec{r}_1 - \vec{r}_2|} + E_{xc}[\rho] = V_{classical}[\rho] + E_{xc}[\rho]$$

Eqn.18

If the new definition is inserted into Eqn.17, total energy equation can be written as:

$$E[\rho] = \int v_{ext}(\vec{r}) \rho(\vec{r}) d\vec{r} + T_s + V_{classical}[\rho] + E_{xc}[\rho]$$

Eqn.19

Derivation steps and Eqn.19 do not depend on any approximations and directly comes from Schrödinger equation. Moreover, all the functions and functionals are known apart from the exchange correlation functional. Total energy can be minimized from Eqn.19 for the electron density. This minimization yields Kohn-Sham equation (Eqn.20). Eqn.20 can be seen as a modified version of Schrödinger equation using Kohn-Sham orbitals, φ_i , instead of wavefunction Ψ [50].

$$\left[-\frac{1}{2} \nabla^2 + v_{ext} + v_{classical} + v_{xc} \right] \varphi_i = \varepsilon_i \varphi_i$$

Eqn.20

where

$$v_{classical}(\vec{r}) = \int d\vec{r}' \frac{\rho(\vec{r}')}{|\vec{r} - \vec{r}'|}$$

Eqn.21

$$v_{xc}(\vec{r}) = \frac{\delta E_{xc}[\rho(\vec{r})]}{\delta \rho(\vec{r})}$$

Eqn.22

Kohn-Sham approach depends on the self-consistent calculation of the molecular energy as a summation of known terms with a relatively small exchange correlation functional. Method assumes that even large errors in the approximations for exchange correlation should not cause large errors in the calculation of total energy [39].

1.3.3. Approximations of Density Functional Theory

As it is mentioned in the previous section, exchange correlation of the Kohn-Sham equation is an unknown property which is making the equation unsolvable. In order to handle this problem, different approximations have been developed to find exchange correlation energy. Most common exchange correlation approximations can be classified as local density approximations (LDA), generalized gradient approximations (GGA) and hybrid approximations [35,42,50,51].

a. Local Density Approximation

Local density approximation can be considered as the simplest approximation to find exchange correlation energy. Method assumes that the electron density is uniform throughout the molecule. According to this assumption exchange correlation energy can be formulated with Eqn.23. ϵ_{xc}^{LDA} term in the equation represents the exchange correlation energy distribution per unit volume at the location of the sampled electron density. LDA generally gives reasonably good results for band structure calculations. However, for the determination of the geometries and prediction of the binding energies, LDA is known to yield less accurate results than the other methods [35,42,50].

$$E_{xc}^{LDA} = \int \epsilon_{xc}^{LDA} [\rho(\vec{r})] \rho(\vec{r}) d\vec{r} \quad \text{Eqn.23}$$

b. Generalized Gradient Approximation

Generalized gradient approximation uses electron density and its gradients to calculate exchange correlation energy by considering the system as a non-uniform electron gas. Alongside with electron density, method uses derivatives of the electron density to make corrections according to changes in the density and can be formulated as Eqn.24. GGA approximation improves the accuracy of the results for the estimation of bond energies and bond distances. GGA is known to give successful results with the systems containing metals and oxides [35,42,50,51]. Therefore, GGA is used in this study.

$$E_{xc}^{GGA}[\rho] = \int d\vec{r} \epsilon_{xc}[\rho, |\nabla\rho|, \nabla^2\rho] \quad \text{Eqn.24}$$

c. Hybrid Approximations

Hybrid methods combine the approximations of DFT and Hartree-Fock methods to find the exchange correlation energy and generally use electron density, its derivatives and its laplacians for the computations. B3LYP can be named as one of the most popular functional derived with hybrid approximations. Hybrid methods generally gives the very accurate results, with some exceptions, for the determination of geometries, total energies and bond lengths [42,52–54].

CHAPTER 2

HISTORY OF PROPYLENE EPOXIDATION RESEARCH

Due to economic and environmental issues of conventional production techniques, alternative propylene oxide production methods and enhancements to the present techniques are highly desirable. There is a considerable amount of work in the literature on propylene epoxidation to fulfill this aim, among them photocatalytic processes, usage of alternative oxygen sources with environmental friendly byproducts and direct propylene epoxidation on the silver based catalyst are the most popular directions. This chapter gives information about the research efforts mentioned above, but mainly focuses on the direct propylene epoxidation studies with silver-based catalyst.

2.1. Photocatalyst Studies

Photocatalytic epoxidation of propylene by the molecular oxygen is mentioned as one of the most environmentally friendly methods to produce propylene oxide [55]. Yoshida and coworkers screened 50 different metal oxides supported with silica for their PO activity under photooxidation. They found that TiO_x and ZnO_x supported on SiO_2 can produce PO effectively. Yoshida reported PO selectivity up to 33% with 24% propylene conversion as their best trial [56]. Since the photo-epoxidation study by Pichat and coworkers on TiO_2 and ZnO structures reports very low PO selectivity and selective complete oxidation to CO_2 in their early work, Yoshida et al. emphasized the importance of the silica matrix for the photo-epoxidation of propylene with molecular

oxygen [56,57]. Zhao and Wachs reported the selectivity of photocatalytic epoxidation of propylene to PO on V_2O_5 on FSM-16 as 40% by stating that the process has high conversion [58]. Nguyen and coworkers evaluated the performances of SiO_2 , TiO_2 , V-Ti/MCM-41, V_2O_5/SiO_2 , Au/TiO_2 and TS-1 catalysts for the photocatalytic epoxidation of propylene and reached 47% PO selectivity by using Ti and V catalyst loaded on MCM-41 under UVA irradiation of 0.2 mW/cm^2 . Nguyen et al. stated that propylene mainly forms propylene oxide, acetone and propanal when it interacts with atomic oxyradicals on the surface [55]. In 2013 Marimuthu and coworkers came up with a different usage of photo-excitation for propylene epoxidation. They used photo-excitation to alter the oxidation state of Cu catalyst to sustain metallic form which is found as a selective catalyst for propylene epoxidation under vacuum conditions. In commercial production conditions, Cu is easily oxidized to Cu_2O and CuO which have nearly zero activity for propylene oxide. Cu_2O gives high selectivity for acrolein and CuO leads to complete combustion [59]. Marimuthu et al. used the photo-excitation to weaken Cu-O bond strength for switching oxidation state and achieved ~20% to ~50% propylene oxide selectivity under visible light illumination [60].

2.2. Alternative Oxygen Source Studies

As it is mentioned in the introduction chapter, byproducts of the conventional industrial PO production methods cause either economic or environmental problems. Therefore, instead of using conventional hydroperoxides, usage of N_2O and H_2O_2 as oxygen sources for epoxidation are investigated by many research groups. N_2 and H_2O are the only side products of the N_2O and H_2O_2 usage respectively. Chimentao and coworkers studied propylene epoxidation by N_2O over $Au-Cu/TiO_2$ catalyst and observed 40% propylene conversion yielding >70% propanal selectivity alongside with acetone, acrolein and CO_2 . They claimed that the propanal formation is the result of the PO isomerization [61]. Horvath and coworkers found that nano-sized MoO_2 particles with a diameter smaller than 10nm give a promising performance for propylene epoxidation with N_2O . They state that monoclinic MoO_2 nanoparticles with a diameter less than 10 nm gives PO selectivity around 40%. In their work, the importance of size selectivity of the catalyst is emphasized [62]. Moens and coworkers

also used N_2O for the epoxidation of propylene to PO. According to their study, Rb_2SO_4 -modified iron oxide on silica gives PO selectivity around 90%. However, they stated that the catalyst lifetime is limited and there is coke formation [63]. Duma and Hönigke used sodium-promoted iron oxide catalyst supported with silica and reported propylene oxide selectivity up to 60% and propylene conversion up to 12% by using N_2O as oxidant [64]. Zhang and coworkers tested Fe-MFI and Fe-MCM-41 catalysts with N_2O as oxidant and found the allylic oxidation products at the end of the reaction. They reported that after the after the modifications of the catalysts with KCl, PO formation became favorable with selectivity around 80% and propylene conversion of 3% [65]. Nijhuis mentioned that potassium promoted iron oxide catalyst with SBA-15 support can reach 80% PO selectivity with 5% propylene conversion [7]. In summary, according to the results of these researchers mentioned above, N_2O can be a good oxidant for the propylene epoxidation. However, commercial availability of N_2O is limited. If the propylene epoxidation methods using N_2O can be further developed to fulfill the industrial needs, additional investment to produce N_2O will also be required [7].

In 1990s hydrogen peroxide usage as oxidant for the propylene epoxidation on titanium silicate-1 (TS-1) catalyst was proposed and very high selectivity over 90% was achieved. However, the comparable market prices of hydrogen peroxide and propylene oxide and issues caused by the constant supply requirement and the transportation of concentrated hydrogen peroxide channeled the research effort to the in-situ production of hydrogen peroxide with hydrogen and oxygen co-feed [7,66–68]. Hölderich and coworkers used Pd supported on TS-1 catalyst in the liquid phase slurry reactor using methanol/water mixture as the slurry liquid. Propylene epoxidation on this system is tested by using H_2O_2 and O_2+H_2 mixtures and led 21.3% and 5.3% PO yield respectively. According to these result, they concluded that the rate determining step of the propylene epoxidation by O_2/H_2 co-feed is the in-situ H_2O_2 formation [69,70]. Haruta et al. observed 90% PO selectivity and 2% propylene conversion in gas phase reaction on Au- TiO_2 surface by using feed gas mixture including propylene, oxygen and hydrogen. It is emphasized that the products are strongly related to the

size of gold particles deposited on TiO₂. Gold nanoparticles larger than 2 nm produce PO however, smaller gold particles produce propane, and gold particles larger than 5nm results combustion [71]. Haruta et al. mentioned two different hypotheses for the duty of the gold particles during the epoxidation reaction. The first hypothesis assumes that gold nanoparticles located in the pores of titanium oxide structure are responsible from the epoxidation of propylene to propylene oxide whereas the second hypothesis assumes that the gold nanoparticles with diameters between 2 nm and 5 nm, and dispersed on the titanium oxide (or titanium silicate for TS-1 case), are responsible from the oxidization of the hydrogen to hydrogen peroxide [72]. Although low propylene conversion was reported, the discovery of Haruta led further studies on the usage of Au catalyst on TiO₂ and TS-1 support with hydrogen co-feed. Taylor and coworkers found similar results with the Haruta's works. They suggested that reaction proceeds through H₂O₂ formation on the Au site and activation of H₂O₂ on Ti site resulting PO formation like Haruta et al. proposed. However, Taylor's mechanism proposes that the formation and the usage of H₂O₂ should be simultaneous rather than sequential as Haruta suggested [73,74]. Nijhuis and coworkers used TS-1 loaded with dispersed gold and TiO₂ dispersed on SiO₂. Propylene epoxidation reaction on this catalyst with propylene, oxygen and hydrogen feed gas achieved 99% PO selectivity, however, propylene conversion was reported as 2%. Nijhuis explained the low propylene conversion by the strong adsorption of propylene oxide to the catalyst surface. They also proposed a mechanism slightly different than the mechanism Haruta proposed before. According to this new proposal, hydrogen and oxygen react on the gold site of the catalyst to produce "hydrogen peroxide like" compound. Then, this compound reacts with propylene on the titanium site to produce propylene oxide [7,67,75]. Wang and coworkers tested Ag/TS-1 catalyst with different Ag loading by using propylene, oxygen, hydrogen and nitrogen mixture. They reported 91.2 % PO selectivity and 0.9% propylene conversion for catalyst with 2% Ag loading. They also claimed that higher conversions could be reached with the use of H₂O₂ instead of H₂/O₂ mixture [76]. Guo and coworkers also studied the Ag/TS-1 catalyst by following different synthesis methods. They reported 57.9% PO selectivity and 0.5% propylene conversion for the catalyst prepared by impregnation. They also synthesized

the Ag/TS-1 catalyst by using K_2CO_3 and Cs_2CO_3 as precipitating agents. Propylene oxide selectivities of 84.1% and 85.4% were reported with 1.3% and 1.1% propylene conversion respectively for catalysts prepared by K_2CO_3 and Cs_2CO_3 methods. Guo emphasized that the new synthesis routes also improved the stability of the catalyst [77]. As a summary, using gold-titania systems with O_2/H_2 feed gained attention due to high propylene oxide selectivity, however low propylene conversion, low hydrogen efficiency and catalyst stability are still important problems of this propylene oxide production technique [78,79].

2.3. Direct Epoxidation Studies

Direct partial oxidation of propylene to propylene oxide by molecular oxygen has received a considerable attention from the researchers [10]. The process aims to produce propylene oxide from the gas phase reaction of propylene and molecular oxygen, which is the cheapest oxidant, without side products. Hence, the process does not suffer from the environmental issues and the economic drawbacks of additional feeds and side/co-products. However, no industrial-scale process using molecular oxygen for the direct partial epoxidation of propylene is achieved yet and no catalyst is not reported with both high conversion and selectivity toward propylene oxide either. Therefore, PO from propylene and molecular oxygen is still one of the most challenging goals of catalysis [9,10,12,75,80,81].

Silver catalyst has been used in nearly all ethylene oxide production plants built after the 1940s. Ethylene oxide selectivity is higher than 90% in these plants and the ethylene conversion is kept limited to prevent combustion of ethylene to CO_2 because of the heat released from the exothermic epoxidation reaction [7]. Due to its important achievement in ethylene epoxidation, silver is one of the most studied catalysts for propylene epoxidation. In early publications, propylene oxide selectivity and propylene conversion on the unpromoted silver catalyst was reported lower than 15% and 10% respectively [7,80–84]. There is an extensive effort for the utilization of silver catalyst for propylene epoxidation, however, propylene conversion and propylene oxide selectivity is still lower than the requirements of industrial production [85].

Current research on the silver catalyst basically focuses on promoter and size effects. There is also a limited amount of studies for the detection of the reaction mechanism on the metallic silver surfaces and silver surfaces with low oxygen coverages. However, there is no consensus on the results of the mechanism studies and further studies are needed for the clarification.

Zemichael and coworkers used K promoted silver catalyst and observed only PO, CO₂ and water during their experiments. Silver catalyst with 1.7% K content is reported to give 6% propylene conversion and 15.2% PO selectivity. According to Zemichael et al., the unpromoted silver catalyst gives the lowest conversion and catalysts with higher K content result lower selectivity and conversion than the catalyst with 1.7% K loading. Effect of the K loading on conversion and selectivity was explained by the change in the size distribution of Ag particles. It is stated that Ag catalyst with 1.7% K loading has 20-40nm sized Ag particles which are active for epoxidation, whereas bigger and smaller particles are less selective towards epoxidation [86]. Takahashi and coworkers modified Ag based catalyst with Mn, Fe, Ni and Co metals. They reported that the Ni & Ag catalyst with 1/2 atomic Ni/Ag ratio results in the highest PO selectivity, which is 11.8% at 170 °C, among their catalysts. Takahashi explained that the Ni addition increases the dispersion of the Ag catalyst and controls the size of the Ag particles. In this manner, Takahashi et al. emphasized that the epoxidation performance of silver catalyst depends on the size of silver particles like Zemichael et al. mentioned previously [83]. Zheng et al. reported 55.1% PO selectivity and 3.6% propylene conversion on Ag₉₅-Cu₅ catalyst with BaCO₃ support by stating that Cu is helping the adsorption of active oxygen species to Ag sites [87]. Zhang and coworkers used Ag catalyst with BaCO₃ support pretreated with ethylene diamine. 12.5% propylene conversion with 36.9% PO selectivity in this study. They emphasized the diversity of the proposals about the mechanisms and size/structure sensitivity of the Ag based catalyst for the epoxidation reaction and proposed that the gas phase propylene should react with the adsorbed molecular oxygen by following Eley-Rideal type mechanism to produce PO on Ag/BaCO₃ catalyst [15]. Lee and coworkers run catalytic tests on Ag/ZrO₂ and Ag/ZrO₂ with Mo and W promoters. 13% propylene

conversion and 60% PO selectivity was reported for $\text{Ag}_{95}\text{Mo}_{3.75}\text{W}_{1.25}/\text{ZrO}_2$ catalyst whereas unpromoted Ag/ZrO_2 gives 48.8% propylene conversion and 2.3% PO selectivity [16]. Ghosh and coworkers loaded Ag nanoparticles on WO_3 nanorods and reported 15.5% propylene conversion with 83% PO selectivity for 4.8% Ag loading. They reported that increasing the silver loading increases the conversion but decreases the PO selectivity. They stated that silver oxide is formed with the help of the dissociation of molecular oxygen on the WO_3 nanorods and they proposed that the oxygen of the silver oxide structure is responsible from the PO formation [88].

Alloy structure of gold and silver can be prepared at any desired compositions [7]. Geenen and coworkers used this feature of silver and gold and they prepared Au-Ag alloys with high gold content up to >70% to create isolated silver sites. They tested their catalysts for ethylene and propylene epoxidation reactions and reported epoxidation activity for alloys up to 50% gold content. According to study, no ethylene oxide formation was reported, and propylene oxide formation was said to shift towards acrolein formation for the catalyst with gold content around 70% [89]. Zemichael and coworkers also tested high gold content Au/Ag alloy using electro-catalytic conditions. They reported that gold catalyst with 14% mole Ag loading has no activity towards propylene oxide [90]. The reason for no PO activity and increased selectivity towards acrolein was explained with the necessity of creating atomic oxygen at the silver site. It was stated that gold sites of the catalyst adsorb oxygen as molecular form and isolated sites cannot dissociate the di-oxygen structure. Therefore, this catalyst is advised to be tested by using N_2O [7,75,89,90]. However, no other study using gold and silver alloy is reported. Özbek theoretical studied metallic and oxide phases of Au catalyst for ethylene epoxidation alongside with Cu and Ag catalysts. For the metallic phase, gold was reported to have no activity for oxygen adsorption or dissociation. However, even Au_2O is unstable, it was reported as a selective catalyst towards ethylene oxide formation. It was also found in the study that desorption of ethylene oxide from Au_2O is much easier than that the ethylene oxide desorption from Ag_2O and Cu_2O [91].

Effect of Cl on the propylene epoxidation on the silver catalyst is studied by many research groups. Lu and coworkers studied NaCl loaded silver catalyst and reported 54% propylene conversion and 26.3% PO selectivity with 3.8% NaCl loading [92]. In another study, Lu worked on the silver catalyst loaded with 10% NaCl and achieved 31.6% PO selectivity with 12.4% propylene conversion. This time they also studied the effects of the Cl addition. According to their study, AgCl particles formed during the catalyst preparation were found inactive for epoxidation reaction. They reported that Cl addition helps propylene epoxidation by altering the electronic structure of the adsorbed oxygen species. They also emphasized that the highly oxidized Ag structure is important for the epoxidation [68]. Monnier mentioned that chlorine can be added to the reaction medium with the feed gas. According to the patent of Thorsteinson et al., a catalyst composed of 40% Ag and 1.5% K on CaCO_3 can result in 34% propylene conversion and 47% PO selectivity with the help of 200ppm $\text{C}_2\text{H}_5\text{Cl}$ addition to the feed stream [75]. Lu et al. also mentioned the work of Cooker et al. stating the use of 5 ppm EtCl, 10% CO_2 and 5ppm NO in the feed stream increased their PO selectivity to 60-64%. Propylene conversion is reported as 1.5%-2.5% for the study [92]. Jin and coworkers studied the chlorination of Ag-MoO₃/ZrO₂ catalyst in the presence of NaCl, CsCl and CaCl₂ and reported that the Cl regulates the electronic properties of the catalyst. According to their results, electron flow between Cl and oxygen inhibits the isomerization and oxidation of PO and enhances the PO selectivity of the catalyst [93]. Seubsai and coworkers proposed that the Cl addition to the silver catalyst weakens the bond strength between Ag and O and increases the activity towards epoxidation. They also mentioned that the Cl and chlorinated compounds reduce the number of available sites for oxygen adsorption, hence they decrease the catalyst activity [94]. Studies with modification generally proposed that the most important effect of Cl is to change the electronic properties of oxygen species. Özbek theoretically studied the effect of Cl on silver oxide surface for ethylene epoxidation and reported that even Cl changes the electronic properties of Ag and O, the most important effect of Cl is to block oxygen adsorption sites causing combustion [91,95]. However, no theoretical work presents for the theoretical investigation of propylene epoxidation on silver oxide surface either with or without Cl.

There are different opinions about the epoxidation mechanism and the active form of the silver catalyst for the propylene epoxidation. However, nearly all studies agree that the allylic hydrogen atoms of the methyl group are the main reason for the low PO selectivity for propylene epoxidation reaction. According to Torres, the orientation of methyl group of the propylene determines the path of the reaction. If one of the hydrogen atoms of the methyl group comes close to the surface oxygen, it leads to combustion. If carbons with double bond can reach an oxygen, they form an oxametallocycle leading PO formation [96]. The most accepted mechanism of propylene epoxidation consists of two pathways. The first pathway proceeds through allylic hydrogen abstraction from the 3rd C of propylene followed by oxygen insertion to 1st C of propylene. This path forms an allylic oxide intermediate and hydroxyl group on the surface. Further reactions of the allylic intermediate on the surface give acrolein or combustion products. The second pathway includes the activation of the double bond by the surface. This activation forms propylene oxametallocycle structures on the surface. These intermediate structures produce PO or its isomers, i.e. propanal and acetone [82,96–99]. Researchers with opposing view to this mechanism accept the PO formation pathway following surface intermediates; however, they propose that the allylic intermediate formation pathway should follow oxametallocycle formation on the catalyst surface [7,10,14,100–103]. As well as reaction mechanism, the rate determining step of the propylene epoxidation on the silver catalyst is also a matter of discussion. Khatib and Oyama mentioned in their review that there are multiple proposals for the rate determining step of the propylene epoxidation with molecular oxygen on the silver based catalyst, but it is most likely the desorption of propylene oxide according to the predictions from ethylene and butadiene cases [6].

Phase and morphology of the silver catalyst are also investigated by different research groups. Among them, the works of Lei et al. and Molina et al. presented the most notable results. Lei and coworkers experimentally and theoretically studied unpromoted Ag₃ clusters and Ag nanoparticles with ~3.5Å diameter on an alumina support. Their experiments showed high propylene oxide selectivities with the negligible CO₂ formation at low temperatures. With the help of theoretical studies,

they reported that atomic oxygen adsorbed on the silver site is responsible for propylene epoxidation whereas oxygen atom at the interface results in acrolein formation [10]. On the other hand, Molina and coworkers studied silver nanoparticles with diameters between 9 to 23 nm. In their study, 23 nm particles were reported to be far more selective towards propylene oxide than the larger catalyst reported in the literature. Shift towards silver oxide phase was reported as the reason for high PO selectivity on 23 nm particles [100]. Stoukides reported, without giving the values, that the active phase of the silver catalyst is in the oxide form and the activity of the catalyst can be increased by using electrochemical oxygen pumping [104]. Kaichev used XPS for the analysis of the silver catalyst and detected that, in the epoxidation conditions, the surface reconstructs to a structure very close to bulk Ag_2O [105]. Pulido and coworkers investigated the Ag(111) and Ag(100) surfaces both experimentally and theoretically for oxygen dissociation. They reported that the Ag(100) surface is more active towards oxygen dissociation. After the oxidation study, they also analyzed the epoxidation performance of these surfaces and reported that the Ag(111) surface only gives combustion products whereas the Ag(100) surface results in propylene oxide and acetone alongside with CO_2 and H_2O [98]. In another publication, Wang et al. reported that oxidized silver sites are the main active sites for propylene epoxidation [106]. Cheng and coworkers studied the propylene epoxidation mechanism for silver aggregates on alumina. They reported that the silver-support interface is responsible for the dissociation of molecular oxygen. It was stated that when oxygen atoms are positioned at the interface or on the silver aggregate by forming silver oxide, PO can be produced selectively whereas oxygen on the support is responsible for the combustion pathway [107]. Molina et al. stated that at medium and high oxygen coverages on the Ag(100) surface, subsurface oxygens are favored for silver oxide phase formation. They reported that the Ag(111), Ag(110) and Ag(100) surfaces result in acrolein production at low oxygen coverages [100]. Zheng and coworkers tested the hypotheses of the previous proposals stating that Ag_2O is the active phase for epoxidation by running the epoxidation experiment on Ag_2O under anaerobic conditions. They reported that the lattice oxygen of the Ag_2O structure is active for PO and CO_2 production [108].

In the works of Özbek and coworkers, mechanism of gas phase ethylene reaction with surface lattice oxygen on silver oxide (Ag_2O) (001) surface has been theoretically investigated using DFT calculations. Özbek et al. stated that the oxygen at the bridge position are highly reactive towards epoxidation on the silver oxide surface. They also reported an alternative way of ethylene oxide formation pathway different than the oxametallo intermediates. According to these studies, Ag_2O (001) surface has a positive effect on ethylene oxide formation by enabling direct oxygen insertion to the double bond. They reported that this Eley-Rideal type reaction is only possible with the absence of oxygen vacancy [44-46]. Fella and Önal theoretically studied the propylene epoxidation on model Ag_{14}O_9 cluster representing Ag_2O surface. They reported that allyl radical formation pathway is in competition with the two propylene adsorption paths resulting in PO formation. Oxametallocycle formation on the model silver oxide cluster was not possible according to their relative energy diagram. It is reported that acetone and propanal formation barriers are higher than the PO formation barrier. Therefore, PO formation is easier than acetone and propanal formation when the surface propylene-oxy is formed [109]. Molina and coworkers modeled partially oxidized single layer Ag(111) surface on a three-layer periodic Ag(111) surface. Compositions of these oxide clusters were given in the study as Ag_{12}O_6 and Ag_{11}O_6 . Adsorption of propylene to the metal and oxygen sites of the (111) surface was simulated in the study. They reported that the adsorption of the propylene on the middle unoxidized silver site of Ag-O-Ag-O honeycomb structure by keeping the double bond is stronger than the adsorption to the oxygen site by forming oxametallocycle. They stated that this conformation is equally selective for PO and acrolein, but PO selectivity should be higher due to a more stable intermediate formation. They stated that when oxametallocycle is formed on the surface, acrolein formation should be more selective than PO formation pathway. It was emphasized that at least two close oxygen adatoms are required for acrolein formation, one for the oxametallocycle and one for the allylic hydrogen transfer from propylene. Propanone (acetone) and propanal formations were also mentioned in the study, but they are less selective [101]. Unlike the works of Özbek et al., direct epoxide formation pathway without surface intermediate was not considered in the studies of Fella and Molina.

Moreover, except the silver oxide like surface study of Molina and model cluster study of Fella, there is no theoretical study for propylene epoxidation on silver oxide (Ag_2O).

CHAPTER 3

MOTIVATION, COMPUTATIONAL METHOD AND SURFACE MODELS

3.1. Motivation and Goals

Traditional production methods for propylene oxide either have environmental, economic or supply issues. Recently introduced methods somewhat reduced environmental issues, however, they still need additional feeds beside propylene and oxygen and require additional complex separation, and/or regeneration steps. The direct epoxidation of propylene with molecular oxygen ($C_3H_6 + \frac{1}{2} O_2 \rightarrow C_3H_6O$) does not require complex pre- and after-treatment steps and does not suffer from the economy of the side products. It also does not require expensive or dangerous side reactants like H_2 or H_2O_2 . Therefore, direct epoxidation of propylene with molecular oxygen is a very important development for the industry. The silver catalyst is an important candidate for direct propylene epoxidation due to its success in the industrial direct ethylene epoxidation process. Unfortunately, its performance for propylene epoxidation could not be increased to industrial standards until this date. In order to make modifications on the silver catalyst, knowing the active phase and the reaction mechanism on the catalyst is essential. However, there is still a debate on the reaction mechanism and the real reason of low PO selectivity. Therefore, this study is triggered by the need for better explanation for the reaction of propylene on the silver catalyst.

This study has two main goals. The first goal of the project is to theoretically investigate the partial oxidation reaction pathways of propylene to propylene oxide

alongside the side reactions on Ag₂O (001) surface and to detect the reason of the low PO selectivity on the silver catalyst. To the best of our knowledge, there have been only two theoretical publications on this subject which cannot explain the experimental findings. Therefore, exploring reaction mechanism to find the reasons behind the low PO formation in the experiments is essential. After finding the reasons of the low PO selectivity, the second goal of the study is to eliminate these hindrances on the PO production pathway(s) on silver oxide surface by making appropriate modifications on the catalyst surface.

3.2. Computational Method and Surface Models

Vienna Ab-initio Simulation Package (VASP) is used throughout this study for the DFT calculations [110,111]. Plane wave basis sets are used with projector augmented wave (PAW) method, Perdew-Wang91 exchange-correlation (PW91) and generalized gradient approximations (GGA) with the implementation of supercell approach [112–114]. 500eV cutoff energy is used for the calculations. The net force acting on the ions is taken as lower than 0.015eV/Å for the convergence criteria of the relaxation. Main active sites for the propylene epoxidation are determined by Wang as the oxidized silver sites [106]. Therefore, silver oxide is studied as the active phase of silver catalyst. k-point sampling for the optimization of cubic Ag₂O bulk (Pn-3m) is generated by Monkhorst–Pack procedure with (15 × 15 × 15) mesh [115,116]. By using the optimization procedure with supplied parameters, the lattice constant of Ag₂O bulk is found as 4.82Å which is in agreement with the results of Özbek [91]. The experimental and theoretical results of Pulido state that the Ag (100) (or (001)) surface is the most reactive surface of silver for oxygen, therefore, (001) surface is cleaved from Ag₂O bulk for the slab preparation step [98]. By using the optimized bulk data, oxygen terminated periodic p(2x2) slab of Ag₂O (001) is prepared with 8 atomic layers (4 Ag and 4 O layers) including 32 Ag and 16 O atoms. The periodicity of the slab in z-direction is avoided by the addition of a vacuum region with the thickness of 15Å. Because of the asymmetry of the resultant slab after vacuum region addition, parameters for dipole corrections in z-direction are supplied in the input (INCAR) file[110]. Final optimization of the slab is carried out using (4 × 4 × 1) k-

point mesh. Additional to the ideal Ag_2O (001) slab, Ag_2O (001) slab with one oxygen vacancy is also prepared by optimizing Ag_2O (001) slab after removing one of the O atoms from the top layer. Obtained Ag_2O (001) slab with 32 Ag and 16 O atoms, i.e. $\text{Ag}_{32}\text{O}_{16}$ (001) slab, and Ag_2O (001) slab with 32 Ag and 15 O atoms, i.e. $\text{Ag}_{32}\text{O}_{15}$ (001) slab, are given in Figure 7. Computations to investigate the interaction of the catalyst surface and the propylene molecule are carried out using $(4 \times 4 \times 1)$ k-point mesh. In these calculations, the bottom layer of the slab is kept fixed to simulate the bulk layer of the catalyst. To be able to calculate the adsorption energy of propylene and the desorption barriers of the products, gamma point calculations are performed for the gas phase propylene, propylene oxide, propanal and acetone molecules. Spin polarization parameter is included for all calculations.

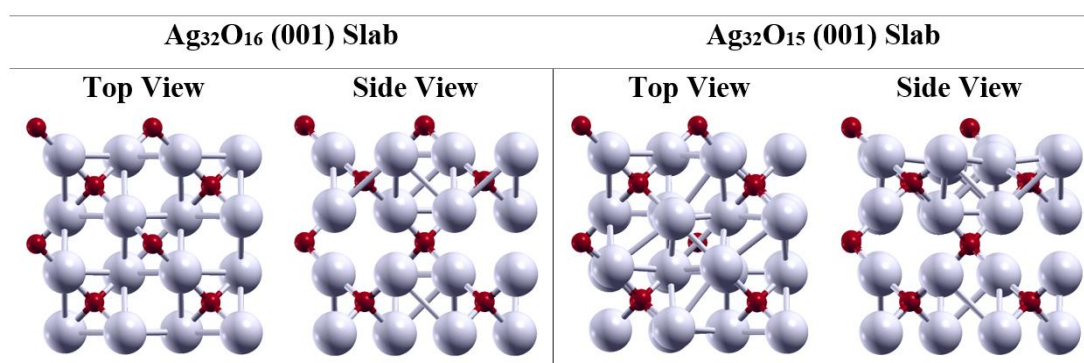


Figure 7: Geometries of optimized $\text{Ag}_{32}\text{O}_{16}$ (001) and $\text{Ag}_{32}\text{O}_{15}$ (001) Slabs (Grey atoms = silver, Red atoms = oxygen)

In order to investigate reaction mechanism and to generate relative energy plots, the methodology given in Figure 8 is used. Geometries and energies of reactants and products on the silver oxide surface are obtained by optimization calculations. Climbing image nudged elastic band (CI-NEB) method is used to determine the transition state (TS) candidates. NEB method optimizes the intermediate images generated between known reactant and products to find saddle points and minimum energy paths. During NEB procedure, each image maintains equal spacing to the neighboring images while it is trying to find the minimum energy level. CI modification to the NEB method enables the highest energy image to shift towards

saddle point. For the TS search, use of 8 intermediate images is decided and the geometries of the intermediate images are prepared accordingly by implementing the transition state tools developed by the Henkelman group [117,118]. After the completion of CI-NEB calculations, the saddle point, i.e. the step with the highest energy, is taken as TS candidate and additional relaxation run is carried out for this geometry. Then, frequency calculations are conducted for the optimized TS candidate geometry and the result is checked for the imaginary frequency value to verify the transition state [35]. After the verification of the imaginary frequency, energy results of the TS geometry are used to calculate reaction barriers.

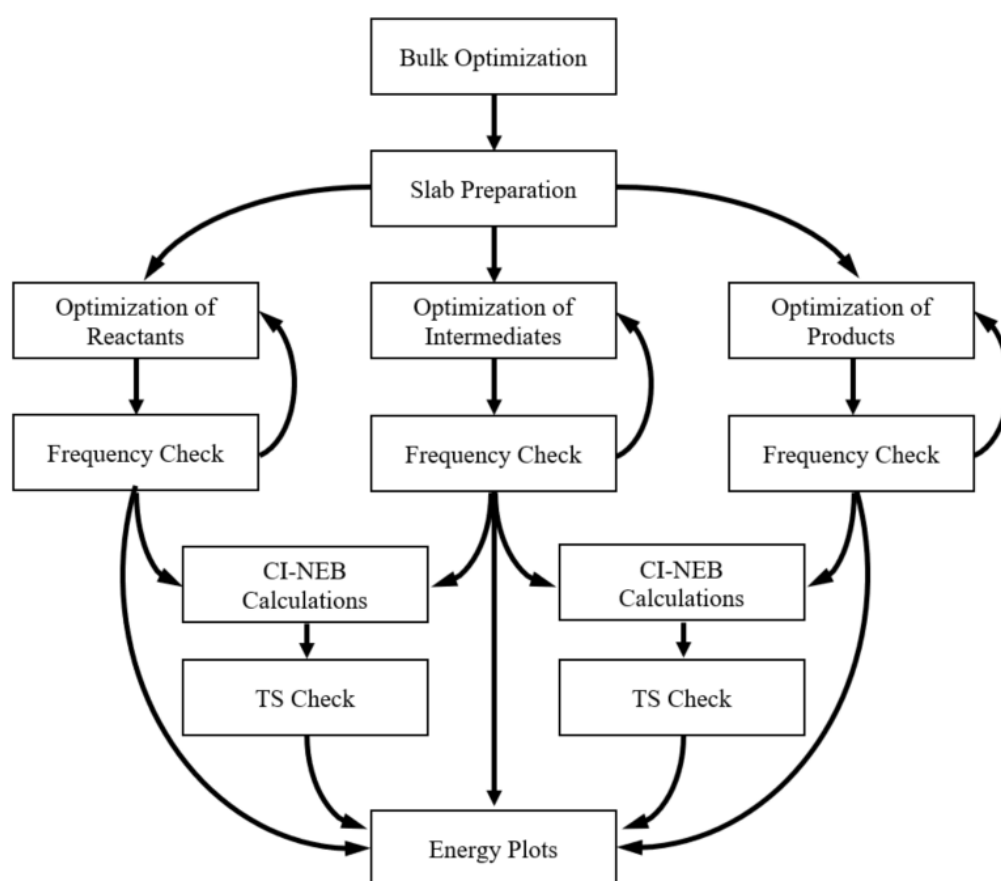


Figure 8: Schematic diagram of the steps followed through the study

Energies obtained from optimization and TS calculations are used to prepare relative energy plots. Summation of the energy of the studied slab and the energy of the gas

phase propylene is taken as the reference point for the plots. Corresponding relative energies for all mechanism steps included in the energy plots are calculated by subtracting reference energy from the energy of the investigated step. The reaction energies are calculated by subtracting the energy of the reactants from the energy of products and activation barriers are calculated by subtracting the energy of reactants from the energy of the transition state. Energies of the gas phase propylene oxide, propanal and acetone molecules are used for the calculation of the desorption energies of these products from the catalyst surface. In order to calculate the desorption energy, energy of the surface with the adsorbed product is subtracted from the sum of the energy of the gas phase molecule and the energy of the surface with oxygen vacancy. Finally, the energy of oxygen adsorption to the oxygen vacancy on the catalyst surface is calculated by subtracting the energy of silver oxide surface with one oxygen vacancy and the half of the energy of gas phase oxygen molecule from the energy of the ideal silver oxide surface. This oxygen adsorption step completes the catalyst cycle after the desorption of the propylene oxide from the surface by restoring the initial silver oxide surface and fulfills the $C_3H_6 + \frac{1}{2} O_2 \rightarrow C_3H_6O$ reaction.

Gold or chlorine doped surfaces are prepared by the re-relaxation of the silver oxide slab after the modification. Slabs with 1/7 and 1/3 top layer Au/Ag ratio, represented as $Ag_{31}Au_1O_{16}$ and $Ag_{30}Au_2O_{16}$, are prepared by replacing one or both silver atoms neighboring to the top center lattice oxygen atom with gold respectively. Slabs with 1/3 and 1/1 top layer Cl/O ratio, represented as $Ag_{32}O_{15}Cl_1$ and $Ag_{32}O_{14}Cl_2$, are prepared by replacing one or both closest top layer oxygen atoms neighboring to the top center lattice oxygen with chlorine respectively. Obtained geometries for the gold and chlorine doped slabs are given in Figure 9. In order to investigate the effect of gold and/or chlorine doping to the electronic property of the surface oxygen, Bader charge analysis is conducted for the all catalyst surfaces before sending the propylene. For this aim, additional optimization run is conducted with 300x300x300 charge density grid. Procedure by Henkelman group is utilized for the analysis of the charge output (CHGCAR) files obtained from this additional run to find the valance charge densities of the individual atoms in the structures [119–121].

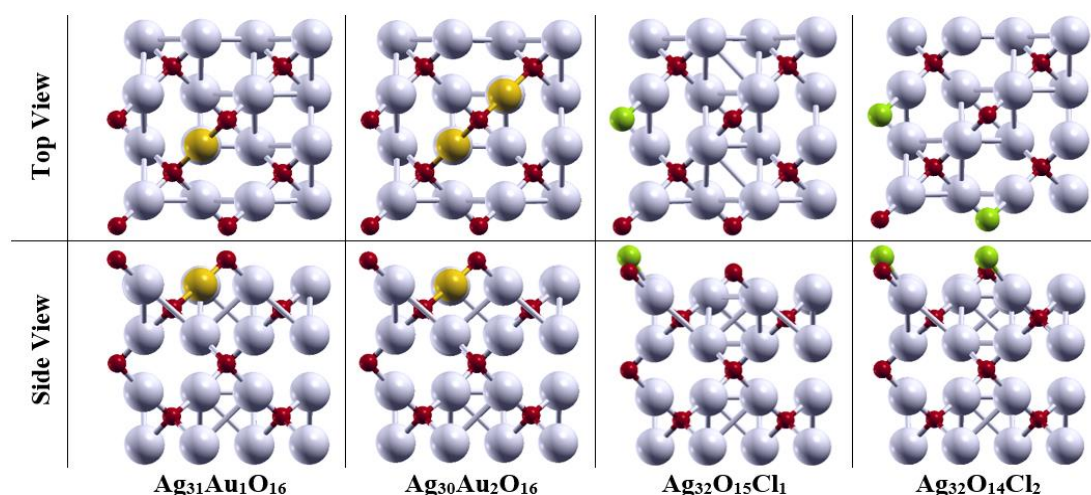


Figure 9: Geometries of $\text{Ag}_{31}\text{Au}_1\text{O}_{16}$, $\text{Ag}_{30}\text{Au}_2\text{O}_{16}$, $\text{Ag}_{32}\text{O}_{15}\text{Cl}_1$ and $\text{Ag}_{32}\text{O}_{14}\text{Cl}_2$ (001) slabs after optimization (Grey atoms = silver, Red atoms = oxygen, Yellow atoms = gold, Green atoms = chlorine)

The same procedure is followed to prepare gold and chlorine doped slabs. $\text{Ag}_{31}\text{Au}_1\text{O}_{15}\text{Cl}_1$, $\text{Ag}_{31}\text{Au}_1\text{O}_{14}\text{Cl}_2$ and $\text{Ag}_{30}\text{Au}_2\text{O}_{14}\text{Cl}_2$ (001) slabs are prepared to investigate the combined effect of gold and chlorine promotion. These slabs have 1/7, 1/7 and 1/3 top layer Au/Ag ratio and 1/3, 1/1 and 1/1 top layer Cl/O ratio respectively. Figure 10 shows the final geometries of these three slabs after optimization.

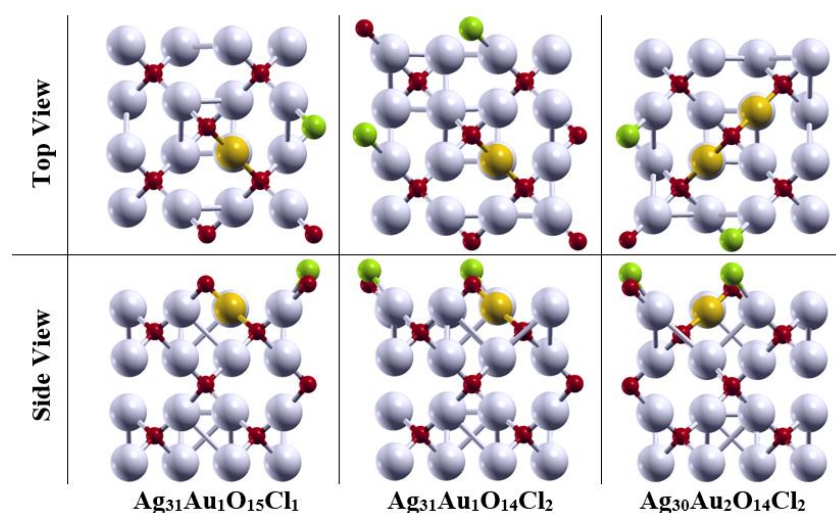


Figure 10: Geometries of $\text{Ag}_{31}\text{Au}_1\text{O}_{15}\text{Cl}_1$, $\text{Ag}_{31}\text{Au}_1\text{O}_{14}\text{Cl}_2$ and $\text{Ag}_{30}\text{Au}_2\text{O}_{14}\text{Cl}_2$ (001) slabs after optimization (Grey atoms = silver, Red atoms = oxygen, Yellow atoms = gold, Green atoms = chlorine)

CHAPTER 4

RESULTS AND DISCUSSIONS

Since the primary goal of this thesis was the investigation of the partial oxidation mechanism of propylene and to find the reasons of low PO selectivity reported in the experimental literature, all possible reaction pathways mentioned in the literature are used to construct a mechanism proposal as the first step. After the determination of the possible reactions, silver oxide surface was used to test this mechanism. Then, Au and Cl doping are studied to increase the activity of silver oxide catalyst for propylene epoxidation.

4.1. Construction of the Partial Oxidation Mechanism of Propylene

Propylene oxide, propanal, acetone and allyl formation possibilities on Ag₂O (001) were studied based on the proposals in the literature. According to the most popular mechanism proposals, pathways through PO and PO isomers, i.e. PA and Ace, are studied by using surface intermediates whereas allyl formation is studied through hydrogen stripping followed by oxygen insertion path [82,96–99]. In order to cover the proposals of the opposing publications, oxametallo-propylene intermediate to allyl pathway is included as an alternative allyl formation path [7,14,101–103]. Özbek observed direct ethylene oxide formation following Eley-Rideal type mechanism on the silver oxide surface, however, this kind of reaction is not mentioned for propylene epoxidation except one study for the O₂/H₂ system on gold catalyst [91,103]. Therefore, direct PO path is also included in the study. Finally, PO to allyl pathway is

included to check the combustion and acrolein formation possibility from PO. Even the product desorption from the catalyst is assumed as the rate determining step of PO production, H stripping from PO is interestingly neglected by the previous researchers. By adding the new pathways on top of the previous proposals from the literature, possible partial oxidation mechanism for propylene on the silver oxide (001) surface is prepared and presented in Figure 11.

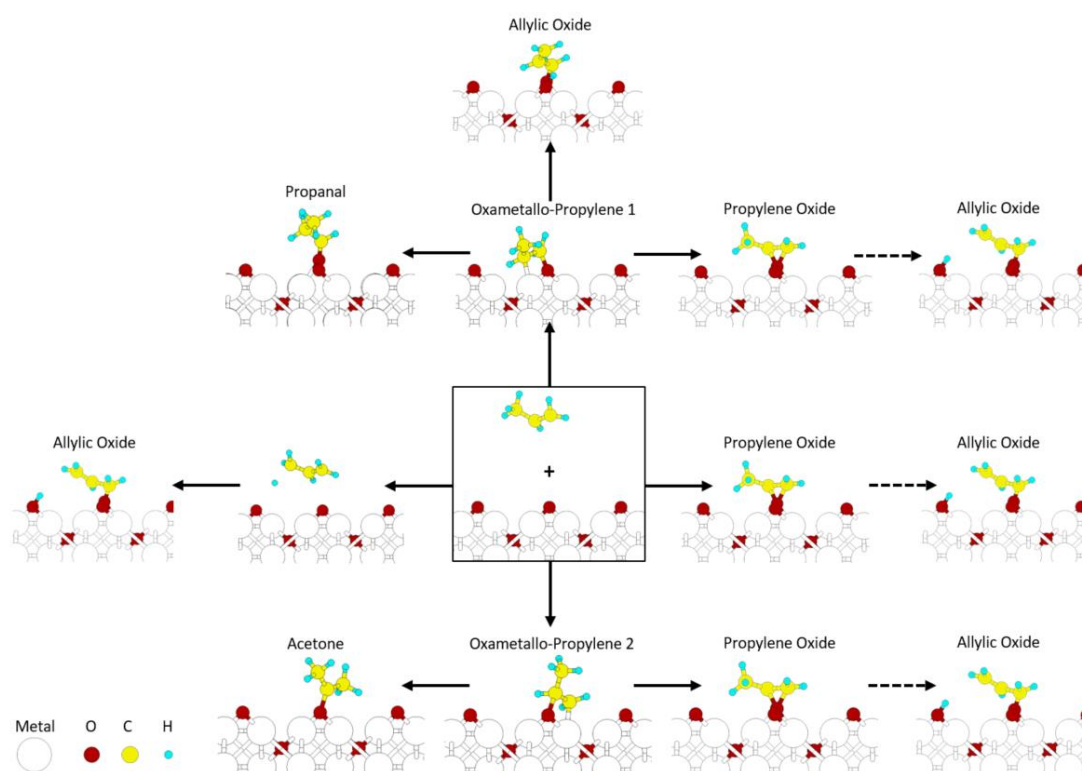
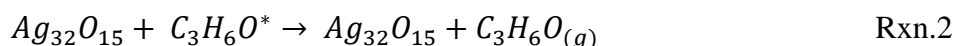
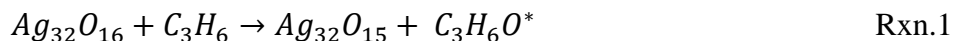


Figure 11: Partial oxidation mechanism of propylene on Ag_2O (001) Surface

4.2. Completion of Catalysis Cycle for Propylene Epoxidation

The catalysis cycle for the propylene epoxidation reaction ($\text{C}_3\text{H}_6 + \frac{1}{2} \text{O}_2 \rightarrow \text{C}_3\text{H}_6\text{O}$) on silver oxide and modified silver oxide surfaces ideally starts with the reaction of propylene with the lattice oxygen following Eley-Rideal type mechanism to produce propylene oxide on the catalyst surface, Rxn.1. Then this PO desorbs from the surface by leaving one oxygen vacancy behind, Rxn.2. Finally, mechanism proceeds with an oxygen adsorption step to regenerate the silver oxide catalyst to its initial state, Rxn.3. Thus, the catalysis cycle is completed. Overall reaction gives $\text{C}_3\text{H}_6 + \frac{1}{2} \text{O}_2 \rightarrow \text{C}_3\text{H}_6\text{O}$

reaction as it is aimed at the beginning. Example reaction order for the catalysis cycle on $\text{Ag}_{32}\text{O}_{16}$ (001) slab are given as follows.



The oxygen adsorption steps (Rxn.3 in the example above) for the catalyst recovery are not given in the relative energy plots for the simplicity but they are supplied in Tables 2-10. Among the surfaces studied, only the Cl-doped surfaces (except $\text{Ag}_{30}\text{Au}_2\text{O}_{14}\text{Cl}_2$) achieved selective PO formation pathway. Therefore, only Cl-doped surfaces (except $\text{Ag}_{30}\text{Au}_2\text{O}_{14}\text{Cl}_2$) follow and complete this catalysis cycle. Since the reactions on the surfaces resulting allyl formation have further reaction steps towards acrolein formation and/or further oxidation, their reaction mechanisms and catalyst recovery reactions to complete catalysis cycle are different and not in the scope of this study.

4.3. Energetics on the Unpromoted Silver Oxide Slabs

4.3.1. Energetics on the Silver Oxide ($\text{Ag}_{32}\text{O}_{16}$) Slab

As the first step of the mechanism, direct interactions of propylene with the $\text{Ag}_{32}\text{O}_{16}$ (001) slab are investigated. Hence, direct PO, oxametallo-propylene (OMP) intermediate and allyl formation steps are simulated and obtained energy profile is given in Figure 12. The interaction of propylene with the lattice oxygen of the $\text{Ag}_{32}\text{O}_{16}$ (001) slab follows Eley-Rideal type mechanism. Allyl formation via allylic hydrogen stripping is the main argument of the literature for the allyl radical formation. Since the experimental study of Zhang points out the CO_2 production on silver oxide, activation barrier for allyl radical (or allylic oxide) formation pathway, which is the primer of CO_2 formation, is expected to be lower than PO and OMP formation pathways [108]. However, allylic hydrogen stripping before the oxygen insertion step has significant activation barrier of 1.9 eV whereas other propylene-surface interaction steps have no activation barrier. C=C bond of the propylene can be activated by the

lattice oxygen of the Ag_2O (001) surface to produce propylene oxide without a barrier. Also, two types of oxametallo-propylene structures can be achieved without a barrier by the activation of $\text{C}=\text{C}$ by one lattice oxygen atom and one surface silver atom. Among them, the first oxametallo-propylene intermediate (OMP1) is formed when the lattice oxygen activates the first carbon of propylene and the second oxametallo-propylene intermediate (OMP2) is formed when the lattice oxygen activates the second carbon of propylene. Structures of these cyclic intermediates are included in Figure 12 alongside with the structures of allyl and PO. According to Figure 12. and the reaction energy values reported in Table 2, PO formation from the direct activation of propylene by the lattice oxygen of the $\text{Ag}_{32}\text{O}_{16}$ (001) slab is found as the most probable result of the first interaction of propylene with the catalyst surface. In this way, PO should be the most probable structure on the silver oxide contrary to the findings in the literature.

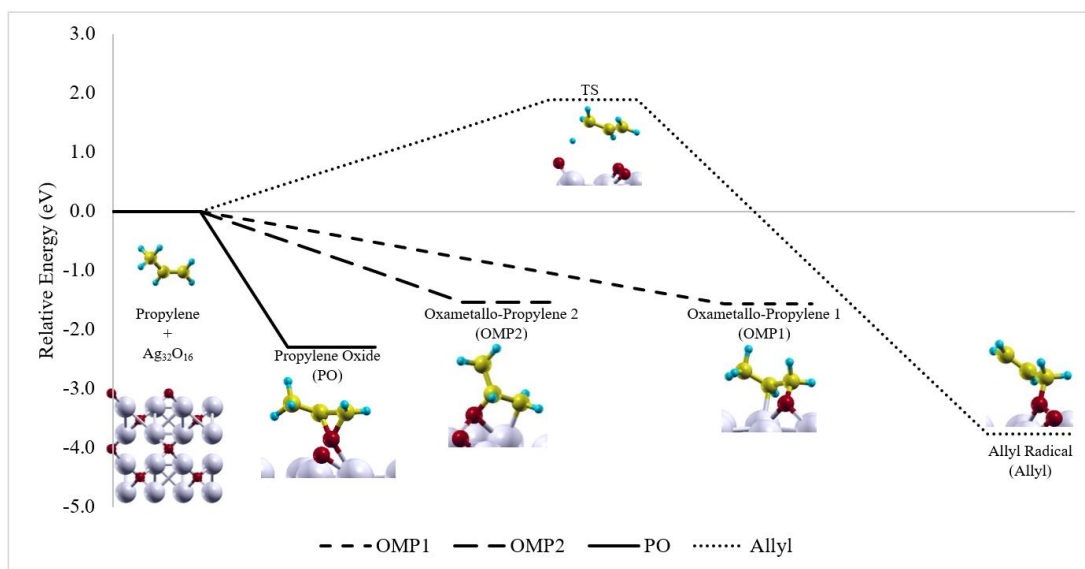


Figure 12: Energetics of direct propylene-surface interactions on $\text{Ag}_{32}\text{O}_{16}$ (001) slab

Even though there is no activation barrier for their formation, relative energy levels of OMP1 and OMP2 intermediate structures indicated that their stability (and presence probability) on the $\text{Ag}_{32}\text{O}_{16}$ (001) slab are lower than PO. However, pathways following these intermediates are studied to reveal the pathways towards PA and Ace, which should be formed through surface intermediates as it is mentioned in the

literature. By following OMP1 intermediate PA, PO and allyl formation and by following OMP2 intermediate Ace and PO formation pathways are investigated. The position of propylene in the OMP1 intermediate enables neighbor lattice oxygen to easily strip one of the allylic hydrogen atoms of the third carbon of the propylene without activation barrier. Again, without activation barrier, the bond between the second carbon and silver can be activated and PO can be formed via ring closing by the interaction of the second carbon with the oxygen. PA formation proceeds through hydrogen transfer from the first carbon to second carbon of OMP1 intermediate and cleavage of the bond between the silver atom and the second carbon atom of the OMP1. This process requires an activation barrier of 0.2 eV. By just considering one step ahead of the OMP1 formation, it can be stated that if the interaction of $\text{Ag}_{32}\text{O}_{16}$ (001) slab and the propylene forms OMP1 on the surface, next step should mostly proceed through allyl formation according to the Figure 13.

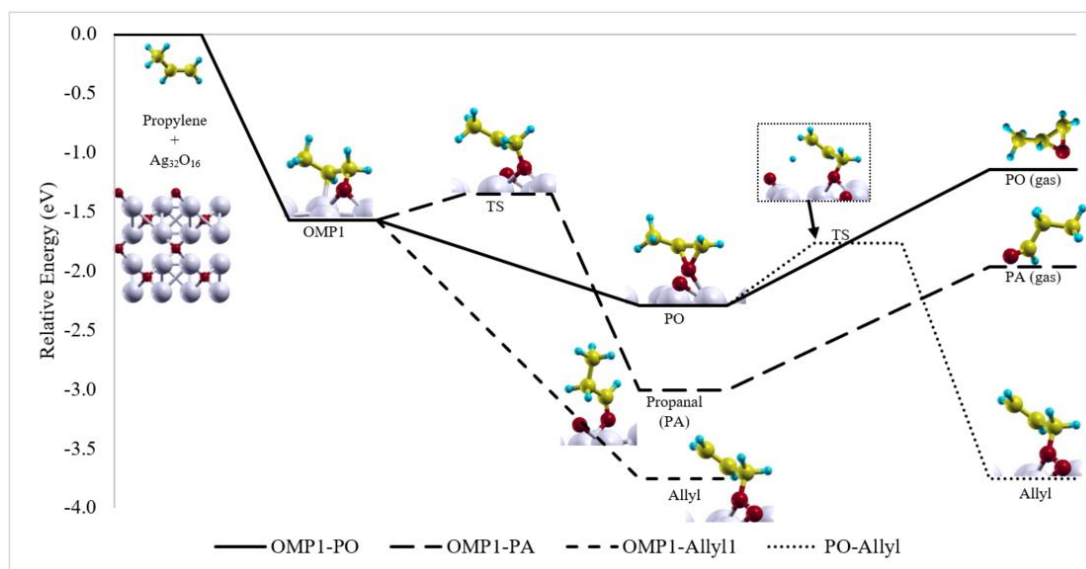


Figure 13: Energetics of the reactions through OMP1 on $\text{Ag}_{32}\text{O}_{16}$ (001) slab

Congruently with the OMP1 intermediate, the OMP2 intermediate can lead PO formation without an activation barrier. Acetone (Ace) formation from OMP2 intermediate proceeds through hydrogen transfer from the second carbon to the first carbon of the intermediate structure and the termination of the silver-carbon bond of the OMP2 intermediate. This process requires an activation barrier of 0.3eV. As it can

be seen from Figure 12 and Figure 14, the hydrogens attached to the 3rd carbon of the OMP2 intermediate points upward and away from the surface. Therefore, allylic hydrogen stripping from OMP2 intermediate is not feasible. As a result, if the interaction of Ag₃₂O₁₆ (001) slab and the propylene forms OMP2 on the surface, next step should proceed through PO formation according to the Figure 14.

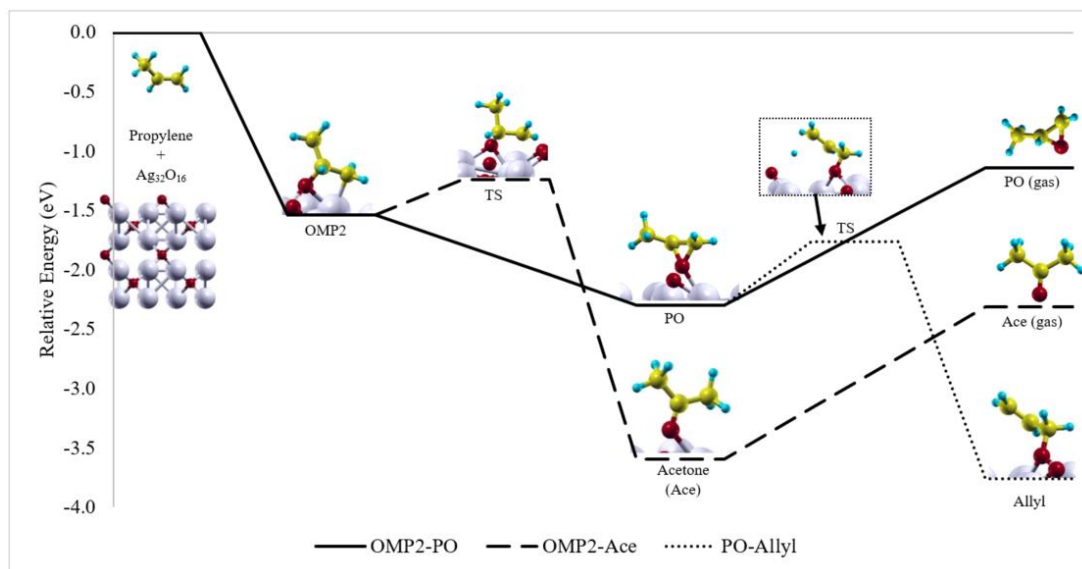


Figure 14: Energetics of the reactions through OMP2 on Ag₃₂O₁₆ (001) slab

By just analyzing the activation barrier and reaction energy data, propylene oxide should be the major product of the propylene – silver oxide interaction. Additional to PO, some amount of allyl derivatives should also be observed due to the OMP1 formation. However, as it can be seen in Figure 13 and Figure 14, desorption of the PO from the surface limits the process and alters the composition of the product stream in favor of allyl derivatives, i.e. combustion products. Even there is no activation barrier for PO formation, desorption energy of PO is 1.2 eV. This desorption barrier for PO is higher than the barriers of the reactions towards OMP1 and OMP2 intermediates from PO, which are 0.7 eV and 0.8 eV respectively. A significant finding of this study is that allylic hydrogen stripping from PO has an activation barrier of 0.5 eV, which is less than the half of PO desorption energy (see Table 2). Therefore, selective PO production process on the Ag₃₂O₁₆ (001) slab ends up with the allyl formation from PO as it is shown in Figure 15. In other words, silver oxide surface

shows high activity for PO formation but fails to fulfill the Sabatier's Principle for the PO production due to high desorption barrier.

Table 2: Activation barriers and reaction energies on $\text{Ag}_{32}\text{O}_{16}$ (001) slab

Reaction	Activation Barrier (eV)	Energy of Reaction (eV)
<i>Propylene</i> (g) \rightarrow <i>OMP1</i>	-	-1.6
<i>Propylene</i> (g) \rightarrow <i>OMP2</i>	-	-1.5
<i>Propylene</i> (g) \rightarrow <i>PO</i>	-	-2.3
<i>Propylene</i> (g) \rightarrow <i>Allyl</i>	1.9	-3.6
<i>OMP1</i> \rightarrow <i>PO</i>	-	-1.1
<i>OMP1</i> \rightarrow <i>PA</i>	0.2	-1.4
<i>OMP1</i> \rightarrow <i>Allyl</i>	-	-2.2
<i>OMP2</i> \rightarrow <i>PO</i>	-	-1.2
<i>OMP2</i> \rightarrow <i>Ace</i>	0.3	-2.1
<i>PO</i> \rightarrow <i>Allyl</i>	0.5	-1.0
<i>PO</i> \rightarrow <i>PO</i> (g)		1.2
<i>PA</i> \rightarrow <i>PA</i> (g)		1.0
<i>Ace</i> \rightarrow <i>Ace</i> (g)		1.3
$\text{Ag}_{32}\text{O}_{15} + 1/2 \text{O}_2 \rightarrow \text{Ag}_{32}\text{O}_{16}$		-0.1

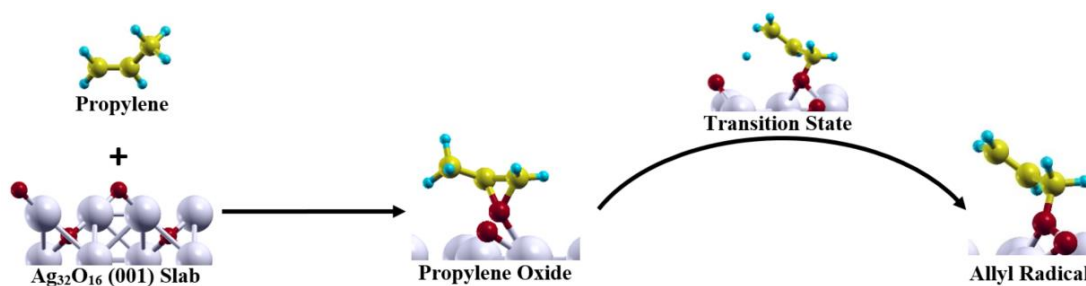


Figure 15: The most probable pathway on $\text{Ag}_{32}\text{O}_{16}$ (001) slab

4.3.2. Energetics on the Silver Oxide Slab with Oxygen Vacancy ($\text{Ag}_{32}\text{O}_{15}$)

Özbek [91] reported that direct ethylene epoxidation only happens when there is no oxygen vacancy. On the other hand, Molina [101] proposed that oxygen vacancies can increase PO selectivity. In order to check the effect of the oxygen vacancy on the propylene epoxidation, this scenario is studied with $\text{Ag}_{32}\text{O}_{15}$ (001) slab. On the oxygen vacancy site, adsorption of the propylene to the surface is observed without activation barrier. In this step, two carbon atoms of the propylene interact with the silver atom of the surface. Consequently, in the absence of one lattice oxygen, a new reaction

network following Langmuir-Hinshelwood type mechanism, which is not possible on the silver oxide surface with ideal stoichiometry, becomes possible. Similar to the $\text{Ag}_{32}\text{O}_{16}$ (001) slab, formation of OMP1 and OMP2 surface intermediates and PO are observed on the neighbor lattice without activation barriers. Energetics of these steps are supplied in Figure 16. Direct gas phase allyl formation via allylic hydrogen stripping followed by oxygen insertion is found improbable due to high activation barrier around 3.0 eV. This step is excluded from Figure 16 for better representation of the other pathways, but it is included in Table 3 for the comparison. According to Figure 16 only, direct formation of PO on a lattice oxygen is the most probable pathway when the gas phase propylene interacts with $\text{Ag}_{32}\text{O}_{15}$ (001) slab.

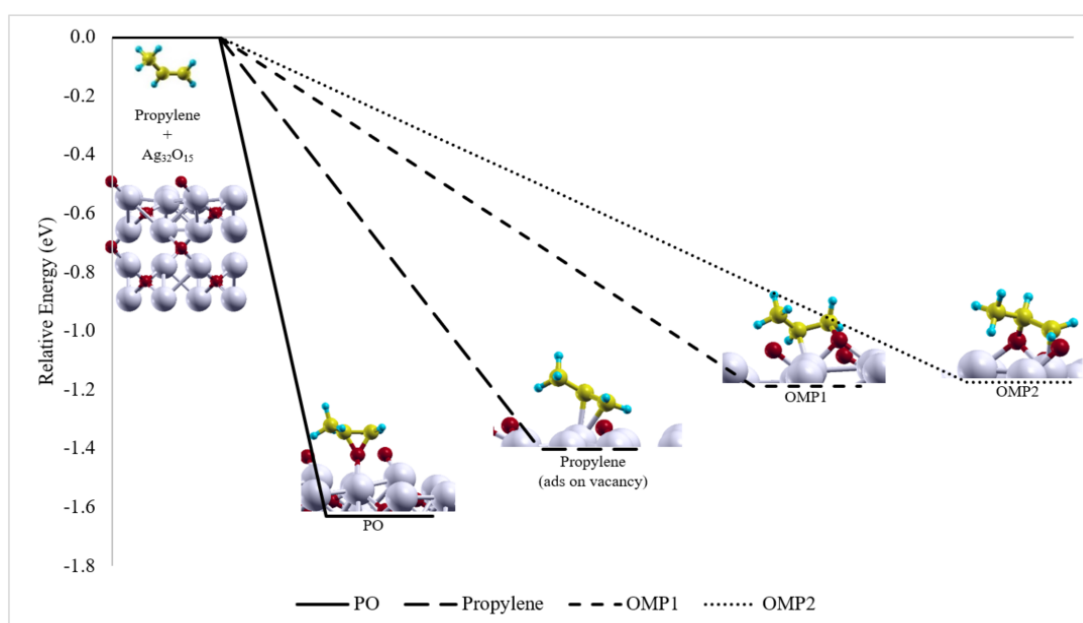


Figure 16: Energetics of direct propylene-surface interactions on $\text{Ag}_{32}\text{O}_{15}$ (001) slab

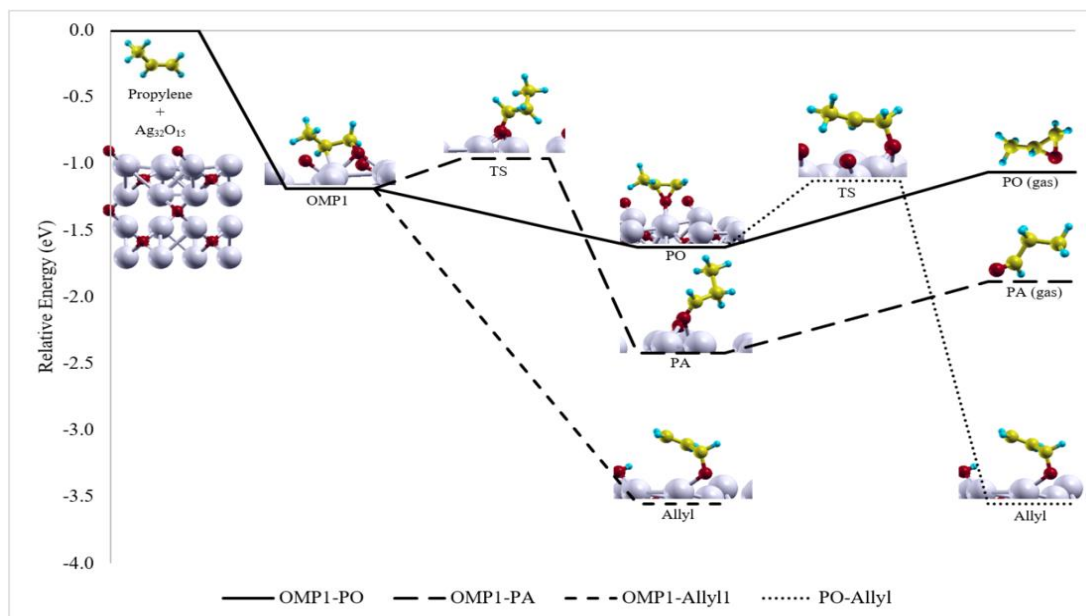


Figure 17: Energetics of the reactions through OMP1 on $\text{Ag}_{32}\text{O}_{15}$ (001) slab

If OMP1 intermediate is formed on the $\text{Ag}_{32}\text{O}_{15}$ (001) slab, allyl radical and propylene oxide formation pathways proceed without activation barrier. Like in the $\text{Ag}_{32}\text{O}_{16}$ (001) slab case, PA formation pathway proceeds through an activation barrier of 0.2 eV. Therefore, according to Figure 17, OMP1 formation on the silver oxide (001) surface with an oxygen vacancy leads allyl radical formation.

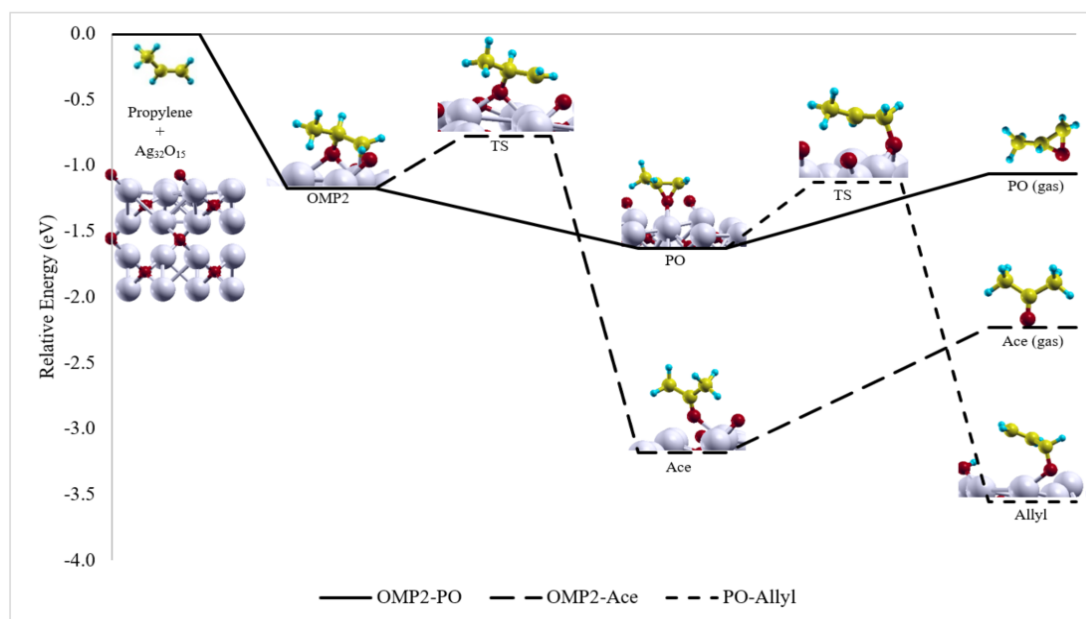


Figure 18: Energetics of the reactions through OMP2 on $\text{Ag}_{32}\text{O}_{15}$ (001) slab

OMP2 formation also gives similar results with the ideal Ag_2O (001) surface. It is observed that PO formation from OMP2 intermediate has no activation barriers whereas acetone formation via a hydrogen transfer from the second carbon atom to first carbon atom of the OMP2 intermediate and silver carbon bond termination needs to overcome an activation barrier of 0.4 eV. PO has a desorption barrier of 0.6 eV on $\text{Ag}_{32}\text{O}_{15}$ (001) slab and activation barriers towards 0.5 eV for allyl formation and 0.4 eV towards OMP1 formation, which also leads allyl formation without a barrier. Therefore, pathways following OMP2 formation leads allyl radical at the end.

Unlike the $\text{Ag}_{32}\text{O}_{16}$ (001) slab, propylene can be adsorbed on the silver of the $\text{Ag}_{32}\text{O}_{15}$ (001) slab at the oxygen vacancy (shown as Propylene* in Table 3). This adsorbed propylene can interact with one of the neighbor oxygen atoms according to Langmuir-Hinshelwood mechanism to form PO, OMP1 or OMP2. As it is supplied in Table 3 and Figure 19, these reaction steps have activation barriers of 0.6, 0.9 and 1.0 eV respectively. On the other hand, adsorbed propylene can interact with two neighbor surface lattice oxygen atoms to form allyl radical in a two-step reaction without forming an OMP intermediate. In the first step, the allylic hydrogen of the propylene is attacked by the closest surface lattice oxygen with an activation barrier of 0.2 eV. Then the remaining C_3H_5 migrates towards another surface lattice oxygen for the oxygen insertion step with an activation barrier of 0.9 eV. Consequently, propylene adsorption to the oxygen vacancy site most probably follows two-step allyl formation pathway according to Figure 19.

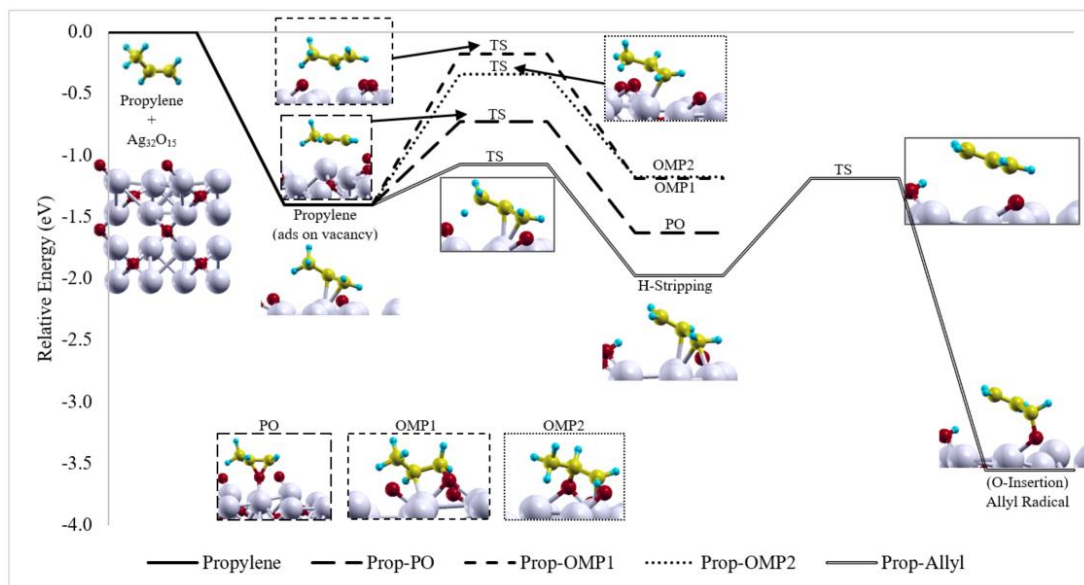
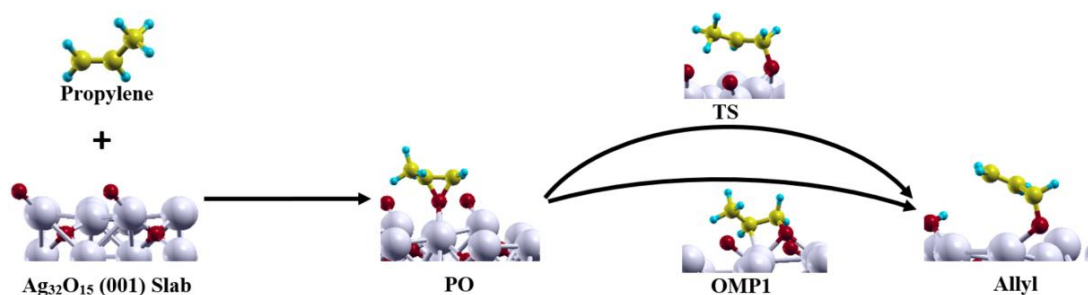


Figure 19: Energetics of the reactions through adsorbed propylene on $\text{Ag}_{32}\text{O}_{15}$ (001) slab

As a summary, silver oxide slab with an oxygen vacancy more or less acts like the ideal silver oxide slab investigated at the beginning. Propylene prefers the two-fold oxygen site instead of free silver site exposed to the vacuum region. Considering its stability, propylene forms propylene oxide on the $\text{Ag}_{32}\text{O}_{15}$ (001) slab instead of OMP1 or OMP2 intermediates. The silver oxide with vacancy has lower binding energies for surface intermediates and products. Therefore, desorption of the products is easier than the ideal silver oxide surface. However, produced propylene oxide cannot selectively leave the surface because of easier OMP1 and allyl formation pathways. As a result, the interaction of propylene with the $\text{Ag}_{32}\text{O}_{15}$ (001) slab follows the pathway given in Figure 20 and ends up with allyl radical formation. Nevertheless, slightly higher PO selectivity can be expected from the silver oxide surface with oxygen vacancy.

Table 3: Activation barriers and reaction energies on Ag₃₂O₁₅ (001) slab

Reaction	Activation Barrier (eV)	Energy of Reaction (eV)
Propylene (g) → OMP1	-	-1.2
Propylene (g) → OMP2	-	-1.2
Propylene (g) → PO	-	-1.6
Propylene (g) → Allyl	2.9	-3.6
Propylene (g) → Propylene*	-	-1.4
Propylene* → OMP1	0.9	0.2
Propylene* → OMP2	1.0	0.2
Propylene* → PO	0.6	-0.2
Propylene* → Allyl (2step)	0.2 & 0.9	-0.6 & -1.6
OMP1 → PO	-	-0.4
OMP1 → PA	0.2	-1.2
OMP1 → Allyl	-	-2.4
OMP2 → PO	-	-0.5
OMP2 → Ace	0.4	-2.0
PO → Allyl	0.5	-1.9
PO → PO (g)		0.6
PA → PA (g)		0.5
Ace → Ace (g)		0.9
Ag ₃₂ O ₁₄ + 1/2 O ₂ → Ag ₃₂ O ₁₅		-0.2

**Figure 20:** The most probable pathway on Ag₃₂O₁₅ (001) slab

Both the ideal silver oxide surface and the silver oxide surface with surface oxygen vacancy are active for the propylene oxide formation on the surface. However, high desorption energy makes PO vulnerable to the interaction with the neighbor oxygen atom to produce allyl radical instead of gas phase propylene oxide. Therefore, to make propylene oxide the favorable product, promoters decreasing the strength of the interaction between the catalyst surface and the propylene oxide are required.

Additionally, promoters should be able to reduce the interaction of the neighbor lattice oxygen atom(s) with PO and surface intermediates OMP1 and OMP2.

4.4. Energetics on the Silver Oxide Slabs with Gold Doping

4.4.1. Energetics on the $\text{Ag}_{31}\text{Au}_1\text{O}_{16}$ (001) Slab

The top layer of the unit cell of the $\text{Ag}_{31}\text{Au}_1\text{O}_{16}$ (001) slab has the Au/Ag ratio of 1/7 and the central oxygen atom of the top layer is bonded to one silver and one gold atoms. Since the oxametallocycles have a bond with the surface metal, there are two different possibilities for the formation of both oxametallo-propylene intermediates with the gold side (Au-OMP1 and Au-OMP2) and with the silver side (Ag-OMP1 and Ag-OMP2). Therefore, $\text{Ag}_{31}\text{Au}_1\text{O}_{16}$ (001) slab has four different surface intermediates. Formation of these four oxametallo-propylene intermediates and the formation of propylene oxide requires no activation barriers as it is shown in Figure 21. Like in the $\text{Ag}_{32}\text{O}_{16}$ (001) surface, direct allylic hydrogen stripping from propylene has a high activation barrier. According to data supplied in Table 4, direct hydrogen stripping step needs to overcome an activation barrier of 2.3 eV to produce allyl radical.

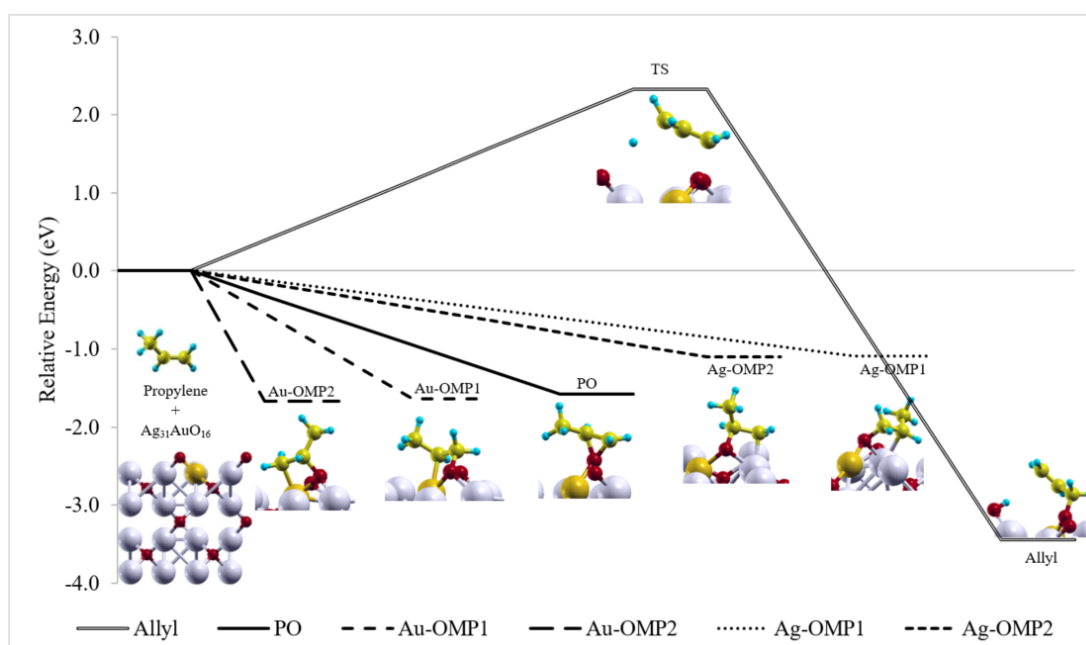


Figure 21: Energetics of direct propylene-surface interactions on $\text{Ag}_{31}\text{Au}_1\text{O}_{16}$ (001) slab

According to Figure 21 and Table 4, the interaction of propylene with the gold side of the top center oxygen molecule of the $\text{Ag}_{31}\text{Au}_1\text{O}_{16}$ (001) unit cell is stronger than its interaction with the silver side of the top center oxygen molecule of the $\text{Ag}_{31}\text{Au}_1\text{O}_{16}$ (001). Unlike the pure silver oxide case, energy levels of the gold side intermediates, Au-OMP1 and Au-OMP2, are comparable with the energy level of PO on the surface. The Ag-O bond distance of 1.99 Å on the $\text{Ag}_{32}\text{O}_{16}$ surface becomes 2.02 Å with the Au-Ag replacement on the $\text{Ag}_{31}\text{Au}_1\text{O}_{16}$ (001) slab. Also, Au-O bond distance is measured as 1.93 Å. The valence electron density of the gold atom (10.54) is slightly higher than the electron density of the silver atom (10.44). These two factors break the symmetry of the lattice oxygen atom and result in the different interaction strengths with the gold side and the silver side.

As mentioned above, gold side OMP1 and OMP2 intermediates have stronger interaction energies than their silver side equivalents on the $\text{Ag}_{31}\text{Au}_1\text{O}_{16}$ (001) slab. Because of their stability, further reactions from Au-OMP1 and Au-OMP2 intermediates are harder than the reactions from the OMP1 and OMP2 structures on the silver side. As it is shown in Figure 22, Figure 23 and Table 4, PO formation from Au-OMP1 and Au-OMP2 become slightly endothermic for both intermediates with reaction energy and activation barrier of 0.1 eV. Activation barriers for PA formation from OMP1 and Ace formation from OMP2 are 0.6eV and 0.8 eV respectively. Additionally, gold doping introduces a 0.2 eV activation barrier for the allyl formation step from Au-OMP1 intermediate. As a result, if the formation pathways are considered alone, allyl formation from Au-OMP1 intermediate becomes comparable with the propylene oxide formation with the help of gold doping.

Gold doping helps propylene oxide formation from Au-OMP1 by introducing an activation barrier to the allyl formation pathway. With gold doping, the position of the propylene oxide formed on the $\text{Ag}_{31}\text{Au}_1\text{O}_{16}$ (001) slab is around 0.63 Å higher than the level of the other surface lattice oxygens. This pre-desorption position helps to reduce the PO desorption energy from 1.2 eV to 1.0 eV. On the other hand, allyl formation from the propylene oxide requires only 0.3 eV as activation barrier.

Therefore, PO desorption from $\text{Ag}_{31}\text{Au}_1\text{O}_{16}$ (001) slab still limits the overall reaction and reaction proceeds through ally formation pathway.

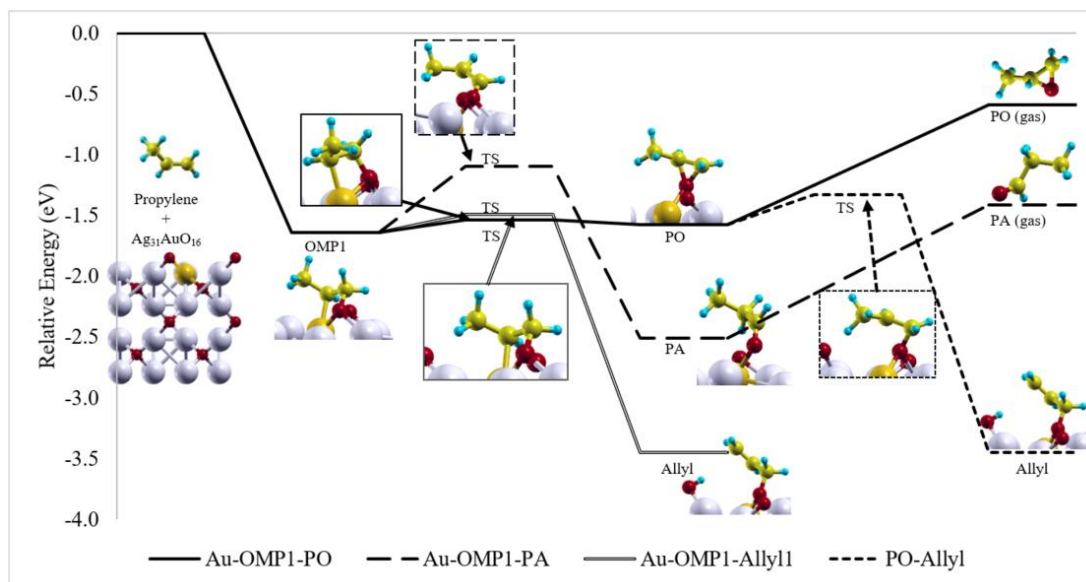


Figure 22: Energetics of the reactions through Au-OMP1 on $\text{Ag}_{31}\text{Au}_1\text{O}_{16}$ (001) slab

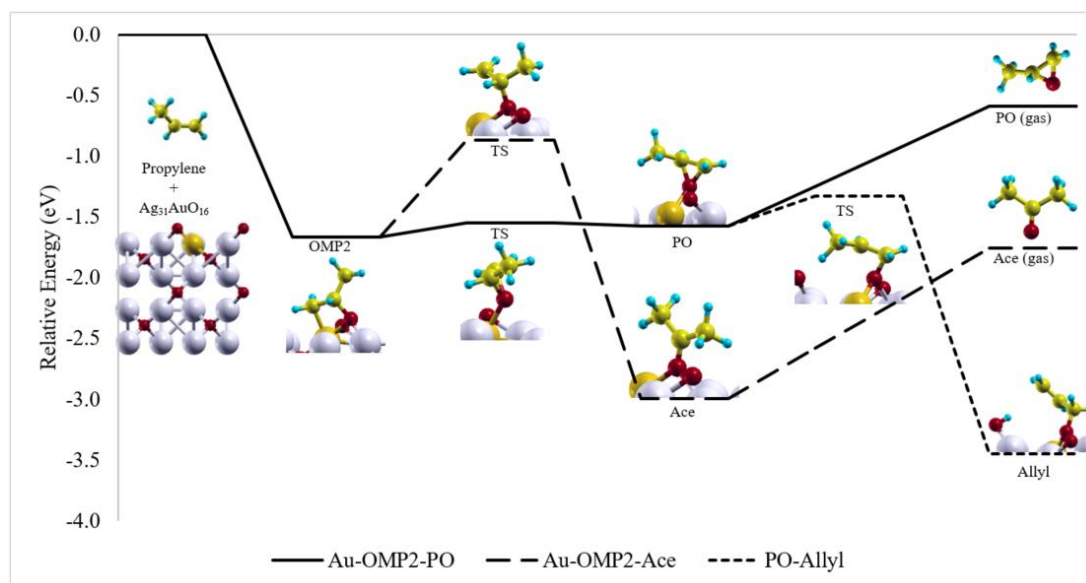


Figure 23: Energetics of the reactions through Au-OMP2 on $\text{Ag}_{31}\text{Au}_1\text{O}_{16}$ (001) slab

As explained above, the new position of the lattice oxygen due to lack of symmetry reduces the interaction of the Ag-OMP1 and Ag-OMP2 intermediates with the slab which is making them less favorable than the gold side alternatives. However, if the silver side surface intermediates, Ag-OMP1 and Ag-OMP2, are formed on the

$\text{Ag}_{31}\text{Au}_1\text{O}_{16}$ (001), they give very similar energetics with the $\text{Ag}_{32}\text{O}_{16}$ surface as it is given in Figure 24 and Figure 25. PA formation from Ag-OMP1 and Ace formation from Ag-OMP2 have activation barriers of 0.3 eV and 0.4 eV respectively, whereas allyl formation from Ag-OMP1 and PO formation from Ag-OMP1 and Ag-OMP2 intermediates have no activation barriers. Additionally, allyl formation from PO is still easier than PO desorption. Therefore, reactions on the silver side of the $\text{Ag}_{31}\text{Au}_1\text{O}_{16}$ (001) slab suffers from the same problems of the $\text{Ag}_{32}\text{O}_{16}$ slab.

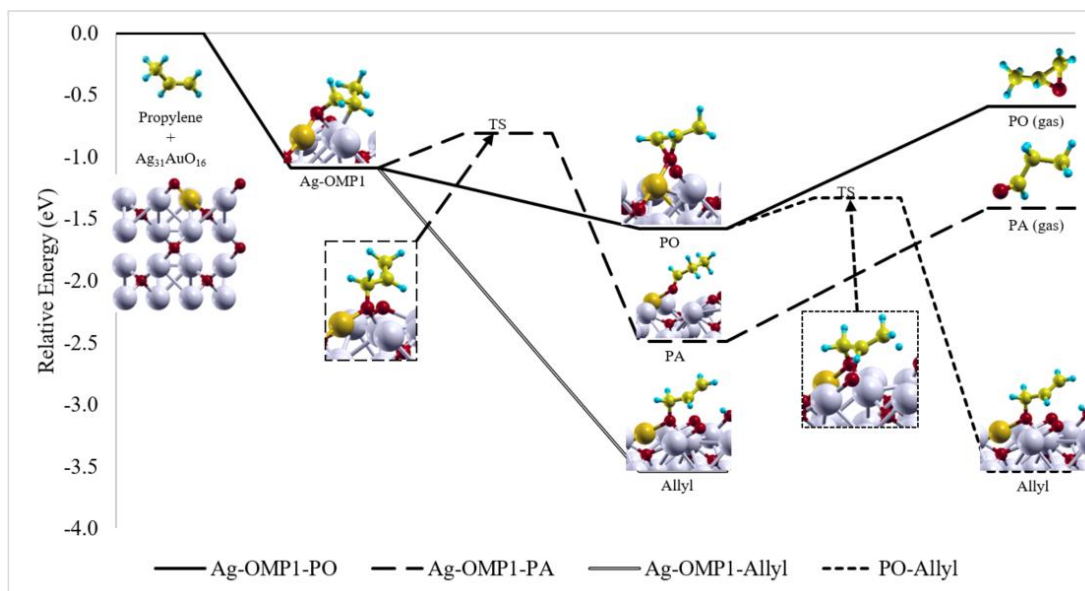


Figure 24: Energetics of the reactions through Ag-OMP1 on $\text{Ag}_{31}\text{Au}_1\text{O}_{16}$ (001) slab

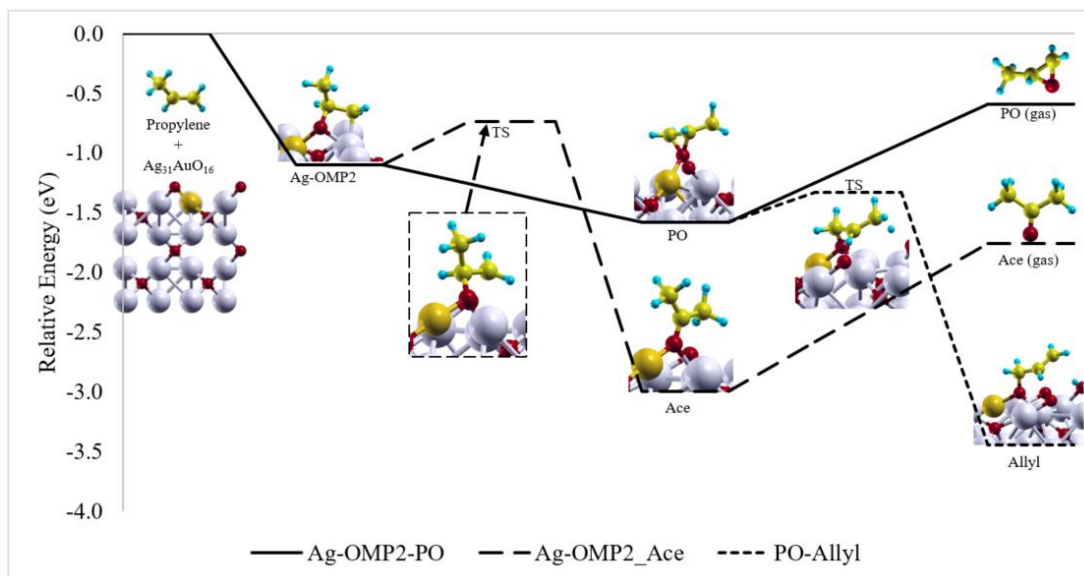


Figure 25: Energetics of the reactions through Ag-OMP2 on Ag₃₁Au₁O₁₆ (001) slab

Table 4: Activation barriers and reaction energies on Ag₃₁Au₁O₁₆ (001) slab

Reaction	Activation Barrier (eV)	Energy of Reaction (eV)
<i>Propylene</i> → <i>Au-OMP1</i>	-	-1.6
<i>Propylene</i> → <i>Au-OMP2</i>	-	-1.7
<i>Propylene</i> → <i>Ag-OMP1</i>	-	-1.1
<i>Propylene</i> → <i>Ag-OMP2</i>	-	-1.1
<i>Propylene</i> → <i>PO</i>	-	-1.6
<i>Propylene</i> → <i>Allyl</i>	2.3	-3.5
<i>Au-OMP1</i> → <i>PO</i>	0.1	0.1
<i>Au-OMP1</i> → <i>PA</i>	0.6	-0.9
<i>Au-OMP1</i> → <i>Allyl</i>	0.2	-1.8
<i>Au-OMP2</i> → <i>PO</i>	0.1	0.1
<i>Au-OMP2</i> → <i>Ace</i>	0.8	-1.3
<i>Ag-OMP1</i> → <i>PO</i>	-	-0.5
<i>Ag-OMP1</i> → <i>PA</i>	0.3	-1.4
<i>Ag-OMP1</i> → <i>Allyl</i>	-	-2.5
<i>Ag-OMP2</i> → <i>PO</i>	-	-0.5
<i>Ag-OMP2</i> → <i>Ace</i>	0.4	-1.9
<i>PO</i> → <i>Allyl</i>	0.3	-1.9
<i>PO (ads)</i> → <i>PO (g)</i>		1.0
<i>PA (ads)</i> → <i>PA (g)</i>		1.1
<i>Ace (ads)</i> → <i>Ace (g)</i>		1.2
<i>Ag₃₁Au₁O₁₅</i> + ½ <i>O₂</i> → <i>Ag₃₁Au₁O₁₆</i>		-0.7

As a summary, modifying the silver oxide surface with gold to have 1/7 gold/silver ratio on the top layer makes the probable reaction network more complex as it is given in Figure 26. At the first step, the interaction of the propylene with the catalyst produces PO, Au-OMP1 or Au-OMP2 with similar selectivities. Due to high desorption barrier, pathways between PO and Au size intermediates, i.e. Au-OMP1 and Au-OMP2, becomes reversible as it is proposed by Kulkarni and coworkers in their PO isomerization study [102]. When the surface has the equilibrium convergence for the PO, it is expected to see the PO to Au-OMP1 and Au-OMP2 reactions. Finally, mechanism ends up with the allyl formation from Au-OMP1 and PO due to limiting PO desorption reaction.

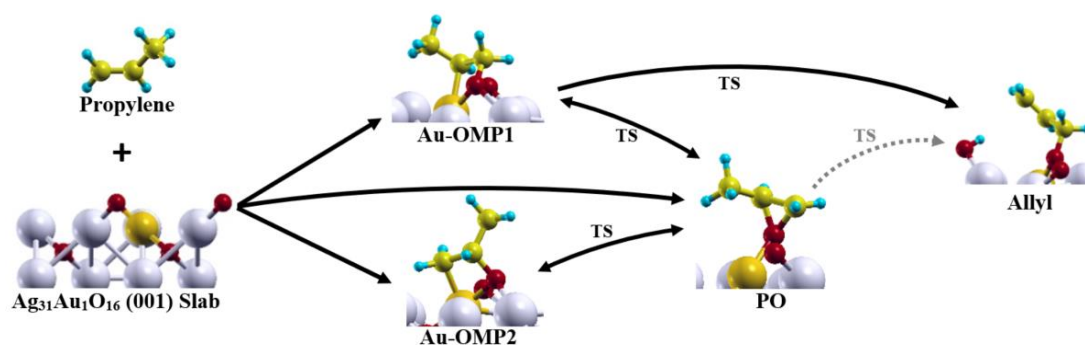


Figure 26: The most probable pathway on $\text{Ag}_{31}\text{Au}_1\text{O}_{16}$ (001) slab

4.4.2. Energetics on the $\text{Ag}_{30}\text{Au}_2\text{O}_{16}$ (001) Slab

The top layer of the unit cell of the $\text{Ag}_{30}\text{Au}_2\text{O}_{16}$ (001) slab has the Au/Ag ratio of 1/3 and the central oxygen atom of the top layer is bonded to two gold atoms as it is demonstrated in Figure 9. Top layer central site can be imagined as an Au_2O piece placed into the Ag_2O slab. At this Au_2O site, surface properties differ from the rest of the surface. Au-O bond length is measured as 1.95 Å whereas the Ag-O bond distance is 1.99 Å for the rest of the top layer. Electron densities of Au atoms are calculated as 10.55 which is slightly higher than the electron density of the silver atoms, 10.44, on the surface. Electron density of the oxygen atom of the Au_2O piece is calculated as 6.64 which is slightly lower than the electron density of the other surface oxygen atoms, 6.67, on the surface. Therefore, gold oxide site on the $\text{Ag}_{30}\text{Au}_2\text{O}_{16}$ (001) slab behaves differently than the $\text{Ag}_{32}\text{O}_{16}$ (001) slab.

Interaction of propylene with the Au₂O site of the Ag₃₀Au₂O₁₆ (001) slab gives OMP1, OMP2 and PO formation pathways without any activation barrier as it is shown in Figure 27. According to Table 5, direct allyl formation on the Ag₃₀Au₂O₁₆ (001) slab has an activation barrier to 3.0 eV, which is not included in Figure 27 for the better representation of the other energy levels. As it is seen from the picture of the PO in Figure 27, propylene oxide is positioned away from the surface. Level of the oxygen of the propylene oxide is measured 1.05 Å higher than the level of the other surface oxygen atoms on average. This pre-desorbed state of the PO makes it less stable and less favorable than the OMP intermediates. However, if the PO is formed, the weak interaction of PO with the surface helps its desorption from the surface.

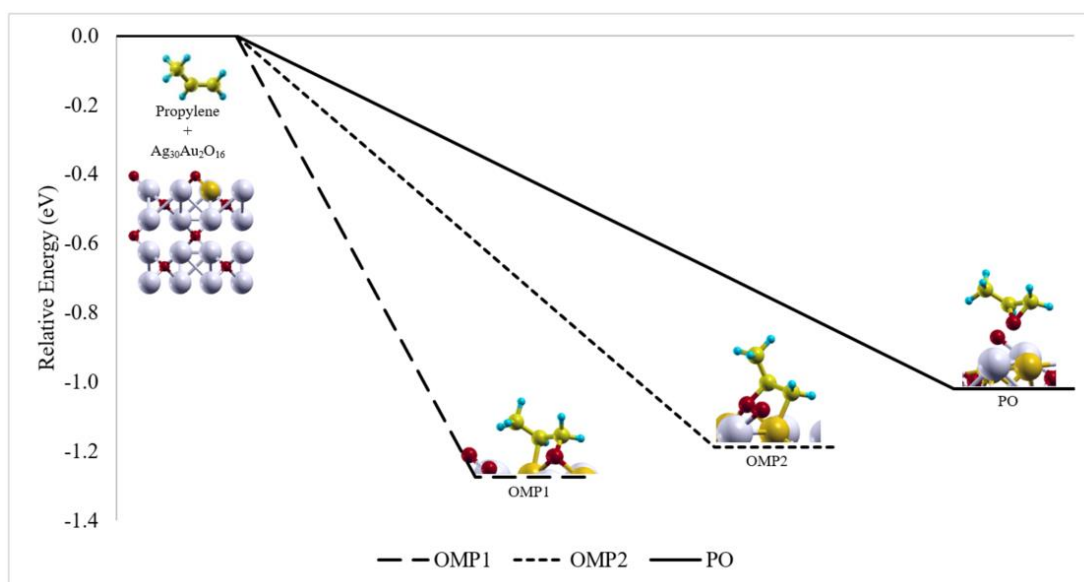


Figure 27: Energetics of direct propylene-surface interactions on Ag₃₀Au₂O₁₆ (001) slab

OMP1 and OMP2 intermediates are the most probable products of the first interaction of propylene and the Ag₃₀Au₂O₁₆ (001) slab. Even though they are more stable than PO, their interaction with the Ag₃₀Au₂O₁₆ (001) slab is weaker than the interaction they have on the pure silver oxide surface. Due to less interaction with the catalyst surface, pathways following the OMP1 and OMP2 intermediates are harder than the pathways on the Ag₃₂O₁₆ (001) slab. As it is given in Figure 28 and Table 5, allyl, PO and PA formation steps from OMP1 intermediate have activation barriers of 0.2 eV, 0.6 eV and 0.8 eV respectively. As it is also given in Table 5 and Figure 29, PO and

Ace formation from OMP2 intermediate have activation barriers of 1.0 eV and 1.1 eV respectively. More importantly, PO formation reactions from both OMP1 and OMP2 intermediates are endothermic on $\text{Ag}_{30}\text{Au}_2\text{O}_{16}$ (001) slab.

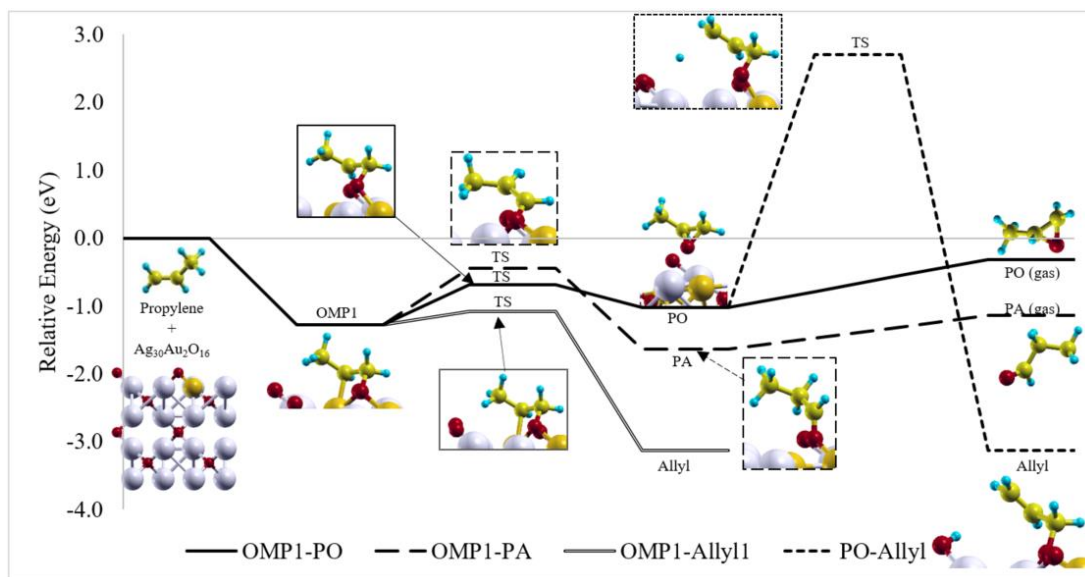


Figure 28: Energetics of the reactions through OMP1 on $\text{Ag}_{30}\text{Au}_2\text{O}_{16}$ (001) slab

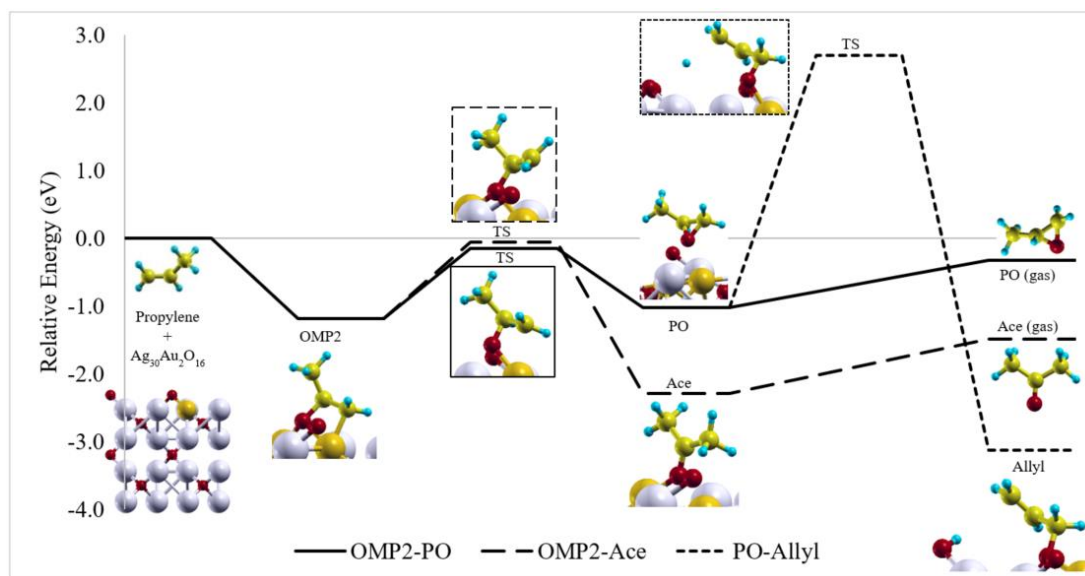


Figure 29: Energetics of the reactions through OMP2 on $\text{Ag}_{30}\text{Au}_2\text{O}_{16}$ (001) slab

Table 5: Activation barriers and reaction energies on Ag₃₀Au₂O₁₆ (001) slab

Reaction	Activation Barrier (eV)	Energy of Reaction (eV)
<i>Propylene</i> → <i>OMP1</i>		-1.3
<i>Propylene</i> → <i>OMP2</i>		-1.2
<i>Propylene</i> → <i>PO</i>		-1.0
<i>Propylene</i> → <i>Allyl</i>	3.0	-3.1
<i>OMP1</i> → <i>PO</i>	0.6	0.3
<i>OMP1</i> → <i>PA</i>	0.8	-0.4
<i>OMP1</i> → <i>Allyl</i>	0.2	-1.9
<i>OMP2</i> → <i>PO</i>	1.0	0.2
<i>OMP2</i> → <i>Ace</i>	1.1	-1.1
<i>PO</i> → <i>Allyl</i>	3.7	-2.1
<i>PO (ads)</i> → <i>PO (g)</i>		0.7
<i>PA (ads)</i> → <i>PA (g)</i>		0.5
<i>Ace (ads)</i> → <i>Ace (g)</i>		0.8
<i>Ag₃₀Au₂O₁₅</i> + ½ <i>O₂</i> → <i>Ag₃₀Au₂O₁₆</i>		-1.0

As Özbek [91] reported for ethylene oxide case, gold oxide results in lower desorption barriers than silver oxide. In propylene case studied here, the geometry and the position of the propylene oxide on the Ag₃₀Au₂O₁₆ (001) slab helps its desorption from the surface as it is expected. The desorption energy of PO from Ag₃₀Au₂O₁₆ (001) slab is calculated as 0.7 eV which is considerably lower than the desorption energy from the Ag₃₂O₁₆ (001) surface. The geometry of PO on Ag₃₀Au₂O₁₆ (001) slab also increases the barrier required to form allyl radical to 3.7 eV. The decrease in the PO desorption barrier and the significant increase in the barrier of the allyl radical formation from PO achieves to block PO to allyl pathway as it is desired at the beginning of the second phase of the study. However, more stable OMP1 intermediate makes direct PO formation pathway unfeasible. Once the OMP1 is formed, the easiest and the most probable pathway from OMP1 is the allyl formation pathway. Therefore, propylene interaction with Ag₃₀Au₂O₁₆ (001) slab follows the mechanism shown in Figure 30 and ends up with the allyl products. Consequently, gold doping cannot block all allyl formation pathways; so, cannot help the performance of the propylene oxide formation process.

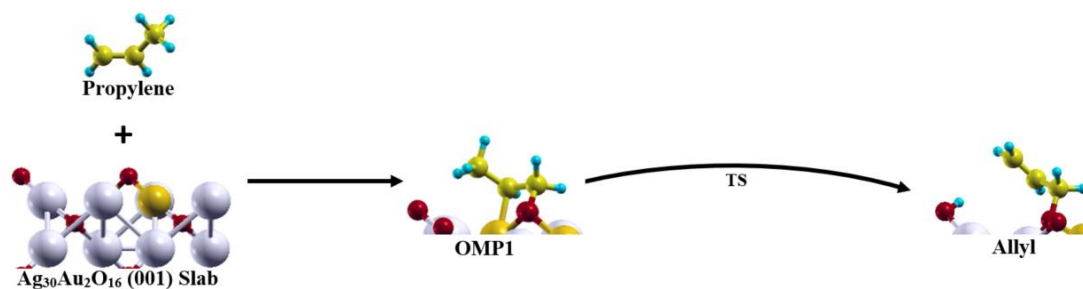


Figure 30: The most probable pathway on $\text{Ag}_{30}\text{Au}_2\text{O}_{16}$ (001) slab

4.5. Energetics on the Silver Oxide Slabs with Chlorine Doping

4.5.1. Energetics on the $\text{Ag}_{32}\text{O}_{15}\text{Cl}_1$ (001) Slab

$\text{Ag}_{32}\text{O}_{15}\text{Cl}_1$ (001) slab has 1/3 Cl/O ratio at the top layer. When the propylene molecule interacts with the top center oxygen atom, there are two different orientation alternatives according to the direction of the allylic end of the propylene molecule. According to the directions given in Figure 31, allylic hydrogens of the propylene, or the surface complexes, are in the vicinity of either chlorine atom (Direction A) or oxygen atom (Direction B). Therefore, first propylene-surface interaction determines the possibility of OH or HCl formation during the course of allyl radical formation pathway.

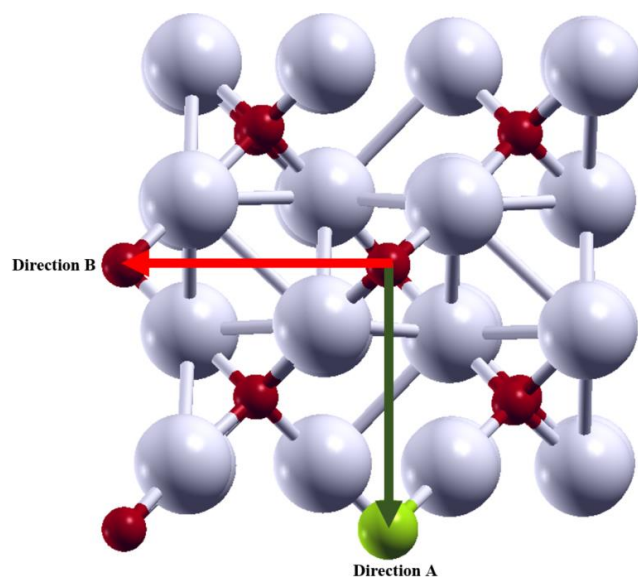


Figure 31: Reaction directions on $\text{Ag}_{32}\text{O}_{15}\text{Cl}_1$ (001) slab

The energetics of the first interaction between propylene and the $\text{Ag}_{32}\text{O}_{15}\text{Cl}_1$ (001) slab is given in Figure 32 and Table 6. Interaction profiles over the Cl modified surface favor direct PO formation and give the same behavior with the $\text{Ag}_{32}\text{O}_{16}$ (001) slab with a small decrease in the interaction energies. Since the direct allyl radical formation is found unfeasible on the first four scenarios, it is not included in the further studies. When the electronic properties of the $\text{Ag}_{32}\text{O}_{15}\text{Cl}_1$ (001) slab are examined, it is seen that the modification of silver oxide surface to have 1/3 Cl/O ratio at the top layer only slightly affects the electron density over the top center Ag_2O group, where the epoxidation is studied. As it is expected from the comments on the effect of Cl on the silver catalyst, the electron densities of the silver atoms are increased from 10.44 to 10.45 and the electron density of the lattice oxygen is increased from 6.68 to 6.69.

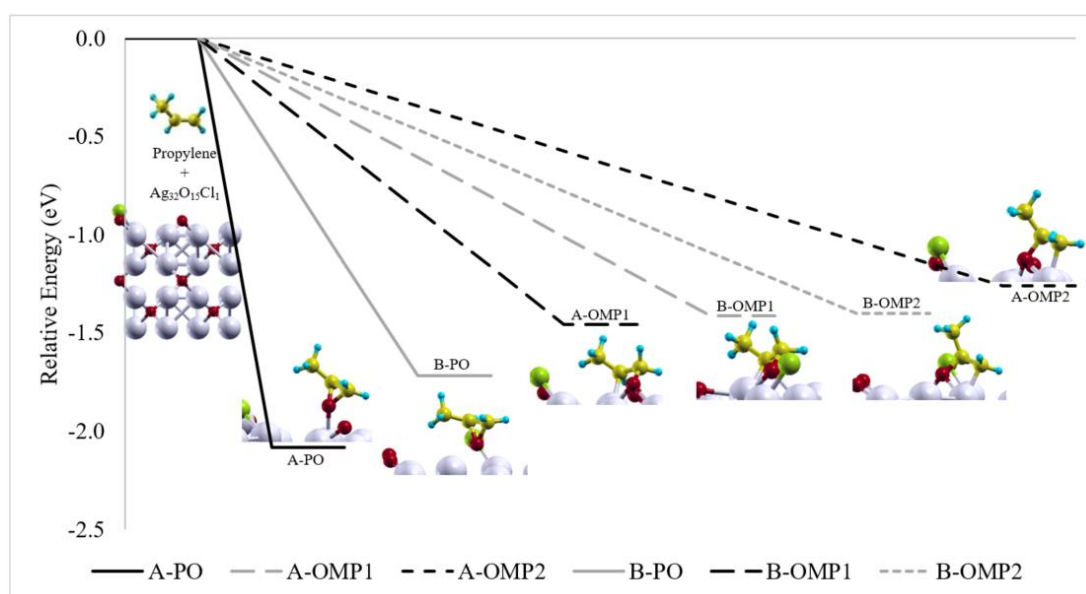


Figure 32: Energetics of direct propylene-surface interactions on $\text{Ag}_{32}\text{O}_{15}\text{Cl}_1$ (001) slab

The most probable pathways on the $\text{Ag}_{32}\text{O}_{15}\text{Cl}_1$ (001) slab should proceed through the direct PO formation pathways. Even their formation probabilities are less, OMP1 and OMP2 pathways are examined in the for both Direction A and B. Also, further reactions through PO formation are explained in this section.

As it is shown in Figure 33 and Table 6, the OMP1 intermediate is formed in the Direction A needs to overcome activation barriers of 0.2 eV and 0.6 eV to produce PO

and PA. Presence of Cl in the vicinity of the allylic hydrogen atoms of the OMP1 changes the allyl formation performance of the OMP1 intermediate drastically. The energy of Cl adsorption to the oxygen vacancy of silver oxide surface is calculated as -1.9 eV whereas oxygen adsorption energy for the same vacancy is only -0.1 eV. Therefore, Cl atom strongly binds the surface silvers and does not attack the allylic hydrogens of the OMP1 intermediate as strong as the oxygen atom. Allyl formation due to H-Cl interaction needs to overcome activation barriers of 0.7 eV for OMP1 and 1.3 eV for PO. Therefore, allyl formation on the Direction A is not probable on the $\text{Ag}_{32}\text{O}_{15}\text{Cl}_1$ (001) slab from neither OMP1 nor PO. As a result, OMP1 formation on Direction A should result in gas phase PO formation.

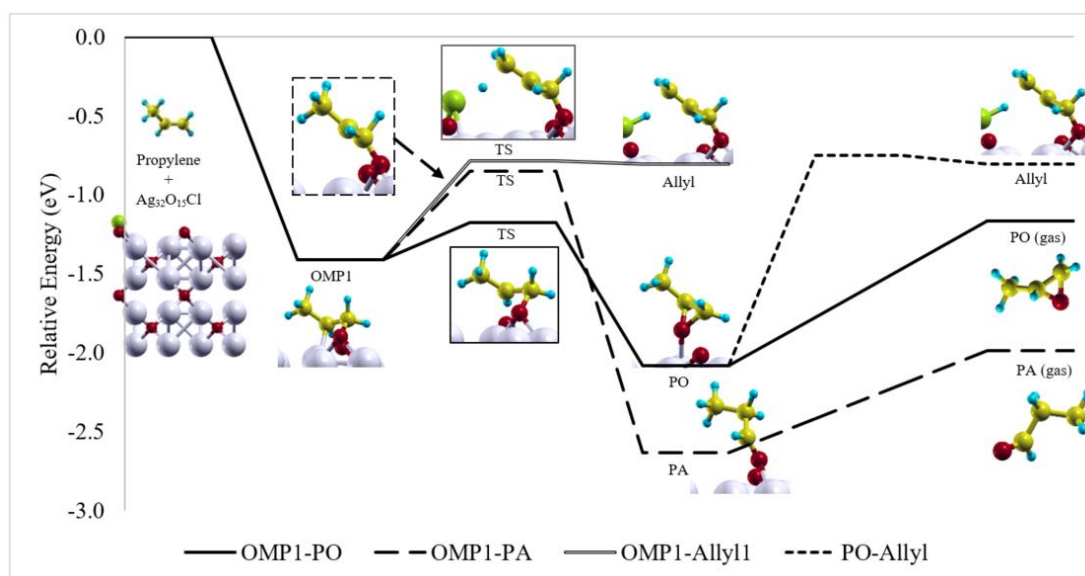


Figure 33: Energetics of the reactions through OMP1 on $\text{Ag}_{32}\text{O}_{15}\text{Cl}_1$ (001) slab on Direction A

Like in the OMP1 case, both PO and Ace formation from OMP2 in the Direction A have activation barriers as it is given in Figure 34. These activation barriers for PO and Ace formation pathways from OMP2 intermediate are calculated as 0.2 eV and 0.8 eV respectively. Therefore, OMP2 formation also results in gas phase PO.

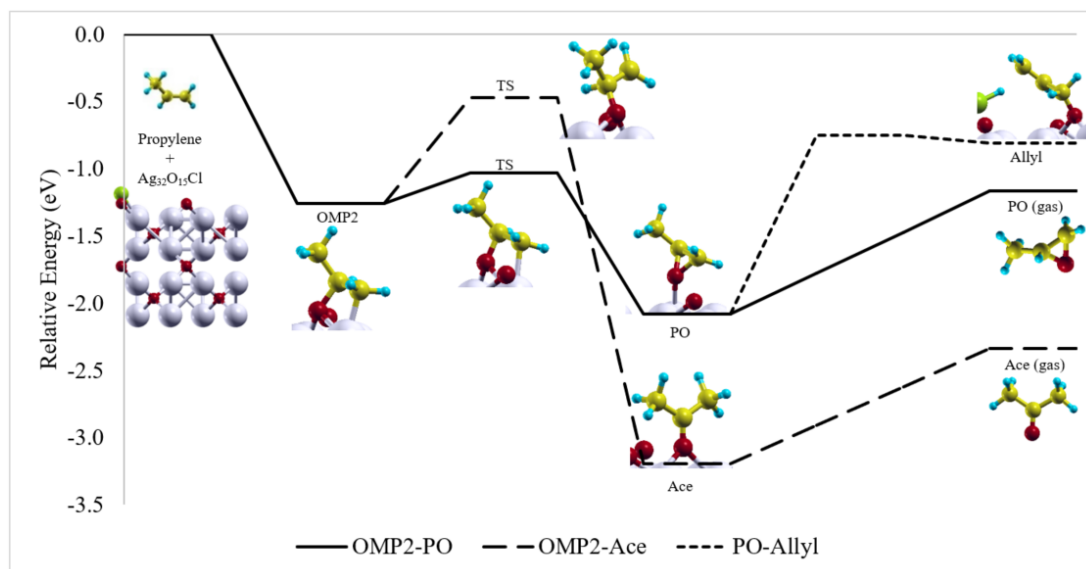


Figure 34: Energetics of the reactions through OMP2 on $\text{Ag}_{32}\text{O}_{15}\text{Cl}_1$ (001) slab on Direction A

When the propylene molecule approaches to the $\text{Ag}_{32}\text{O}_{15}\text{Cl}_1$ (001) slab by positioning its allylic hydrogen towards the neighbor oxygen atom as it is demonstrated as Direction B in Figure 31, allyl formation pathway becomes favorable with small activation barrier as it is shown in Figure 35. According to Figure 35 and Table 6, Allyl, PO and PA formation pathways from OMP1 have activation barriers of 0.1 eV, 0.2 eV and 0.4 eV respectively. Therefore, the formation of OMP1 in Direction B should result in allyl radical formation.

Even though OMP1 cannot produce PO, direct PO formation is more probable than OMP1 formation in Direction B. Therefore, reactions and the desorption of propylene oxide are still important on this surface. It is calculated that 0.6 eV is required for the desorption of PO whereas allyl radical formation and OMP1 formation from PO needs to overcome activation barriers of 0.4 eV and 0.5 eV. Therefore, it is concluded that the possible PO formation on the $\text{Ag}_{32}\text{O}_{15}\text{Cl}_1$ (001) slab in Direction B ends up with products associated with allyl production.

OMP2 formation in Direction B can be followed by the reactions towards PO and Ace with activation barriers of 0.4 eV and 0.9 eV as shown in Figure 36. Therefore, PO formation pathway should be followed after the OMP2 formation step. However, like

in the OMP1 case, PO produced from OMP2 proceeds through allyl formation routes instead of desorption to the gas phase.

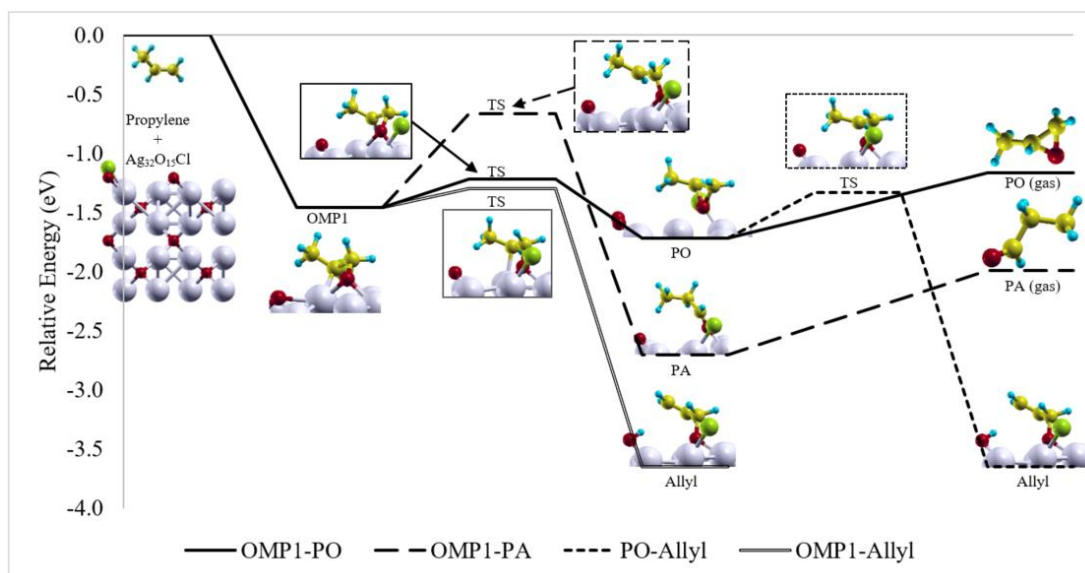


Figure 35: Energetics of the reactions through OMP1 on $\text{Ag}_{32}\text{O}_{15}\text{Cl}_1$ (001) slab on Direction B

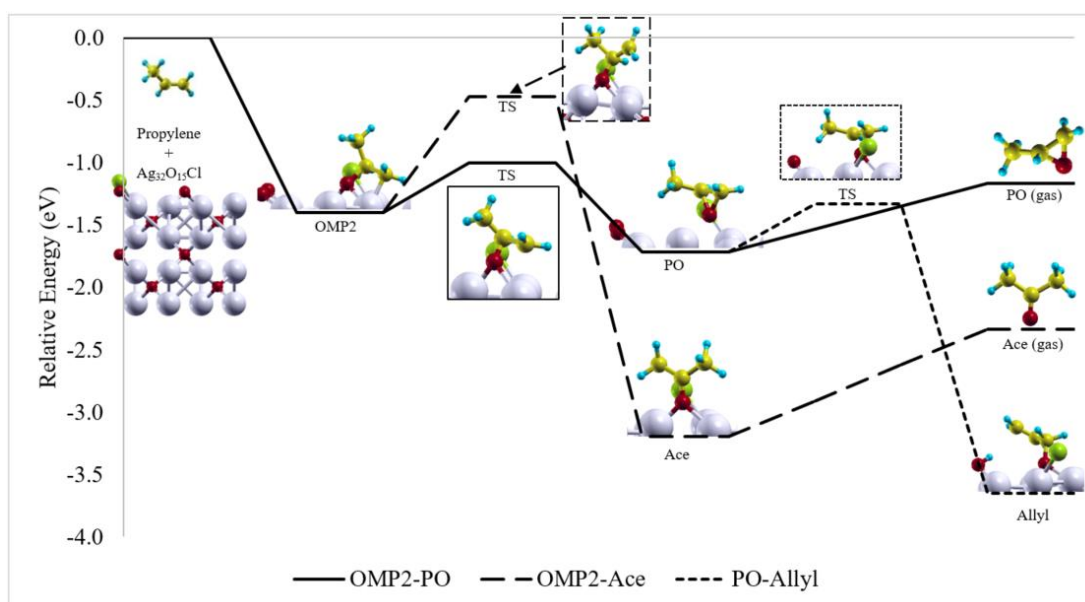


Figure 36: Energetics of the reactions through OMP2 on $\text{Ag}_{32}\text{O}_{15}\text{Cl}_1$ (001) slab on Direction B

Table 6: Activation barriers and reaction energies on Ag₃₂O₁₅Cl₁ (001) slab

Reaction	Activation Barrier (eV)	Energy of Reaction (eV)
<i>Propylene</i> → <i>OMP1</i> (Direction A)	-	-1.4
<i>Propylene</i> → <i>OMP2</i> (Direction A)	-	-1.3
<i>Propylene</i> → <i>PO</i> (Direction A)	-	-2.1
<i>OMP1</i> → <i>PO</i> (Direction A)	0.2	-0.7
<i>OMP1</i> → <i>PA</i> (Direction A)	0.6	-1.2
<i>OMP1</i> → <i>Allyl</i> (Direction A)	0.7	0.6
<i>OMP2</i> → <i>PO</i> (Direction A)	0.2	-0.8
<i>OMP2</i> → <i>Ace</i> (Direction A)	0.8	-1.9
<i>PO</i> → <i>Allyl</i> (Direction A)	1.3	1.3
<i>PO</i> (ads) → <i>PO</i> (g) (Direction A)		0.9
<i>PA</i> (ads) → <i>PA</i> (g) (Direction A)		0.6
<i>Ace</i> (ads) → <i>Ace</i> (g) (Direction A)		0.9
<i>Propylene</i> → <i>OMP1</i> (Direction B)	-	-1.5
<i>Propylene</i> → <i>OMP2</i> (Direction B)	-	-1.4
<i>Propylene</i> → <i>PO</i> (Direction B)	-	-1.7
<i>OMP1</i> → <i>PO</i> (Direction B)	0.2	-0.3
<i>OMP1</i> → <i>PA</i> (Direction B)	0.4	-1.3
<i>OMP1</i> → <i>Allyl</i> (Direction B)	0.1	-1.0
<i>OMP2</i> → <i>PO</i> (Direction B)	0.4	-0.3
<i>OMP2</i> → <i>Ace</i> (Direction B)	0.9	-1.8
<i>PO</i> → <i>Allyl</i> (Direction B)	0.4	-1.9
<i>PO</i> (ads) → <i>PO</i> (g) (Direction B)		0.6
<i>PA</i> (ads) → <i>PA</i> (g) (Direction B)		0.7
<i>Ace</i> (ads) → <i>Ace</i> (g) (Direction B)		0.9
Ag ₃₂ O ₁₄ Cl ₁ + ½ O ₂ → Ag ₃₂ O ₁₅ Cl ₁		-0.1

As a conclusion, the interaction of propylene molecule with Ag₃₂O₁₅Cl₁ (001) slab produces propylene oxide in Direction A in the first interaction step as it is shown in Figure 37. Thanks to the presence of Cl atom instead of oxygen, this propylene oxide cannot react to form allyl radical easily and desorbs from the surface by leaving an oxygen vacancy behind. In order to complete the catalysis cycle and the stoichiometry of the (C₃H₆ + ½ O₂ → C₃H₆O) reaction, oxygen adsorption follows the desorption step with -0.1 eV adsorption energy. Therefore, Ag₃₂O₁₅Cl₁ (001) slab favors gas phase propylene oxide formation pathway and achieves the second goal of the study.

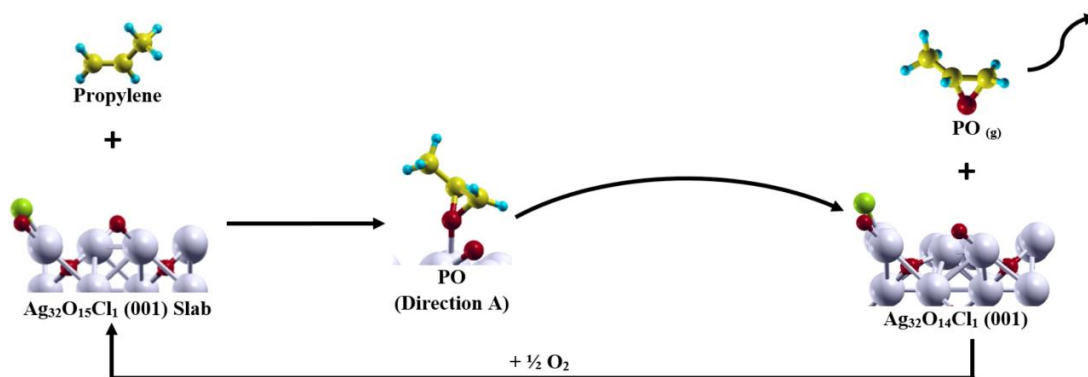


Figure 37: The most probable pathway on $\text{Ag}_{32}\text{O}_{15}\text{Cl}_1$ (001) slab

4.5.2. Energetics on the $\text{Ag}_{32}\text{O}_{14}\text{Cl}_2$ (001) Slab

$\text{Ag}_{32}\text{O}_{14}\text{Cl}_2$ (001) slab has one to one Cl to O ratio at the top layer. Modification of the top layer of silver oxide surface by replacing two lattice oxygen atoms with two chlorine atoms increases the electron density of the surface lattice oxygen atom from 6.68 to 6.74. Electron density of the silver atoms connected to the surface lattice oxygens also increases from 10.44 to 10.47. This shift in the electron density decreases the PO, OMP1 and OMP2 formation energies on the silver oxide surface. As it is shown in Figure 38 and Table 7, the interaction between the propylene molecule and the $\text{Ag}_{32}\text{O}_{14}\text{Cl}_2$ (001) slab results -1.1 eV, -1.2 eV and -1.7 eV for OMP1, OMP2 and PO respectively. According to energetics in Figure 38, the interaction of propylene molecule with the $\text{Ag}_{32}\text{O}_{14}\text{Cl}_2$ (001) slab most probably results in direct PO formation.

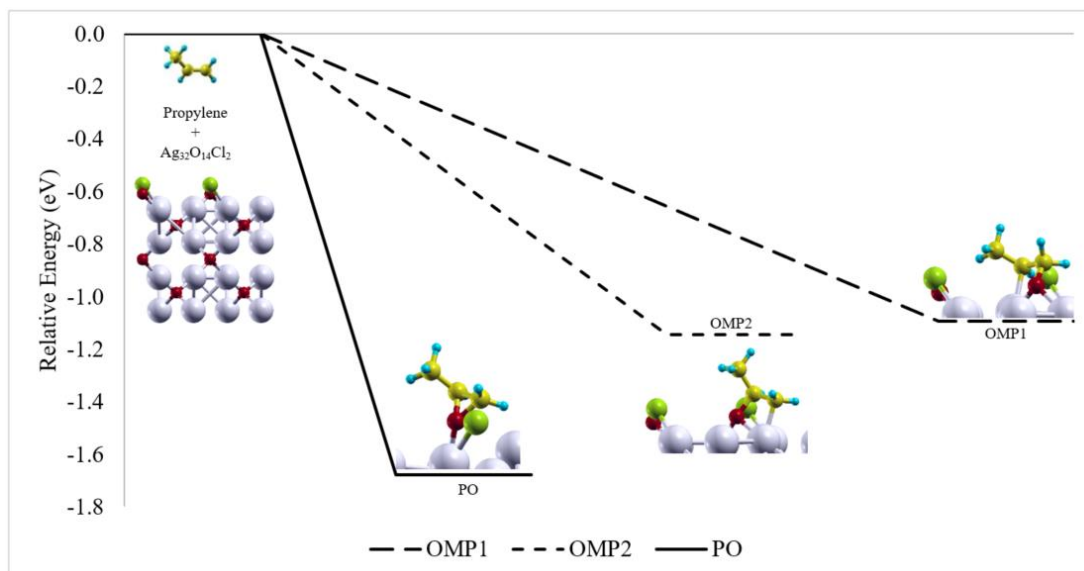


Figure 38: Energetics of direct propylene-surface interactions on $\text{Ag}_{32}\text{O}_{14}\text{Cl}_2$ (001) slab

Figure 39 and Figure 40 showing the possible pathways from OMP1 and OMP2 intermediates give similar profiles to the figures supplied for the Direction A of the $\text{Ag}_{32}\text{O}_{15}\text{Cl}_1$ (001) slab. Activation barriers for PO and PA pathways are calculated as 0.2 eV and 0.3 eV for OMP1 intermediate and the barriers for PO and Ace are calculated as 0.3 eV and 0.8 eV for OMP2 intermediate. It is found that the allyl radical formation from OMP1 intermediate and PO via hydrogen abstraction by chlorine atom have activation barriers of 0.4 eV and 0.9 eV respectively. Like in the $\text{Ag}_{32}\text{O}_{15}\text{Cl}_1$ (001) slab case, Cl atoms of the $\text{Ag}_{32}\text{O}_{14}\text{Cl}_2$ (001) slab prefers to connect silver atoms of the surface. Hence, their effect on the allylic hydrogens of propylene is weaker than the oxygen atoms. The interaction between the allylic hydrogen of the OMP1 intermediate and the only neighbor lattice oxygen atom, which is 3.5 Å away from the hydrogen, is additionally investigated and activation barrier for this reaction is calculated as 2.9 eV. Therefore, this reaction is definitely not probable. In the end, the formation of both OMP1 and OMP2 intermediates favored the propylene oxide formation in the gas phase.

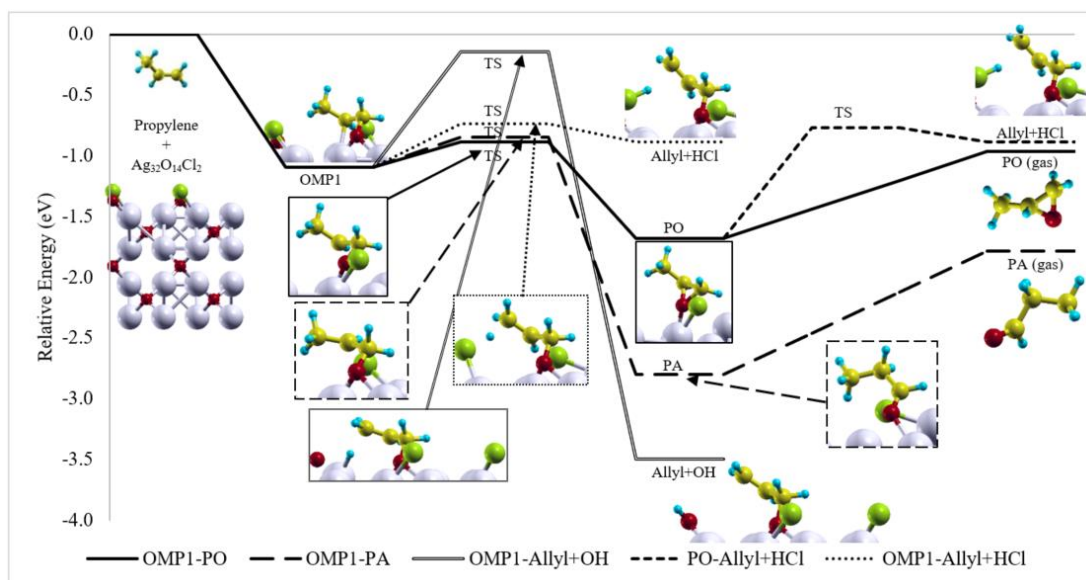


Figure 39: Energetics of the reactions through OMP1 on $\text{Ag}_{32}\text{O}_{14}\text{Cl}_2$ (001) slab

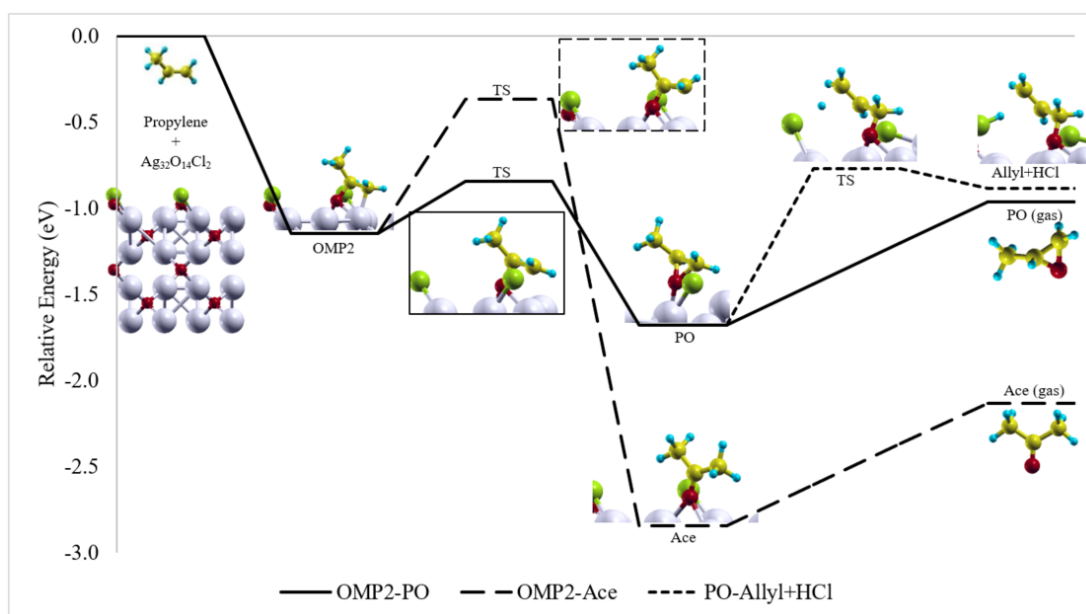


Figure 40: Energetics of the reactions through OMP2 on $\text{Ag}_{32}\text{O}_{14}\text{Cl}_2$ (001) slab

Table 7: Activation barriers and reaction energies on Ag₃₂O₁₄Cl₂ (001) slab

Reaction	Activation Barrier (eV)	Energy of Reaction (eV)
<i>Propylene</i> → <i>OMP1</i>	-	-1.1
<i>Propylene</i> → <i>OMP2</i>	-	-1.2
<i>Propylene</i> → <i>PO</i>	-	-1.7
<i>OMP1</i> → <i>PO</i>	0.2	-0.6
<i>OMP1</i> → <i>PA</i>	0.3	-1.7
<i>OMP1</i> → <i>Allyl</i> + <i>OH</i>	1.0	-2.4
<i>OMP1</i> → <i>Allyl</i> + <i>HCl</i>	0.4	0.2
<i>OMP2</i> → <i>PO</i>	0.3	-0.5
<i>OMP2</i> → <i>Ace</i>	0.8	-1.7
<i>PO</i> → <i>Allyl</i> + <i>OH</i>	2.9	-1.8
<i>PO</i> → <i>Allyl</i> + <i>HCl</i>	0.9	0.8
<i>PO (ads)</i> → <i>PO (g)</i>		0.7
<i>PA (ads)</i> → <i>PA (g)</i>		1.0
<i>Ace (ads)</i> → <i>Ace (g)</i>		0.7
Ag ₃₂ O ₁₃ Cl ₂ + ½ O ₂ → Ag ₃₂ O ₁₄ Cl ₂		-0.3

Like Ag₃₂O₁₅Cl₁ (001) slab, Ag₃₂O₁₄Cl₂ (001) slab favors PO formation in the gas phase at the end of the mechanism as it is shown in Figure 41. After the propylene oxide is desorbed from the surface by creating a surface vacancy, oxygen adsorption reaction takes place with a reaction energy of -0.3 eV. The adsorption of the oxygen atom to the surface vacancy restores the Ag₃₂O₁₄Cl₂ (001) slab to its initial state and completes the catalytic cycle. In this manner, the Ag₃₂O₁₄Cl₂ (001) slab also fulfills the second goal of the study.

The theoretical results on the Ag₃₂O₁₅Cl₁ (001) and Ag₃₂O₁₄Cl₂ (001) slabs showed that there are indeed electronic changes in the surface oxygen and silver atoms due to the Cl addition as it is proposed by the experimental work of Lu for propylene epoxidation on silver catalyst [81]. This electron flow towards silver and oxygen atoms decreases the interaction energy of PO with the surface and helps PO desorption. However, the theoretical results show that the main reason for the improvement on the PO selectivity made by the Cl addition is the physical effect of Cl on the silver oxide surface. Cl blocks the active oxygen sites by replacing the lattice oxygen. Since the Cl atoms on the silver catalyst have less affinity towards the hydrogen atoms of the

propylene than the oxygen atoms have, Cl presence blocks the allyl formation reactions physically.

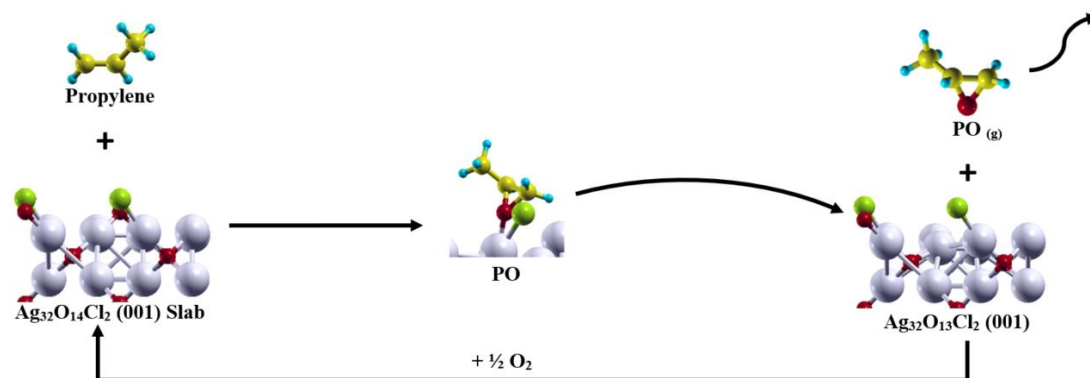


Figure 41: The most probable pathway on $\text{Ag}_{32}\text{O}_{14}\text{Cl}_2$ (001) slab

4.6. Energetics on the Silver Oxide Slabs with both Gold and Chlorine Doping

4.6.1. Energetics on the $\text{Ag}_{31}\text{Au}_1\text{O}_{15}\text{Cl}_1$ (001) Slab

$\text{Ag}_{31}\text{Au}_1\text{O}_{15}\text{Cl}_1$ (001) slab is prepared with one silver-gold and one chlorine-oxygen replacements as it is explained in Chapter 3. The surface of the slab has 1/7 Au/Ag and 1/3 Cl/O ratio and surface layer formula can be simply written as $\text{Ag}_7\text{Au}_1\text{O}_3\text{Cl}_1$. There are four different possibilities for the investigation of the reactions on this surface. Two of the possible interactions are the silver side and gold side interactions over the top center lattice oxygen. Then, these two options also have Cl and O directions according to the position of the propylene molecule. Since the silver side simulations on the $\text{Ag}_{31}\text{Au}_1\text{O}_{16}$ (001) slab give very similar results with the $\text{Ag}_{32}\text{O}_{16}$ (001) slab, only the pathways towards Au side are considered for $\text{Ag}_{31}\text{Au}_1\text{O}_{15}\text{Cl}_1$ (001) slab in directions A and B demonstrated in Figure 42. According to the energetics data supplied in Figure 43 and Table 8, direct PO formation pathways are the most probable result of propylene-surface interaction in both A and B directions. According to data, modifying silver oxide surface with both chlorine and gold reduces the difference between the energy levels of PO and the OMP intermediates. As the initial propylene-surface interaction, $\text{Ag}_{31}\text{Au}_1\text{O}_{15}\text{Cl}_1$ (001) slab favors PO formation like $\text{Ag}_{32}\text{O}_{16}$ and $\text{Ag}_{32}\text{O}_{15}\text{Cl}_1$ slabs. Additionally, like $\text{Ag}_{31}\text{Au}_1\text{O}_{16}$ slab, $\text{Ag}_{31}\text{Au}_1\text{O}_{15}\text{Cl}_1$ (001) slab has close energy levels for PO and the gold side OMP intermediates. Therefore, the impact

of the OMP pathways should be observed alongside with the direct PO pathways in the experimental conditions.

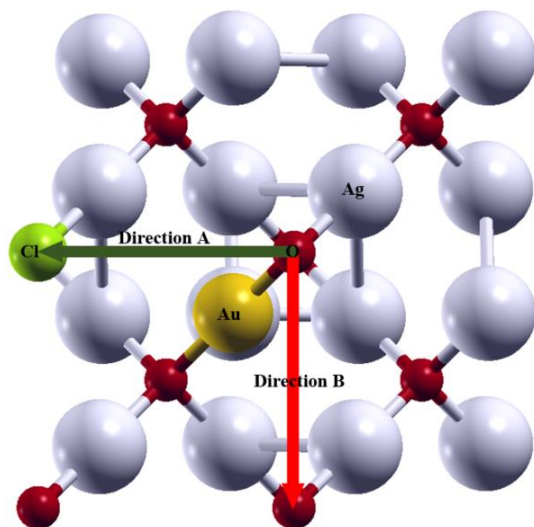


Figure 42: Reaction directions on $\text{Ag}_{31}\text{Au}_1\text{O}_{15}\text{Cl}_1$ (001) slab

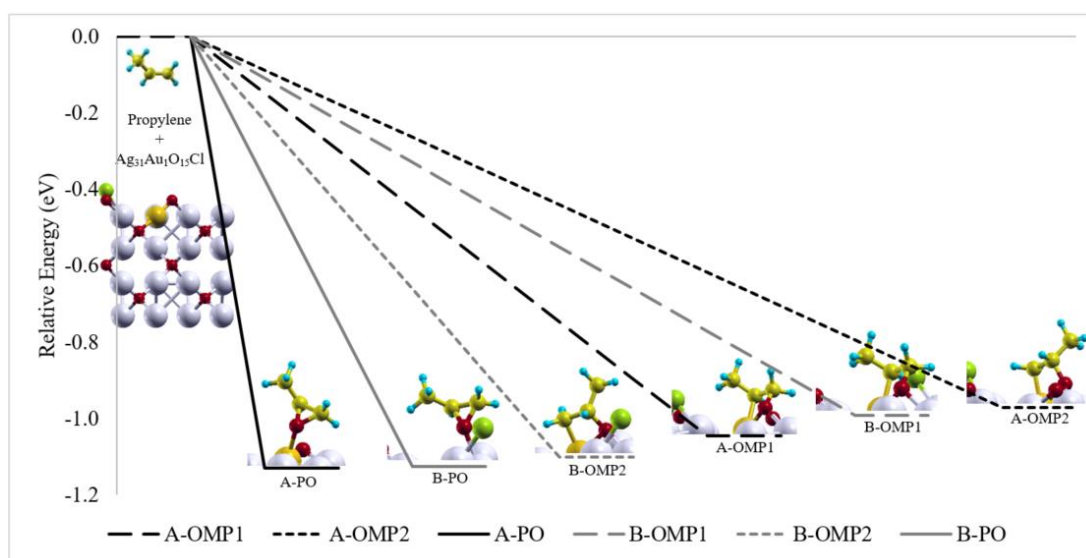


Figure 43: Energetics of direct propylene-surface interactions on $\text{Ag}_{31}\text{Au}_1\text{O}_{15}\text{Cl}_1$ (001) slab

OMP1 and OMP2 intermediates can be formed with the reaction energies around -1.0 eV in the Direction A on $\text{Ag}_{31}\text{Au}_1\text{O}_{15}\text{Cl}_1$ (001). Once the OMP1 intermediate is formed on the surface, the reaction can further proceed through PO, PA or allyl (with Cl-H activation) formation pathways. Since the relatively weaker interaction of OMP1

with the $\text{Ag}_{31}\text{Au}_1\text{O}_{15}\text{Cl}_1$ (001) slab PO, PA and allyl formation from OMP1 steps have relatively high activation barriers of 0.6 eV, 0.7 eV and 0.8 eV respectively. According to this data, also shown in Figure 44, PO formation path is the most probable pathway among these three routes. Since the allyl and OMP1 formation from the propylene oxide is harder than the desorption of PO, OMP1 formation on Direction A on $\text{Ag}_{31}\text{Au}_1\text{O}_{15}\text{Cl}_1$ (001) ends up with gas PO as the product. Like OMP1 mechanism, OMP2 formation on the $\text{Ag}_{31}\text{Au}_1\text{O}_{15}\text{Cl}_1$ (001) slab also follows the PO formation pathway with an activation barrier of 0.8 eV, instead of Ace formation which needs to overcome 1.1 eV. Figure 45 shows the relative energies of these two reaction pathways.

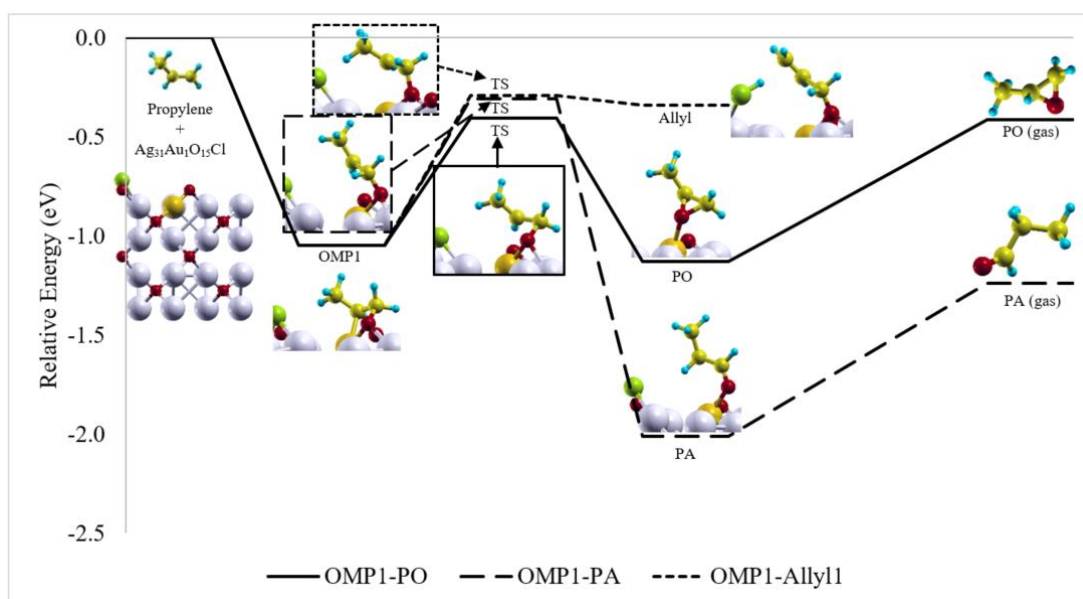


Figure 44: Energetics of the reactions through OMP1 on $\text{Ag}_{31}\text{Au}_1\text{O}_{15}\text{Cl}_1$ (001) slab on Direction A

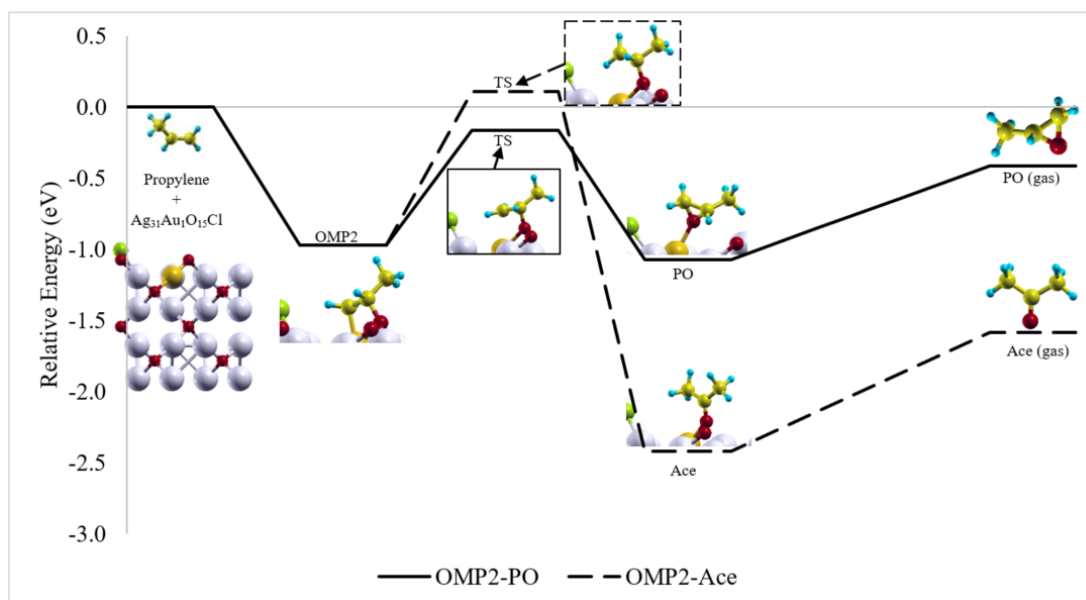


Figure 45: Energetics of the reactions through OMP2 on $\text{Ag}_{31}\text{Au}_1\text{O}_{15}\text{Cl}_1$ (001) slab on Direction A

If the interaction of propylene with the $\text{Ag}_{31}\text{Au}_1\text{O}_{15}\text{Cl}_1$ (001) slab yields OMP1 on Direction B, allylic hydrogen atoms of the propylene molecule come close to the neighbor lattice oxygen. Then lattice oxygen attacks the allylic hydrogen without any activation barrier to form allyl radical and OH on the surface. In order to produce PO and PA from OMP1, activation barriers of 0.4 eV and 0.5 eV should be overcome. Therefore, allyl formation is the most probable pathway from OMP1 as it is also shown in Figure 46. On the other way, when OMP2 is formed, there are 0.8 eV and 0.9 eV activation barriers for PO and Ace formations. As it is shown in Figure 47, PO formed on direction B needs 0.7 eV to desorb from the surface when allyl formation from PO requires 0.9 eV. Therefore, PO desorption is more probable than the allyl formation pathway from PO. However, if Figure 46 is examined again, it can be seen that OMP1 formation from PO requires an activation barrier of only 0.5 eV which is lower than both PO desorption and allyl formation. Therefore, OMP2 formation pathway continues as OMP1 pathway after PO formation and ends up with allyl radical formation.

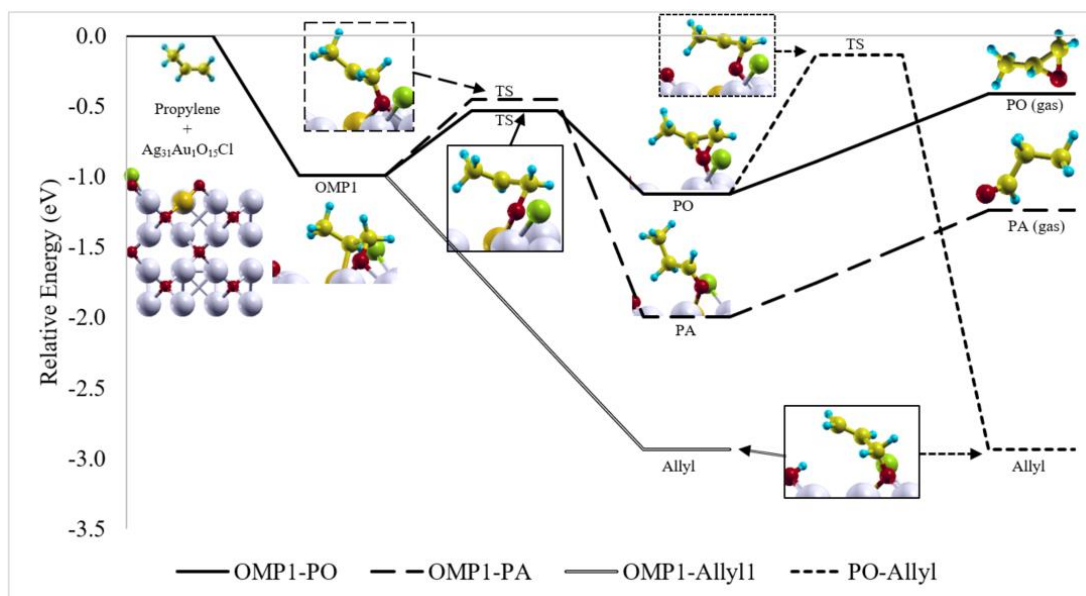


Figure 46: Energetics of the reactions through OMP1 on $\text{Ag}_{31}\text{Au}_1\text{O}_{15}\text{Cl}_1$ (001) slab on Direction B

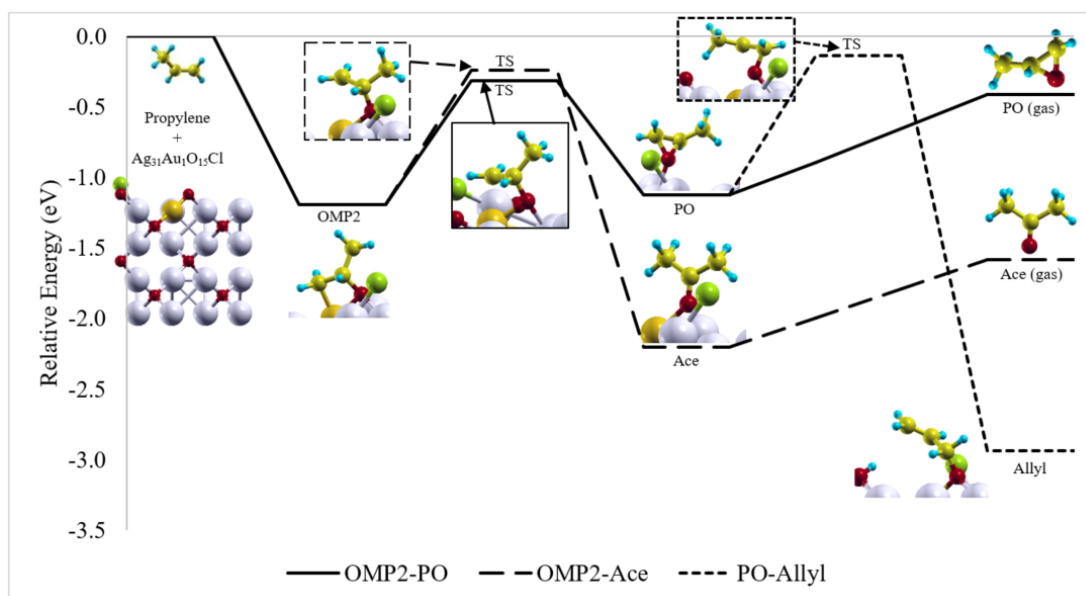


Figure 47: Energetics of the reactions through OMP2 on $\text{Ag}_{31}\text{Au}_1\text{O}_{15}\text{Cl}_1$ (001) slab on Direction B

Table 8: Activation barriers and reaction energies on Ag₃₁Au₁O₁₅Cl₁ (001) slab

Reaction	Activation Barrier (eV)	Energy of Reaction (eV)
<i>Propylene</i> → <i>OMP1</i> (Direction A)	-	-1.0
<i>Propylene</i> → <i>OMP2</i> (Direction A)	-	-1.0
<i>Propylene</i> → <i>PO</i> (Direction A)	-	-1.1
<i>OMP1</i> → <i>PO</i> (Direction A)	0.6	-0.1
<i>OMP1</i> → <i>PA</i> (Direction A)	0.7	-1.0
<i>OMP1</i> → <i>Allyl</i> (Direction A)	0.8	0.7
<i>OMP2</i> → <i>PO</i> (Direction A)	0.8	-0.2
<i>OMP2</i> → <i>Ace</i> (Direction A)	1.1	-1.4
<i>PO</i> → <i>Allyl</i> (Direction A)		0.8
<i>PO</i> (ads) → <i>PO</i> (g) (Direction A)		0.7
<i>PA</i> (ads) → <i>PA</i> (g) (Direction A)		0.8
<i>Ace</i> (ads) → <i>Ace</i> (g) (Direction A)		0.6
<i>Propylene</i> → <i>OMP1</i> (Direction B)	-	-1.0
<i>Propylene</i> → <i>OMP2</i> (Direction B)	-	-1.1
<i>Propylene</i> → <i>PO</i> (Direction B)	-	-1.1
<i>OMP1</i> → <i>PO</i> (Direction B)	0.4	-0.1
<i>OMP1</i> → <i>PA</i> (Direction B)	0.5	-1.0
<i>OMP1</i> → <i>Allyl</i> (Direction B)	-	-1.9
<i>OMP2</i> → <i>PO</i> (Direction B)	0.8	0.0
<i>OMP2</i> → <i>Ace</i> (Direction B)	0.9	-1.1
<i>PO</i> → <i>Allyl</i> (Direction B)	0.9	-1.8
<i>PO</i> (ads) → <i>PO</i> (g) (Direction B)		0.7
<i>PA</i> (ads) → <i>PA</i> (g) (Direction B)		0.8
<i>Ace</i> (ads) → <i>Ace</i> (g) (Direction B)		0.8
Ag ₃₁ Au ₁ O ₁₄ Cl ₁ + ½ O ₂ → Ag ₃₁ Au ₁ O ₁₅ Cl ₁		-0.9

As a summary, the data in Table 8 and Figures 43-47 shows that interaction of propylene molecule with Ag₃₁Au₁O₁₅Cl₁ (001) slab most probably leads PO in both A and B directions indicated in Figure 41. As it is demonstrated in Figure 48, PO formed in direction B cannot desorb from the surface and produce OMP1. Then this OMP1 on the direction B proceeds through allyl formation resulting acrolein production or further oxidation. Fortunately, PO formed in Direction A most probably desorbs from the catalyst surface by leaving an oxygen vacancy behind. Then reaction continues with an oxygen adsorption step with a reaction energy of -0.9 eV to recover the silver oxide slab to its initial state. Hereby, the oxygen adsorption step completes the catalytic cycle and completes the C₃H₆ + ½ O₂ → C₃H₆O reaction. According to these

results, more PO should be observed than the allyl pathway products in the propylene epoxidation reaction on $\text{Ag}_{31}\text{Au}_1\text{O}_{15}\text{Cl}_1$ (001) slab.

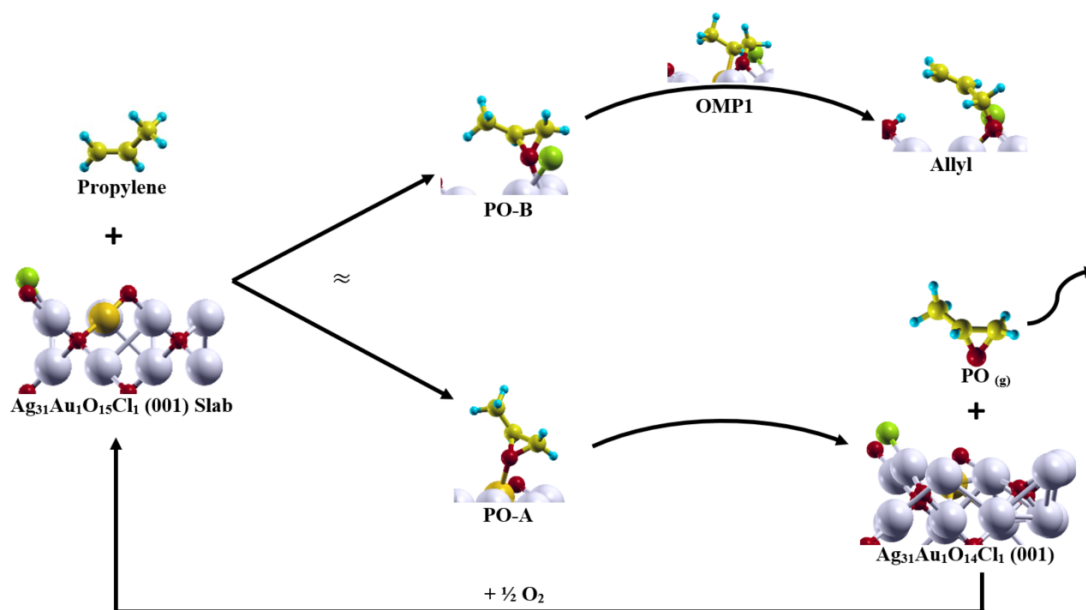


Figure 48: The most probable pathway on $\text{Ag}_{31}\text{Au}_1\text{O}_{15}\text{Cl}_1$ (001) slab

4.6.2. Energetics on the $\text{Ag}_{31}\text{Au}_1\text{O}_{14}\text{Cl}_2$ (001) Slab

Initial interaction between the propylene molecule and the $\text{Ag}_{31}\text{Au}_1\text{O}_{14}\text{Cl}_2$ (001) slab results in OMP1 formation slightly more favorable than the OMP2 and PO options as it is shown in Figure 49. It can be said that the difference between the energy levels become negligibly small for $\text{Ag}_{31}\text{Au}_1\text{O}_{14}\text{Cl}_2$ (001) slab. As a result of the gold and Cl doping, interaction of the OMP intermediates and the propylene oxide with the surface is lower than the interaction energies on the pure silver oxide surface. Bader charge analysis shows that the electron density of the center top oxygen atom slightly decreases from 6.68 to 6.67. Therefore, the effect of gold on the charge distribution around the top center lattice oxygen of the $\text{Ag}_{31}\text{Au}_1\text{O}_{14}\text{Cl}_2$ (001) surface is higher than the effect of the chlorine atoms.

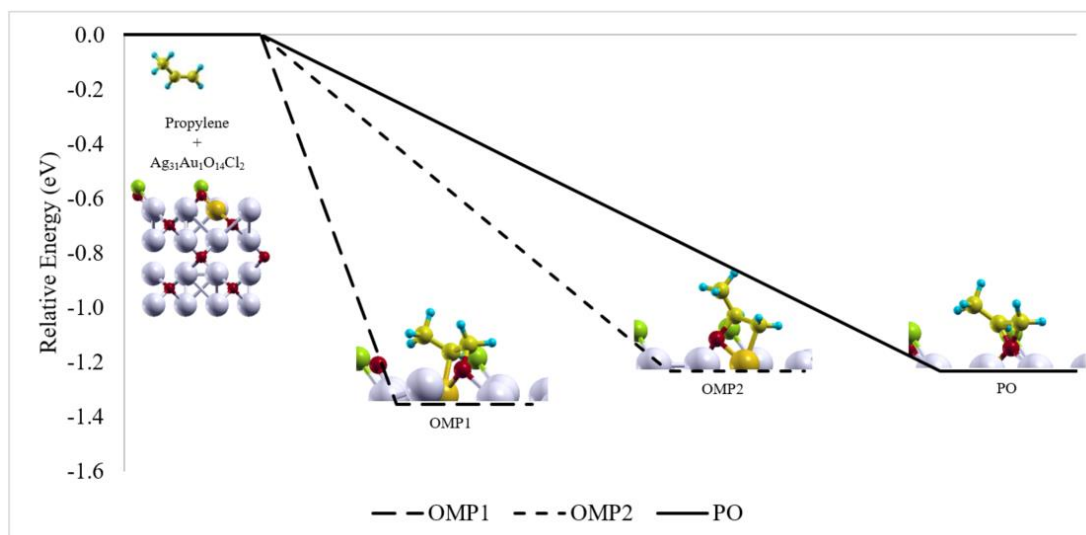


Figure 49: Energetics of direct propylene-surface interactions on $\text{Ag}_{31}\text{Au}_1\text{O}_{14}\text{Cl}_2$ (001) slab

Activation barriers for the formation of PO, PA and allyl radical from OMP1 intermediate are reported as 0.8 eV, 1.1 eV and 1.2 eV respectively. Therefore, PO formation step follows the OMP1 formation on the $\text{Ag}_{31}\text{Au}_1\text{O}_{14}\text{Cl}_2$ (001) slab. As it is also observed in the $\text{Ag}_{32}\text{O}_{14}\text{Cl}_2$ (001) slab, replacement of the nearest two lattice oxygens with chlorine prevents OH formation on the surface and HCl formation becomes the only option leading allyl formation on the surface. Since the interaction of Cl atom with silver is stronger than the interaction of Cl with H, OMP1 to allyl formation pathway on $\text{Ag}_{31}\text{Au}_1\text{O}_{14}\text{Cl}_2$ (001) slab results in this high activation barrier. Similar to the allyl formation from OMP1, allyl formation from PO also requires a high activation barrier value of 1.2 eV, which is shown in Figure 50 and Table 9. When the two allyl formation pathways are eliminated, PO desorption with 0.6 eV desorption barrier becomes the most probable pathway following the OMP1 and PO formation steps. When OMP2 is formed on the $\text{Ag}_{31}\text{Au}_1\text{O}_{14}\text{Cl}_2$ (001) slab, the reaction can proceed through PO formation or acetone formation steps with 0.9 eV and 1.3 eV respectively (see Figure 51). Therefore, OMP2 formation most probably results PO in the product stream.

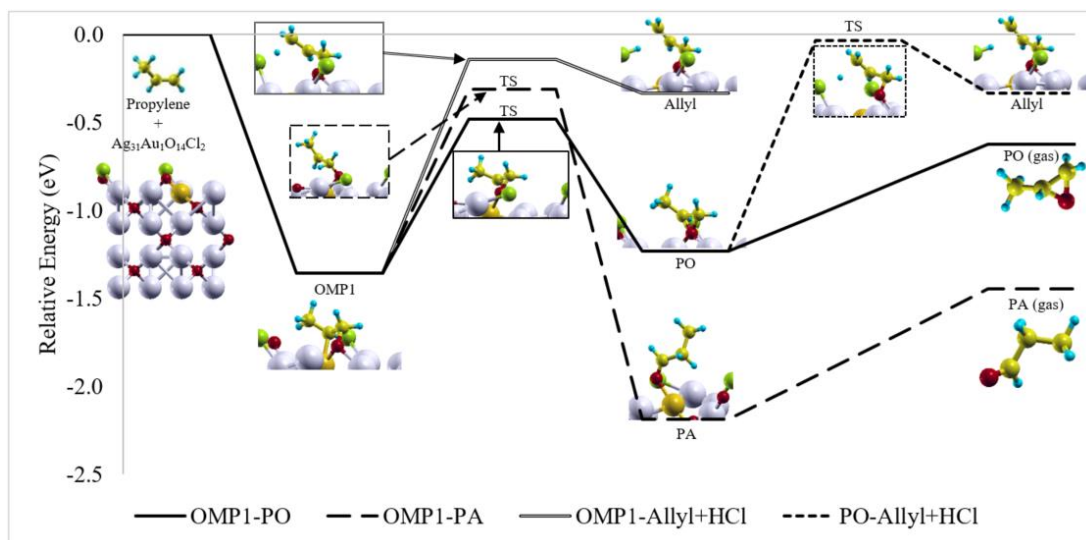


Figure 50: Energetics of the reactions through OMP1 on $\text{Ag}_{31}\text{Au}_1\text{O}_{14}\text{Cl}_2$ (001) slab

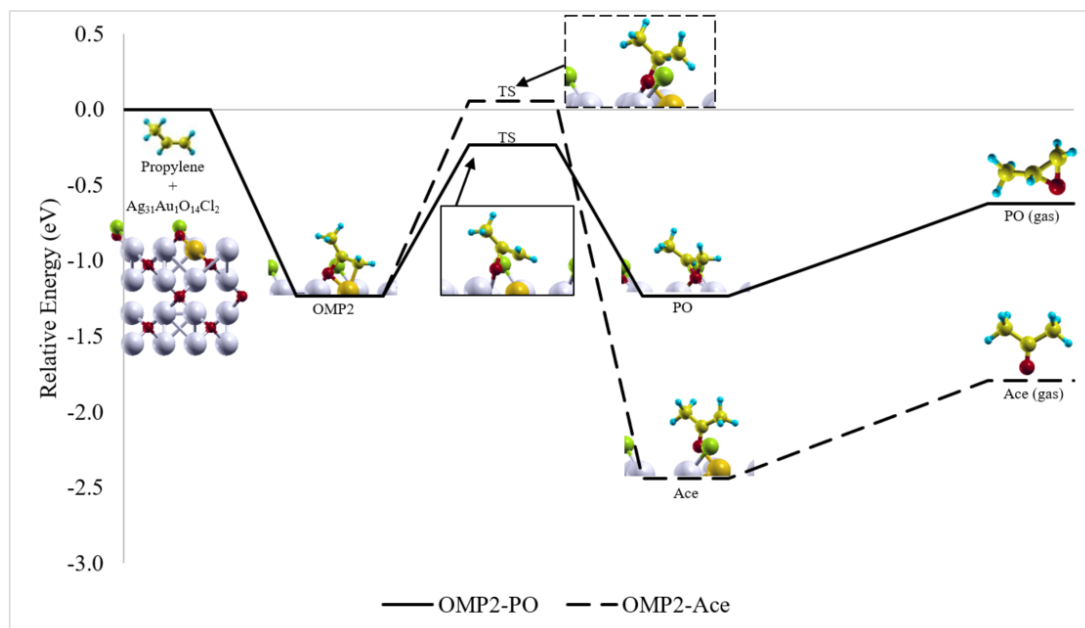
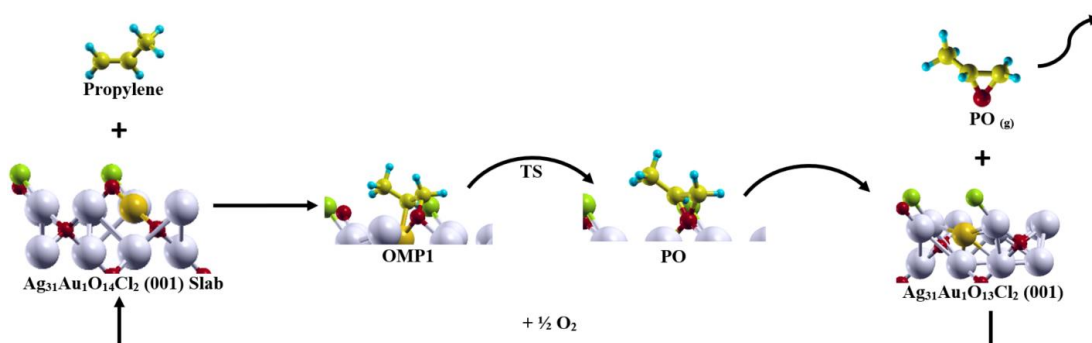


Figure 51: Energetics of the reactions through OMP2 on $\text{Ag}_{31}\text{Au}_1\text{O}_{14}\text{Cl}_2$ (001) slab

Table 9: Activation barriers and reaction energies on $\text{Ag}_{31}\text{Au}_1\text{O}_{14}\text{Cl}_2$ (001) slab

Reaction	Activation Barrier (eV)	Energy of Reaction (eV)
<i>Propylene</i> \rightarrow <i>OMP1</i>	-	-1.4
<i>Propylene</i> \rightarrow <i>OMP2</i>	-	-1.2
<i>Propylene</i> \rightarrow <i>PO</i>	-	-1.2
<i>OMP1</i> \rightarrow <i>PO</i>	0.8	0.1
<i>OMP1</i> \rightarrow <i>PA</i>	1.1	-0.8
<i>OMP1</i> \rightarrow <i>Allyl</i> + <i>HCl</i>	1.2	1.0
<i>OMP2</i> \rightarrow <i>PO</i>	0.9	0.0
<i>OMP2</i> \rightarrow <i>Ace</i>	1.3	-1.2
<i>PO</i> \rightarrow <i>Allyl</i> + <i>HCl</i>	1.2	0.9
<i>PO (ads)</i> \rightarrow <i>PO (g)</i>		0.6
<i>PA (ads)</i> \rightarrow <i>PA (g)</i>		0.7
<i>Ace (ads)</i> \rightarrow <i>Ace (g)</i>		0.7
$\text{Ag}_{31}\text{Au}_1\text{O}_{13}\text{Cl}_2 + \frac{1}{2} \text{O}_2 \rightarrow \text{Ag}_{31}\text{Au}_1\text{O}_{14}\text{Cl}_2$		-0.7

The most probable reaction steps according to the mechanism explained in section 4.1 are represented for $\text{Ag}_{31}\text{Au}_1\text{O}_{14}\text{Cl}_2$ (001) slab in Figure 52. When a gas phase propylene molecule interacts with $\text{Ag}_{31}\text{Au}_1\text{O}_{14}\text{Cl}_2$ (001) slab, chemisorption step gives OMP1 intermediate on the surface. When the required energy to overcome the activation barrier is supplied, this OMP1 intermediate reacts to form adsorbed propylene oxide. With the help of neighbor Cl atoms, PO cannot be oxidized further. Therefore, PO desorbs from the surface by creating a surface oxygen vacancy. Finally, oxygen adsorption to this surface vacancy happens and completes the catalysis cycle.

**Figure 52:** The most probable pathway on $\text{Ag}_{31}\text{Au}_1\text{O}_{14}\text{Cl}_2$ (001) slab

4.6.3. Energetics on the $\text{Ag}_{30}\text{Au}_2\text{O}_{14}\text{Cl}_2$ (001) Slab

Modification of silver oxide surface with two gold and two chlorine atoms makes the Au/Ag and Cl/O ratios on the top layer 1/3 and 1/1 respectively. In the new surface, gold modification affects the top center oxygen atom (oxygen of Au_2O group) more than the chlorine doping. According to Bader analysis, the presence of two chlorine atoms on the surface changes the electron densities of the top center oxygen and gold atoms. The electron density of the oxygen atom increases from 6.64 to 6.65 and the electron densities of the gold atoms increase from 10.55 to 10.58 with respect to $\text{Ag}_{30}\text{Au}_2\text{O}_{16}$ slab. These changes also affect the interaction energy of the propylene molecule with the $\text{Ag}_{30}\text{Au}_2\text{O}_{14}\text{Cl}_2$ (001) slab and make PO and oxametallo-propylene intermediates less stable than their equivalents on the $\text{Ag}_{32}\text{O}_{16}$ slab. According to data supplied in Table 10 and Figure 53, OMP2 formation from the interaction of the propylene with the $\text{Ag}_{30}\text{Au}_2\text{O}_{14}\text{Cl}_2$ (001) slab is the most probable route with reaction energy of -1.0 eV, whereas OMP1 and PO formation steps have the reaction energies of -0.8 eV and -0.7 eV respectively.

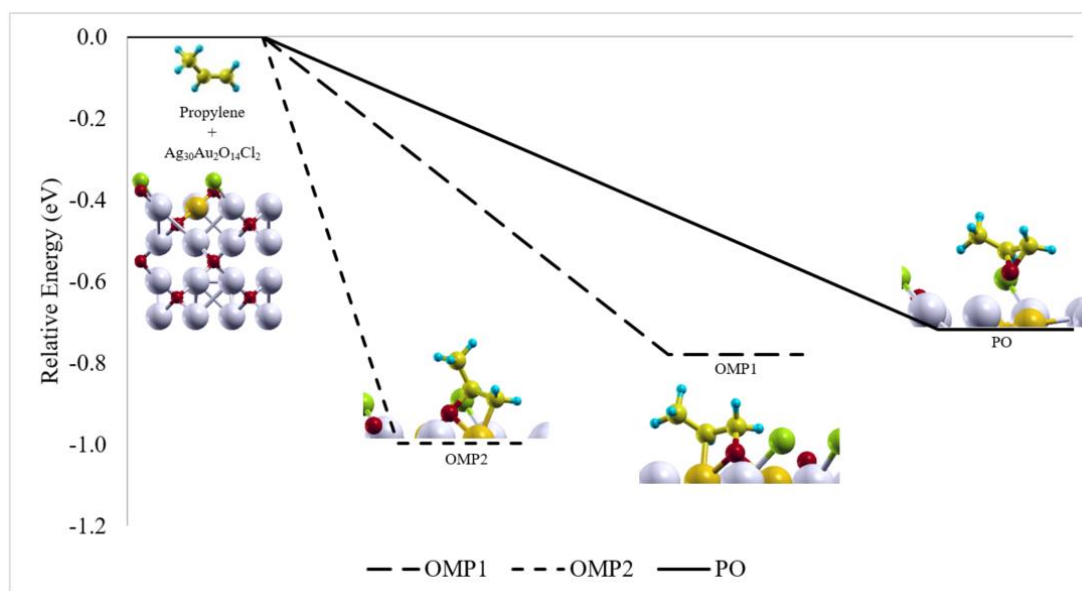


Figure 53: Energetics of direct propylene-surface interactions on $\text{Ag}_{30}\text{Au}_2\text{O}_{14}\text{Cl}_2$ (001) slab

When OMP1 intermediate is formed on the surface, PO, PA and allyl formation reactions may occur. According to Figure 54 and Table 10, activation barriers for PO,

PA and allyl formation steps are calculated as 0.9 eV, 1.0 eV and 0.7 eV respectively. It is considered that the weak interaction between the intermediate structure and the surface cannot help $\text{Ag}_{30}\text{Au}_2\text{O}_{14}\text{Cl}_2$ (001) slab to catalyze these reactions effectively. According to this data OMP1 formation should be followed by allyl radical formation on $\text{Ag}_{30}\text{Au}_2\text{O}_{14}\text{Cl}_2$ (001) slab.

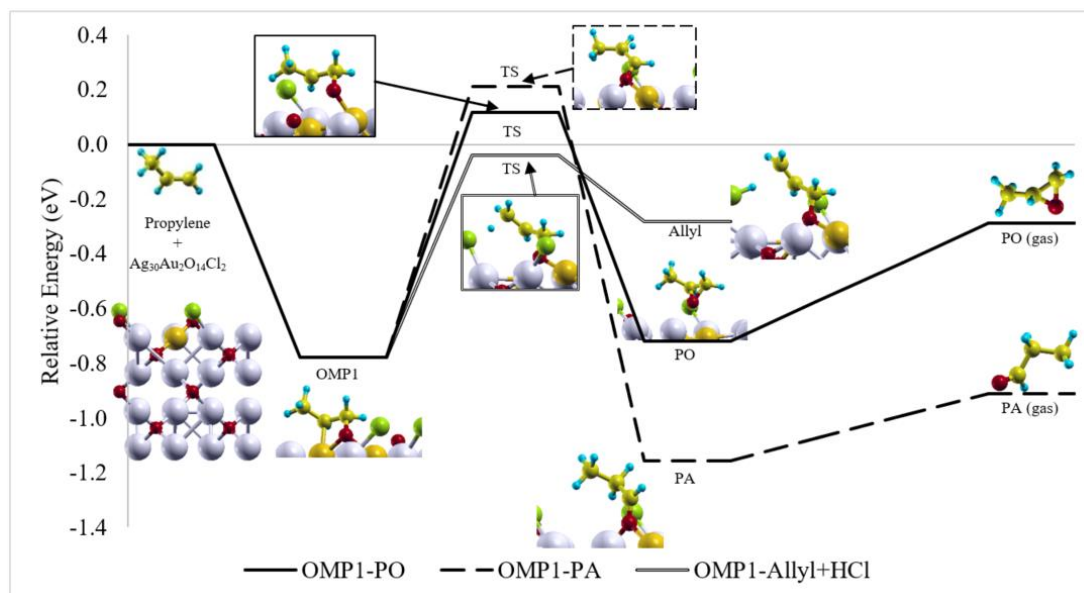


Figure 54: Energetics of the reactions through OMP1 on $\text{Ag}_{30}\text{Au}_2\text{O}_{14}\text{Cl}_2$ (001) slab

When OMP2 is formed on $\text{Ag}_{30}\text{Au}_2\text{O}_{14}\text{Cl}_2$ (001) slab, which is the most probable path in Figure 53, 1.2 eV and 1.3 eV should be supplied for the PO and Ace formation reactions respectively (see Figure 55 and Table 10). On the other way, the desorption of propylene from the surface needs only 1.0 eV. Therefore, PO formation from OMP2 is not probable on $\text{Ag}_{30}\text{Au}_2\text{O}_{14}\text{Cl}_2$ (001) slab.

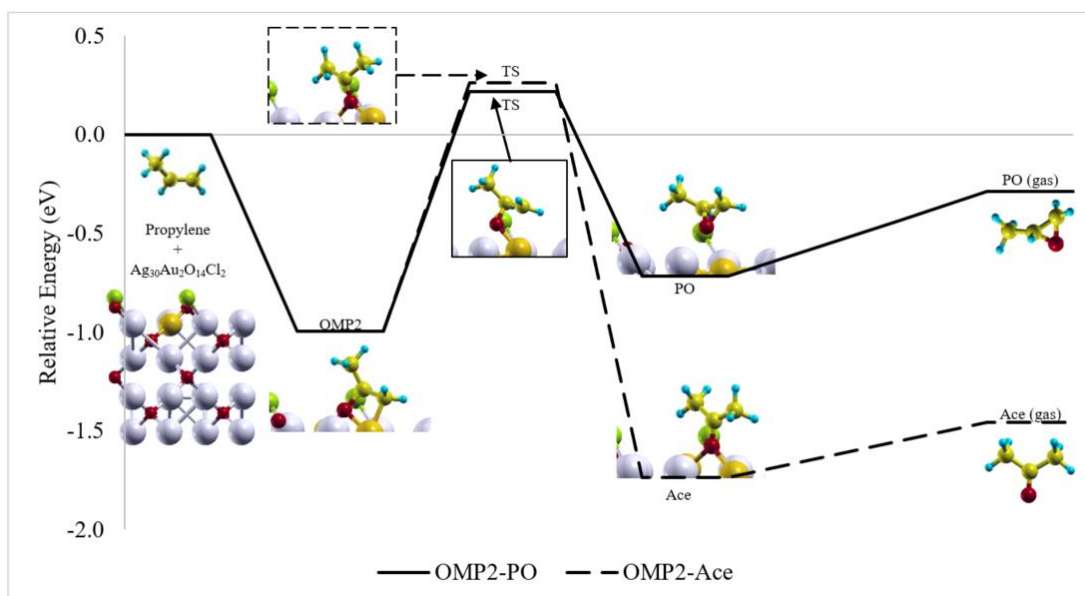


Figure 55: Energetics of the reactions through OMP2 on $\text{Ag}_{30}\text{Au}_2\text{O}_{14}\text{Cl}_2$ (001) slab

Table 10: Activation barriers and reaction energies on $\text{Ag}_{30}\text{Au}_2\text{O}_{14}\text{Cl}_2$ (001) slab

Reaction	Activation Barrier (eV)	Energy of Reaction (eV)
<i>Propylene</i> → <i>OMP1</i>	-	-0.8
<i>Propylene</i> → <i>OMP2</i>	-	-1.0
<i>Propylene</i> → <i>PO</i>	-	-0.7
<i>OMP1</i> → <i>PO</i>	0.9	0.1
<i>OMP1</i> → <i>PA</i>	1.0	-0.4
<i>OMP1</i> → <i>Allyl</i> + <i>HCl</i>	0.7	0.4
<i>OMP2</i> → <i>PO</i>	1.2	0.3
<i>OMP2</i> → <i>Ace</i>	1.3	-0.7
<i>PO</i> → <i>Allyl</i> + <i>HCl</i>	1.0	0.4
<i>PO (ads)</i> → <i>PO (g)</i>		0.4
<i>PA (ads)</i> → <i>PA (g)</i>		0.3
<i>Ace (ads)</i> → <i>Ace (g)</i>		0.3
$\text{Ag}_{30}\text{Au}_2\text{O}_{13}\text{Cl}_2 + \frac{1}{2} \text{O}_2 \rightarrow \text{Ag}_{30}\text{Au}_2\text{O}_{14}\text{Cl}_2$		-1.0

The most probable mechanism for the partial oxidation of propylene on the $\text{Ag}_{30}\text{Au}_2\text{O}_{14}\text{Cl}_2$ (001) slab is represented in Figure 56. According to Figure 53, the interaction of propylene with the $\text{Ag}_{30}\text{Au}_2\text{O}_{14}\text{Cl}_2$ (001) slab most probably results in OMP2 structure. However, the reaction cannot proceed through PO or Ace formation because of high activation barriers. When the equilibrium condition for the OMP2 is

achieved, new propylene-surface interactions should result in OMP1 formation. When the OMP1 intermediate is formed on the $\text{Ag}_{30}\text{Au}_2\text{O}_{14}\text{Cl}_2$ (001) slab, the reaction proceeds through allyl radical formation. At the end, acrolein or combustion products may be expected in the product stream. Therefore, two gold and two chlorine modification on the silver oxide surface cannot help allyl formation problem. Presence of the two gold and the two chlorine atoms in the unit cell of the silver oxide surface substantially decreases the desorption barrier of the propylene oxide from 1.2 eV to 0.4 eV. However, $\text{Ag}_{30}\text{Au}_2\text{O}_{14}\text{Cl}_2$ (001) slab cannot produce PO, due to high activation barriers of the PO formation reaction from the intermediates.

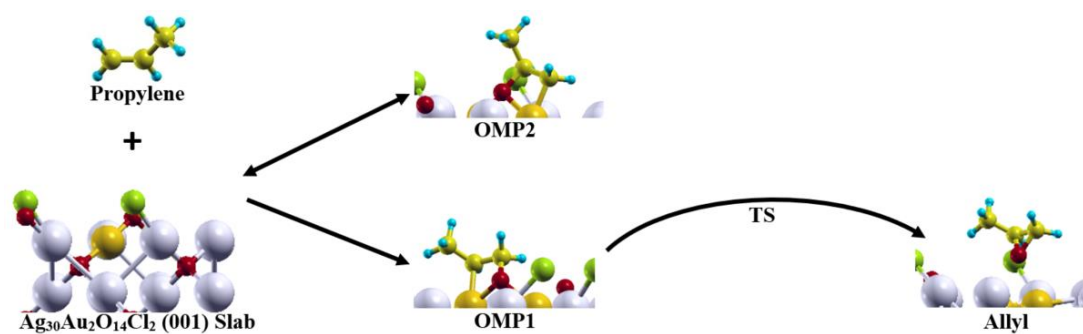


Figure 56: The most probable pathway on $\text{Ag}_{30}\text{Au}_2\text{O}_{14}\text{Cl}_2$ (001) slab

CHAPTER 5

CONCLUSIONS

The goal of this thesis was to investigate the propylene partial oxidation mechanism by using DFT calculations and to find out the possible reasons for low propylene selectivity on silver catalysts and to modify the catalyst to overcome these problems. Throughout the study, the oxide phase of the silver catalyst, i.e. Ag_2O , was used.

Mechanism study on the silver oxide study shows that direct propylene oxide formation on silver oxide surface from the interaction of propylene with surface lattice oxygen is the most probable mechanism. It is found that the direct allylic hydrogen abstraction mechanism, which is shown that the reason of high CO_2 or acrolein selectivity on the silver catalyst by many publications, is not possible because of high activation barrier of 1.9 eV. Even though direct PO formation on the silver oxide surface is the most probable result of the interaction of propylene with the silver oxide surface, desorption of the PO from the surface is detected as the rate-determining step of the gas phase PO formation. Compared with the PO desorption, hydrogen stripping from PO and formation of OMP1 via ring opening are found to have barriers around the half of PO desorption energy. Silver oxide surface with an oxygen vacancy is also studied. It is found that the situation on this surface is similar to the silver oxide surface without vacancy. The only difference is the possibility for the propylene to be adsorbed on oxygen vacant silver site. However, direct propylene epoxidation on one of the neighbor lattice oxygens is energetically more probable than this interaction. At the end, the silver oxide surface with one oxygen vacancy produces PO selectively but

due to the high desorption barrier, PO further reacts with the surface and produces allyl radical. According to these results, the first goal of the study is achieved. The reason for the low PO selectivity is reported as the high desorption barrier of PO and relatively easier allyl formation pathway from PO. According to the findings in this thesis work, silver (oxide) catalyst should be modified such that, the modified catalyst should facilitate the PO desorption and it should also obstruct the allyl radical formation from PO and preferably from OMP1.

In the second part of the study, doping effect is studied. The gold doping is selected because of the previous reports stating that the products can be desorbed more easily from the gold oxide than the silver oxide catalyst for ethylene epoxidation case. Therefore, two different gold modified silver oxide surfaces are prepared with 1/7 and 1/3 gold to silver ratios on the surface. It is found that the desorption energy of PO from the surface is decreased with the Au/Ag replacement. It is observed that even -Ag-O-Au- group decreases the PO desorption barrier, it still cannot prevent the allylic hydrogen abstraction from PO. On the other hand, the -Au-O-Au- group obtained with two Au/Ag replacement reduces the propylene oxide desorption barrier by half of its previous value and increases the barrier of the allyl formation from PO significantly. However, because the gold atoms have higher electron content than the silver atoms of the surface, the most probable pathway for the first interaction of the catalyst with the propylene shifts from PO to the OMP intermediates. With the change of the direction from PO to OMP1, allyl radical formation becomes the most probable result on the gold modified surfaces. Therefore, the only gold modification cannot make gas phase propylene formation feasible.

Cl doping is studied as the second alternative modification on the silver oxide surface. Two surfaces with 1/3 and 1/1 chlorine to oxygen ratio are prepared by replacing surface oxygen atom(s) with chlorine. While gold substitution is withdrawing electrons from the surface oxygen, Cl doping increases the valence electron density of the bridge oxygens. The change in the electronic structure of the surface decreases the desorption barriers of the products from the surface. Both surfaces modified with Cl gives gas phase PO formation as the most probable pathways. After the desorption of

the PO from the catalyst, vacancy is filled with the oxygen adsorption and the catalyst cycle is completed. Besides the electronic effect, the most important effect of Cl for the PO selectivity is observed to be physical. Cl/O replacement on the silver oxide surface reduces the number of active neighbor oxygen sites responsible for the allylic hydrogen abstraction from PO or OMP1. Cl connects to the silver stronger than oxygen and does not react with the hydrogen as oxygen does. Therefore, Cl blocks the allyl radical formation by physically reducing the active oxygen sites on the catalyst surface. On the contrary to the experimental publications stating the effect of the Cl addition is electronic, the results of this thesis show that the main effect of the Cl on the silver catalyst is physical. This finding also explains the reason of the decrease in the propylene conversion reported in the experimental literature when the silver catalyst is promoted with Cl. Such that it could be wise to expect less activity when the active oxygen sites are reduced.

The combined effect of the gold and chlorine substitution is also studied. In the presence of both gold and chlorine, interaction energy of propylene with the surface in the form of PO, OMP1 and OMP2 formation become weaker. It is observed from the Bader analysis that the electronic effect of the gold on the lattice oxygen of the surface is stronger than the effect of the chlorine. Therefore, the gap between the energy difference of PO and OMP intermediates are closed and even OMP intermediates become more stable. On the surface with one gold and one chlorine, PO and allyl formation pathways are found competitive. Hence, chlorine addition enhances the performance of the gold modified surface. Moreover, the addition of the second chlorine makes the surface more selective towards PO by blocking all allyl pathways possible. The surface with one gold and two chlorine modifications also inhibits the isomerization pathways of the propylene oxide due to high activation barriers for OMP1 and OMP2 formation from PO. On the other hand, the addition of the second gold to this structure further weakens the propylene-surface interaction. As unmodified silver oxide surface suffers from the strong interaction, the silver oxide surface with two gold and two chlorine doping fails from the other requirement of the Sabatier Principle. Without the sufficient catalyst-substrate interaction, activation

barriers between OMP structures to PO rises significantly and allyl formation via Cl-H interaction becomes the most probable pathway. Therefore, this study emphasizes that the fine-tuning of the Cl and Au content on the silver oxide surface is essential for the PO selectivity.

REFERENCES

- [1] Kahlich, D., Wiechern, U., and Lindner, J. (2012) Propylene Oxide. *Ullmann's Encycl. Ind. Chem.*, **30**, 313–335.
- [2] Trent, D.L. (2001) Propylene Oxide. *Kirk-Othmer Encycl. Chem. Technol.*
- [3] Shell Global, <https://www.shell.com>, last visited on September 2017.
- [4] lyondellbasel, <https://www.lyondellbasell.com>, last visited on September 2017.
- [5] Data Book (2015), LyondellBasell.
- [6] Khatib, S.J., and Oyama, S.T. (2015) Direct Oxidation of Propylene to Propylene Oxide with Molecular Oxygen: A Review. *Catal. Rev.*, **57** (3), 306–344.
- [7] Nijhuis, T.A., Makkee, M., Moulijn, J.A., and Weckhuysen, B.M. (2006) The production of propene oxide: Catalytic processes and recent developments. *Ind. Eng. Chem. Res.*, **45** (10), 3447–3459.
- [8] The DOW Chemical Company, <https://www.dow.com>, last visited on September 2017.
- [9] Kahn, M., Seubsai, A., Onal, I., and Senkan, S. (2010) High Throughput Synthesis and Screening of New Catalytic Materials for the Direct Epoxidation of Propylene. *Comb. Chem. High Throughput Screen.*, **13** (1), 67–74.
- [10] Lei, Y., Mehmood, F., Lee, S., et al. (2010) Increased Silver Activity for Direct Propylene Epoxidation via Subnanometer Size Effects. *Science* (80-.), **328** (5975), 224–228.
- [11] Cheng, L., Yin, C.R., Mehmood, F., et al. (2014) Reaction Mechanism for Direct Propylene Epoxidation by Alumina-Supported Silver Aggregates: The Role of the Particle/Support Interface. *ACS Catal.*, **4** (1), 32–39.
- [12] Kizilkaya, A.C., Fellah, M.F., and Onal, I. (2010) Direct gas-phase epoxidation of propylene to propylene oxide through radical reactions: A theoretical study. *Chem. Phys. Lett.*, **487** (4–6), 183–189.
- [13] Phon-in, P., Seubsai, A., Chukeaw, T., et al. (2016) Direct epoxidation of propylene to propylene oxide over RuO₂-CuO-NaCl-TeO₂-MnO_x/SiO₂ catalysts. *Catal. Commun.*, **86**, 143–147.

- [14] Yang, X., Kattel, S., Xiong, K., et al. (2015) Direct epoxidation of propylene over stabilized Cu(+) surface sites on titanium-modified Cu₂O. *Angew Chem Int Ed Engl*, **54** (41), 11946–11951.
- [15] Zhang, Q., Guo, Y.Y., Zhan, W., et al. (2016) Gas-phase epoxidation of propylene by molecular oxygen over Ag/BaCO₃ catalysts: Effect of preparation conditions. *Catal. Today*, **276**, 2–10.
- [16] Lee, E.J., Lee, J.W.J., Seo, Y.J., et al. (2017) Direct epoxidation of propylene to propylene oxide with molecular oxygen over Ag–Mo–W/ZrO₂ catalysts. *Catal. Commun.*, **89**, 156–160.
- [17] Chemsystems Inc., (2009) Propylene Oxide: Process Technology (including comparison of Sumitomo's Cumene Hydroperoxide, Hydrogen Peroxide-Based/HPPO, PO/Styrene Monomer, PO/MTBE and Chlorohydrin/CHP Routes), Production Costs (COP), Capacity, Regional Supply/Demand Forecasts.
- [18] Tsuji, J., Yamamoto, J., Ishino, M., and Oku, N. (2006) Development of New Propylene Oxide Process.
- [19] Deutschmann, O., Knözinger, H., Kochloefl, K., and Turek, T. (2011) Heterogeneous Catalysis and Solid Catalysts, 1. Fundamentals. *Ullmann's Encycl. Ind. Chem.*, 457–481.
- [20] Niemantsverdriet, J.W., and Schlögl, R. (2013) Heterogeneous Catalysis: Introduction. *Compr. Inorg. Chem. II (Second Ed. From Elem. to Appl.)*, **7**, 1–6.
- [21] van Santen, R.A. (2017) *Modern Heterogeneous Catalysis*, Wiley-VCH Verlag GmbH & Co. KGaA, Weinheim, Germany.
- [22] Inglezakis, V.J., and Pouloupoulos, S.G. (2006) *Adsorption, Ion Exchange and Catalysis: Design of Operations and Environmental Applications*.
- [23] Farrauto, R.J. (2012) Industrial Catalysis: A Practical Guide, in *Handbook of Industrial Chemistry and Biotechnology*, Springer US, Boston, MA, pp. 201–230.
- [24] Misono, M. (2013) *Basis of heterogeneous catalysis*, Elsevier B.V.
- [25] Howard, P., Morris, G., and Sunley, G. Chapter 1. Introduction: Catalysis in the Chemical Industry, in *Metal-catalysis in Industrial Organic Processes*, Royal Society of Chemistry, Cambridge, pp. 1–22.
- [26] Acmite Market Intelligence (2015) Global Catalyst Market. *Mark. Rep.*, 1–542.
- [27] Fogler, H.S. (2010) *Elements of Chemical Reaction Engineering*.
- [28] Lindström, B., and Pettersson, L.J. (2003) A Brief History of Catalysis. *Cattech*, **7** (1597).
- [29] Roberts, M.W. (2000) Birth of the catalytic concept (1800-1900). *Catal.*

Letters, **67** (1), 1–4.

- [30] Wisniak, J. (2010) The History of Catalysis. From the Beginning to Nobel Prizes. *Educ. quim.*, **21** (1), 60–69.
- [31] Rothenberg, G. (2008) *Catalysis*, Wiley-VCH Verlag GmbH & Co. KGaA, Weinheim, Germany.
- [32] Smith, G. V., and Notheisz, F. (1999) Introduction to Catalysis, in *Heterogeneous Catalysis in Organic Chemistry*, Elsevier, pp. 1–28.
- [33] Lloyd, L. (2011) *Handbook of Industrial Catalysts*, Springer US, Boston, MA.
- [34] Behr, A. (2010) Catalysis, Homogeneous. *Ullmann's Encycl. Ind. Chem.*, 223–269.
- [35] Young, D.C. (2001) *Computational Chemistry*, John Wiley & Sons, Inc., New York, USA.
- [36] Jensen, F. (2007) *Introduction to Computational Chemistry*, John Wiley & Sons Ltd., West Sussex.
- [37] Van Santen, R.A., and Sautet, P. (2009) Challenges to Computational Catalysis, in *Computational Methods in Catalysis and Materials Science* (eds. Santen, R.A. van, and Sautet, P.), Wiley-VCH Verlag GmbH & Co. KGaA, Weinheim, Germany, pp. 441–446.
- [38] Piela, L. (2017) Computational Chemistry: From the Hydrogen Molecule to Nanostructures, in *Handbook of Computational Chemistry*, Springer International Publishing, Cham, pp. 3–19.
- [39] Lewars, E.G. (2016) *Computational Chemistry*, Springer International Publishing, Cham.
- [40] Rode, B.M., Hofer, T.S., and Kugler, M.D. (2007) *The Basics of Theoretical and Computational Chemistry*, Wiley-VCH Verlag GmbH & Co. KGaA, Weinheim, Germany.
- [41] Burke, K. (2007) *The ABC of DFT*, University of California, Irvine.
- [42] Jacobsen, H., and Cavallo, L. (2017) Directions for Use of Density Functional Theory: A Short Instruction Manual for Chemists, in *Handbook of Computational Chemistry*, Springer International Publishing, Cham, pp. 225–267.
- [43] Nobelprize.org The Nobel Prize in Chemistry 1998. *Nobel Media AB 2014*.
- [44] Kedziera, D., and Kaczmarek-Kedziera, A. (2017) Remarks on Wave Function Theory and Methods, in *Handbook of Computational Chemistry*, Springer International Publishing, Cham, pp. 123–171.
- [45] Savin, A., and Johnson, E.R. (2014) Judging Density-Functional Approximations: Some Pitfalls of Statistics, pp. 81–95.

- [46] Mariscal, M.M., Oviedo, O.A., and Leiva, E.P.M. (2013) *Metal Clusters and Nanoalloys*, Springer New York, New York, NY.
- [47] Web of Science. <http://webofknowledge.com>. last visited on September 2017
- [48] Sholl, D.S., and Steckel, J.A. (2009) *Density Functional Theory*, John Wiley & Sons, Inc., Hoboken, NJ, USA.
- [49] Baerends, E.J., Sautet, P., and van Santen, R. Basic Aspects of Density Functional Theory, in *Computational Methods in Catalysis and Materials Science*, Wiley-VCH Verlag GmbH & Co. KGaA, Weinheim, Germany, pp. 23–32.
- [50] Seminario, J.M. (1995) An introduction to density functional theory in chemistry, pp. 1–27.
- [51] Filippi, C., Gonze, X., and Umrigar, C.J. (1996) Generalized gradient approximations to density functional theory: comparison with exact results. *Recent Dev. Appl. Mod. Density Funct. . Theor. Comput. Chem. vol. 4*, **4** (1), 295–326.
- [52] Chermette, H. (1998) Density functional theory: A powerful tool for theoretical studies in coordination chemistry. *Coord. Chem. Rev.*, **178**, 699–721.
- [53] Manz, T.A., and Sholl, D.S. Computing Accurate Net Atomic Charges, Atomic Spin Moments, and Effective Bond Orders in Complex Materials, in *Computational Catalysis*, Royal Society of Chemistry, Cambridge, pp. 192–222.
- [54] Steinmetz, M., Hansen, A., Ehrlich, S., et al. (2014) Accurate Thermochemistry for Large Molecules with Modern Density Functionals, pp. 1–23.
- [55] Nguyen, V.H., Chan, H.Y., Wu, J.C.S.S., and Bai, H. (2012) Direct gas-phase photocatalytic epoxidation of propylene with molecular oxygen by photocatalysts. *Chem. Eng. J.*, **179**, 285–294.
- [56] Yoshida, H., Murata, C., and Hattori, T. (2000) Screening Study of Silica-Supported Catalysts for Photoepoxidation of Propene by Molecular Oxygen. *J. Catal.*, **194** (2), 364–372.
- [57] Pichat, P., Herrmann, J.M., Disdier, J., and Mozzanega, M.N. (1979) Photocatalytic oxidation of propene over various oxides at 320 K. Selectivity. *J. Phys. Chem.*, **83** (24), 3122–3126.
- [58] Zhao, C., and Wachs, I.E. (2008) Selective oxidation of propylene over model supported V₂O₅ catalysts: Influence of surface vanadia coverage and oxide support. *J. Catal.*, **257** (1), 181–189.
- [59] Reitz, J.B., and Solomon, E.I. (1998) Propylene oxidation on copper oxide surfaces: Electronic and geometric contributions to reactivity and selectivity. *J. Am. Chem. Soc.*, **120** (44), 11467–11478.

- [60] Marimuthu, A., Zhang, J., and Linic, S. (2013) Tuning Selectivity in Propylene Epoxidation by Plasmon Mediated Photo-Switching of Cu Oxidation State. *Science* (80-.), **339** (6127), 1590–1593.
- [61] Chimentão, R.J., Medina, F., Fierro, J.L.G., et al. (2007) Propene epoxidation by nitrous oxide over Au-Cu/TiO₂ alloy catalysts. *J. Mol. Catal. A Chem.*, **274** (1–2), 159–168.
- [62] Horvath, B., Hronec, M., Vavra, I., et al. (2013) Direct gas-phase epoxidation of propylene over nanostructured molybdenum oxide film catalysts. *Catal. Commun.*, **34**, 16–21.
- [63] Moens, B., De Winne, H., Corthals, S., et al. (2007) Epoxidation of propylene with nitrous oxide on Rb₂SO₄-modified iron oxide on silica catalysts. *J. Catal.*, **247** (1), 86–100.
- [64] Duma, V., and Honicke, D. (2000) Gas phase epoxidation of propene by nitrous oxide over silica-supported iron oxide catalysts. *J. Catal.*, **191** (1), 93–104.
- [65] Zhang, Q.H., Guo, Q., Wang, X.X., et al. (2006) Iron-catalyzed propylene epoxidation by nitrous oxide: Toward understanding, the nature of active iron sites with modified Fe-MFI and Fe-MCM-41 catalysts. *J. Catal.*, **239** (1), 105–116.
- [66] Jiao, J., Shen, B., and Zhao, J. (2011) Exploration Research on High Selectivity of Propylene Epoxidation over TS-1 Catalyst. *Energy Sources, Part A Recover. Util. Environ. Eff.*, **33** (12), 1147–1154.
- [67] Nijhuis, T.A., Huizinga, B.J., Makkee, M., and Moulijn, J.A. (1999) Direct epoxidation of propene using gold dispersed on TS-1 and other titanium-containing supports. *Ind. Eng. Chem. Res.*, **38** (3), 884–891.
- [68] Lu, J.Q., Luo, M.F., Lei, H., and Li, C. (2002) Epoxidation of propylene on NaCl-modified silver catalysts with direct molecular oxygen as the oxidant. *Appl. Catal. A Gen.*, **237**, 11–19.
- [69] Meiers, R., Dingerdissen, U., and Hölderich, W.F. (1998) Synthesis of Propylene Oxide from Propylene, Oxygen, and Hydrogen Catalyzed by Palladium–Platinum–Containing Titanium Silicalite. *J. Catal.*, **176** (2), 376–386.
- [70] Meiers, R., and Hölderich, W.F. (1999) Epoxidation of propylene and direct synthesis of hydrogen peroxide by hydrogen and oxygen. *Catal. Letters*, **59** (2/4), 161–163.
- [71] Hayashi, T., Tanaka, K., and Haruta, M. (1998) Selective vapor-phase epoxidation of propylene over Au/TiO₂ catalysts in the presence of oxygen and hydrogen. *J. Catal.*, **178** (2), 566–575.
- [72] Haruta, M., and Kawahara, J. (2008) Epoxidation of Propylene with Oxygen-Hydrogen Mixtures. *Mech. Homog. Heterog. Epoxidation Catal.*, 297–313.

- [73] Taylor, B., Lauterbach, J., and Delgass, W.N. (2005) Gas-phase epoxidation of propylene over small gold ensembles on TS-1. *Appl. Catal. A Gen.*, **291** (1–2), 188–198.
- [74] Taylor, B., Lauterbach, J., Blau, G.E., and Delgass, W.N. (2006) Reaction kinetic analysis of the gas-phase epoxidation of propylene over Au/TS-1. *J. Catal.*, **242** (1), 142–152.
- [75] Monnier, J.R. (2001) The direct epoxidation of higher olefins using molecular oxygen. *Appl. Catal.*, **221**, 73–91.
- [76] Wang, R., Hao, J., Guo, X., et al. (2004) Propylene epoxidation over Ag/TS-1 catalysts. *Stud. Surf. Sci. Catal.*, **154**, 2632–2638.
- [77] Guo, X., Wang, R., Wang, X., and Hao, J. (2004) Effects of preparation method and precipitator on the propylene epoxidation over Ag/TS-1 in the gas phase. *Catal. Today*, **93–95**, 211–216.
- [78] Kanungo, S., Keshri, K.S., van Hoof, A.J.F., et al. (2016) Silylation enhances the performance of Au/Ti-SiO₂ catalysts in direct epoxidation of propene using H₂ and O₂. *J. Catal.*, **344**, 434–444.
- [79] Kanungo, S., Perez Ferrandez, D.M., Neira d'Angelo, F., et al. (2016) Kinetic study of propene oxide and water formation in hydro-epoxidation of propene on Au/Ti-SiO₂ catalyst. *J. Catal.*, **338**, 284–294.
- [80] Lambert, R.M., Williams, F.J., Cropley, R.L., and Palermo, A. (2005) Heterogeneous alkene epoxidation: past, present and future. *J. Mol. Catal. A Chem.*, **228** (1–2), 27–33.
- [81] Lu, J.Q., Luo, M.F., Lei, H., and Li, C. (2002) Epoxidation of propylene on NaCl-modified silver catalysts with air as the oxidant. *Appl. Catal. a-General*, **237** (1–2), 11–19.
- [82] Hu, Z.-M., Nakai, H., and Nakatsuji, H. (1998) Oxidation mechanism of propylene on an Ag surface: dipped adcluster model study. *Surf. Sci.*, **401** (3), 371–391.
- [83] Takahashi, A., Hamakawa, N., Nakamura, I., and Fujitani, T. (2005) Effects of added 3d transition-metals on Ag-based catalysts for direct epoxidation of propylene by oxygen. *Appl. Catal. A Gen.*, **294** (1), 34–39.
- [84] Farinha Portela, M., Henriques, C., Pires, M.J., et al. (1987) Catalytic epoxidation and degradation of propylene by dioxygen over silver. *Catal. Today*, **1** (1–2), 101–110.
- [85] Yao, W., Zheng, X., Guo, Y.Y.Y., et al. (2011) Role of chlorohydrocarbon in increasing selectivity of propylene oxide over Ag-Y₂O₃-K₂O/ α -Al₂O₃ catalyst for epoxidation of propylene by molecular oxygen. *J. Mol. Catal. A Chem.*, **342–343**, 30–34.

- [86] Zemichael, F.W., Palermo, A., Tikhov, M.S., and Lambert, R.M. (2002) Propene Epoxidation over K-Promoted Ag/CaCO₃ Catalysts: The Effect of Metal Particle Size. *Catal. Letters*, **80** (3/4), 93–98.
- [87] Zheng, X., Zhang, Q., Guo, Y.Y., et al. (2012) Epoxidation of propylene by molecular oxygen over supported Ag-Cu bimetallic catalysts with low Ag loading. *J. Mol. Catal. A Chem.*, **357**, 106–111.
- [88] Ghosh, S., Acharyya, S.S., Tiwari, R., et al. (2014) Selective oxidation of propylene to propylene oxide over silver-supported tungsten oxide nanostructure with molecular oxygen. *ACS Catal.*, **4** (7), 2169–2174.
- [89] Geenen, P. V., Boss, H. J. and Pott, G.T. (1982) A study of the vapour phase epoxidation of propylene and ethylene on silver and silver gold alloy catalysis. *J. Catal.*, **77**, 499.
- [90] Zemichael, F.W., Al-Musa, A., Cumming, I.W., and Hellgardt, K. (2008) Propene partial oxidation over Au-Ag Alloy and Ag catalysts using electrochemical oxygen. *Solid State Ionics*, **179** (27–32), 1401–1404.
- [91] Özbek, M.O. (2011) Computational Study of Ethylene Epoxidation, *Middle East Technical University*.
- [92] Lu, G., and Zuo, X. (1999) Epoxidation of propylene by air over modified silver catalyst. *Catal. Letters*, **58**, 67–70.
- [93] Jin, G., Lu, G., Guo, Y., et al. (2004) Modification of Ag–MoO₃/ZrO₂ Catalyst with Metallic Chloride for Propylene Epoxidation by Molecular Oxygen. *Catal. Letters*, **97** (3/4), 191–196.
- [94] Seubsai, A., and Senkan, S. (2011) The Effects of Cofeeding Chlorinated Hydrocarbons in the Direct Epoxidation of Propylene by Molecular Oxygen. *ChemCatChem*, **3** (11), 1751–1754.
- [95] Özbek, M.O., Önal, I., and Van Santen, R.A. (2013) Chlorine and Caesium Promotion of Silver Ethylene Epoxidation Catalysts. *ChemCatChem*, **5** (2), 443–451.
- [96] Torres, D., Lopez, N., Illas, F., and Lambert, R.M. (2007) Low-basicity oxygen atoms: a key in the search for propylene epoxidation catalysts. *Angew Chem Int Ed Engl*, **46** (12), 2055–2058.
- [97] Liu, T., Hacıoğlu, P., Oyama, S.T., et al. (2009) Enhanced reactivity of direct propylene epoxidation with H₂ and O₂ over Ge-modified Au/TS-1 catalysts. *J. Catal.*, **267** (2), 202–206.
- [98] Pulido, A., Concepción, P., Boronat, M., and Corma, A. (2012) Aerobic epoxidation of propene over silver (111) and (100) facet catalysts. *J. Catal.*, **292**, 138–147.
- [99] Chukeaw, T., Seubsai, A., Phon-in, P., et al. (2016) Multimetallic catalysts of

- RuO₂-CuO-Cs₂O-TiO₂/SiO₂ for direct gas-phase epoxidation of propylene to propylene oxide. *RSC Adv.*, **6** (61), 56116–56126.
- [100] Molina, L.M., Lee, S., Sell, K., et al. (2011) Size-dependent selectivity and activity of silver nanoclusters in the partial oxidation of propylene to propylene oxide and acrolein: A joint experimental and theoretical study. *Catal. Today*, **160** (1), 116–130.
- [101] Molina, L.M., Lopez, M.J., Alonso, J.A., et al. (2014) Ab initio studies of propene epoxidation on oxidized silver surfaces. *Phys Chem Chem Phys*, **16** (48), 26546–26552.
- [102] Kulkarni, A., Bedolla-Pantoja, M., Singh, S., et al. (2012) Reactions of propylene oxide on supported silver catalysts: Insights into pathways limiting epoxidation selectivity. *Top. Catal.*, **55** (1–2), 3–12.
- [103] Moskaleva, L. V. (2016) Theoretical mechanistic insights into propylene epoxidation on Au-based catalysts: Surface O versus OOH as oxidizing agents. *Catal. Today*, **278**, 45–55.
- [104] Stoukides, M. (1984) Electrocatalytic Rate Enhancement of Propylene Epoxidation on Porous Silver Electrodes Using a Zirconia Oxygen Pump. *J. Electrochem. Soc.*, **131** (4), 839–845.
- [105] Kaichev, V. V., Bukhtiyarov, V.I., Hävecker, M., et al. (2003) The nature of electrophilic and nucleophilic oxygen adsorbed on silver. *Kinet. Catal.*, **44** (3), 432–440.
- [106] Wang, R., Guo, X., Wang, X., and Hao, J. (2004) Gas-phase epoxidation of propylene over Ag/Ti-containing catalysts. *Catal. Today*, **93–95** (July), 217–222.
- [107] Cheng, L., Yin, C., Mehmood, F., et al. (2014) Reaction Mechanism for Direct Propylene Epoxidation by Alumina- Supported Silver Aggregates : The Role of the Particle / Support Interface.
- [108] Zheng, X., Guo, Y.L.Y.Y.-L., Guo, Y.L.Y.Y.-L., et al. (2015) Epoxidation of propylene by molecular oxygen over unsupported AgCu_x bimetallic catalyst. *Rare Met.*, **34** (7), 477–490.
- [109] Fellah, M.F., and Onal, I. (2012) Epoxidation of Propylene on a [Ag₁₄O₉] Cluster Representing Ag₂O (001) Surface: A Density Functional Theory Study. *Catal. Letters*, **142** (1), 22–31.
- [110] Kresse, G., and Furthmüller, J. (1996) Efficiency of ab-initio total energy calculations for metals and semiconductors using a plane-wave basis set. *Comput. Mater. Sci.*, **6** (1), 15–50.
- [111] Kresse, G., and Hafner, J. (1994) Ab initio molecular-dynamics simulation of the liquid-metal–amorphous-semiconductor transition in germanium. *Phys. Rev. B*, **49** (20), 14251–14269.

- [112] Blöchl, P.E. (1994) Projector augmented-wave method. *Phys. Rev. B*, **50** (24), 17953–17979.
- [113] Perdew, J.P., and Wang, Y. (1992) Accurate and simple analytic representation of the electron-gas correlation energy. *Phys. Rev. B*, **45** (23), 13244–13249.
- [114] Perdew, J.P., Chevary, J.A., Vosko, S.H., et al. (1992) Atoms, molecules, solids, and surfaces: Applications of the generalized gradient approximation for exchange and correlation. *Phys. Rev. B*, **46** (11), 6671–6687.
- [115] Monkhorst, H.J., and Pack, J.D. (1976) Special points for Brillouin-zone integrations. *Phys. Rev. B*, **13** (12), 5188–5192.
- [116] Allen, J.P., Scanlon, D.O., and Watson, G.W. (2011) Electronic structures of silver oxides. *Phys. Rev. B - Condens. Matter Mater. Phys.*, **84** (11), 1–14.
- [117] Henkelman, G., Uberuaga, B.P., and Jónsson, H. (2000) A climbing image nudged elastic band method for finding saddle points and minimum energy paths. *J. Chem. Phys.*, **113** (22), 9901.
- [118] Henkelman, G., and Jónsson, H. (2000) Improved tangent estimate in the nudged elastic band method for finding minimum energy paths and saddle points. *J. Chem. Phys.*, **113** (22), 9978–9985.
- [119] Henkelman, G., Arnaldsson, A., and Jónsson, H. (2006) A fast and robust algorithm for Bader decomposition of charge density. *Comput. Mater. Sci.*, **36** (3), 354–360.
- [120] Tang, W., Sanville, E., and Henkelman, G. (2009) A grid-based Bader analysis algorithm without lattice bias. *J. Phys. Condens. Matter*, **21** (8), 84204.
- [121] Sanville, E., Kenny, S.D., Smith, R., and Henkelman, G. (2007) Improved grid-based algorithm for Bader charge allocation. *J. Comput. Chem.*, **28** (5), 899–908.

CURRICULUM VITAE

PERSONAL DETAILS:

Surname, Name : Tezsevin, İlker
Nationality : Turkish
Date and Place of Birth : March 20, 1988 – Biga
e-mail : ilkertezsevin@gmail.com

EDUCATION

2010 – 2012 M.Sc. Chemical Engineering Department, (CGPA:3.50/4.00)
Middle East Technical University (Turkey)
Thesis Title: A study of catalytic nanocarbon synthesis by means of
quantum mechanical methods

2006 – 2010 B.S. Chemical Engineering Department (CGPA:3.42/4.00)
Middle East Technical University (Turkey)

WORK EXPERIENCE

2011 – 2015 Research Assistant: METU Chemical Engineering Dept., Ankara

2014 – 2015 Academic Advisor: Asya Sistem Biomass Plasma Gasification Facility
Asya Sistem Energy, Logistics and Engineering Consultancy, Ankara

2015 – 2017 Visiting Researcher: TU/e Chemical Engineering and Chemistry
Dept. Eindhoven/The Netherlands

SELECTED AWARDS AND SCHOLARSHIPS

- 2015 International Research Scholarship During Ph.D. Study: TÜBİTAK
- 2012 Ph.D. Scholarship: TÜBİTAK
- 2012 Best Poster Award in Nanotechnology: 7th Chemical Engineering Conference for Collaborative Research in Eastern Mediterranean Countries, Corfu, Greece
- 2012 Prof. Dr. Hasan Orbey Memorial Award for Research Excellence in Graduate Studies: METU Chemical Engineering Dept.
- 2010 M.Sc. Scholarship: TÜBİTAK

SELECTED CONFERENCE PAPERS

Ilker Tezsevin, Mehmet Ferdi Fellah, Yuda Yurum, Isik Onal, A Density Functional Theory Study of Carbon Activation of Acetylene on (M- μ O-M)-ZSM-5 Clusters (where M= Fe, Ni, Co and V) as Initial Step of Carbon Nanotube Production. "2nd Nano Today - Nano Technology Conference Waikoloa, Hawaii", (2011)

Ilker Tezsevin, Deniz Onay, Mehmet Ferdi Fellah, Isik Onal, A DFT Study of NO_x Reduction by C₃H₈ Aided Selective Catalytic Reduction Method: Investigation of Reduction Pathways from NO to N₂ on Ag₇ Nanocluster. "2nd Nano Today - Nano Technology Conference Waikoloa, Hawaii", (2011)

Ilker Tezsevin, Duygu Gerceker, Isik Onal, A Study of Catalytic Nanocarbon Synthesis by Means of Quantum Mechanical Methods. "7th Chemical Engineering Conference for Collaborative Research in Eastern Mediterranean Countries, Corfu", (2012)

Ilker Tezsevin, Işık Önal, A DFT Study of Propylene Epoxidation on Ag₂O (001) and Gold Modified Ag₂O (001) Surfaces. "30th European Conference on Surface Science, Antalya", (2014)

İlker Tezsevin, Ivo Filot, Emiel Hensen, Rutger A. van Santen, Işık Önal, Acrolein Formation Mechanism by Propylene Partial Oxidation on Ag₂O (001) Surface. “CHAINS 2015, the Dutch Chemistry Conference, Veldhoven”, (2015)

İlker Tezsevin, Ivo Filot, Emiel Hensen, Rutger A. van Santen, Işık Önal, A Density Functional Theory Study of Propylene Epoxidation over Ag₂O (001) Surface. “N3C, The Netherlands' Catalysis and Chemistry Conference, Noordwijkerhout”, (2016)

PUBLICATIONS

İlker Tezsevin, Mehmet Ferdi Fellah, Isik Onal, Density functional theory investigation of acetylene dehydrogenation on metal exchanged ZSM-5 clusters for initial step of carbon nanotube production. *Microporous and Mesoporous Materials*, Volume 180, 1 November 2013, Pages 102-108.

DOI:10.1016/j.micromeso.2013.06.021

İlker Tezsevin, Deniz Onay, Mehmet Ferdi Fellah, Isik Onal, A Density Functional Theory Study of NO Reduction by C₃H₈ Aided Selective Catalytic Reduction Method. *Catalysis Letters*, Volume 145, 9 January 2015, Pages 964-970.

DOI:10.1007/s10562-014-1475-2

İlker Tezsevin, Cansu Demirtas, Isik Onal, Cerag Dilek, Density functional theory study of interactions between carbon dioxide and functionalized polyhedral oligomeric silsesquioxanes. *International Journal of Quantum Chemistry*, 2017, e25397

DOI: 10.1002/qua.25397